Faculteit Industriële Ingenieurswetenschappen

master in de industriële wetenschappen: nucleaire technologie

Masterthesis

Characterisation of UO2 Spent Nuclear Fuel Samples containing Gd2O3 using Serpent2 Code

Lars Rymenants

Scriptie ingediend tot het behalen van de graad van master in de industriële wetenschappen: nucleaire technologie, afstudeerrichting nucleair en medisch

PROMOTOR :
Prof. dr. ir. Gert VAN DEN EYNDE

PROMOTOR :
Dr. ir. Pablo ROMOJARO

Gezamenlijke opleiding UHasselt en KU Leuven

Universiteit Hasselt | Campus Diepenbeek | Faculteit Industriële Ingenieurswetenschappen | Agoralaan Gebouw H - Gebouw B | BE 3590 Diepenbeek

Universiteit Hasselt | Campus Diepenbeek | Agoralaan Gebouw D | BE 3590 Diepenbeek
Universiteit Hasselt | Campus Hasselt | Martelarenlaan 42 | BE 3500 Hasselt

2023
2024

Faculteit Industriële Ingenieurswetenschappen

master in de industriële wetenschappen: nucleaire technologie

Masterthesis

Characterisation of UO2 Spent Nuclear Fuel Samples containing Gd2O3 using Serpent2 Code

Lars Rymenants

Scriptie ingediend tot het behalen van de graad van master in de industriële wetenschappen: nucleaire technologie, afstudeerrichting nucleair en medisch

PROMOTOR :

Prof. dr. ir. Gert VAN DEN EYNDE

PROMOTOR :

Dr. ir. Pablo ROMOJARO

UHASSELT KU LEUVEN

Acknowledgements

I would like to express my sincere appreciation to all those who contributed to the completion of this master's thesis. Firstly, I would like to express my gratitude towards Prof. dr. ir. Van den Eynde for highlighting this available opportunity at the Belgian Nuclear Research Centre (SCK CEN), and for stimulating my interest in this research topic during my studies as an industrial engineer in nuclear technology at the University of Hasselt (UHasselt) and the Catholic University of Leuven (KU Leuven).

Secondly, I would like to acknowledge my external supervisor Dr. ir. Romojaro for his invaluable assistance in both the conduct and reporting aspects of my master's thesis. All of the accumulated knowledge and expertise that I have acquired as a direct consequence of this great learning opportunity will be carried with me throughout my future engineering career path, for which I am deeply grateful.

Lastly, I would like to express my gratitude towards Dr. Dreesen for his guidance regarding the appropriate academic formulation and correct formatting of all the involved documents.

This page intentionally left blank

Table of Contents

List of Figures

List of Tables

Nomenclature

γ	Cumulative fission yield
ε	Fast fission factor
η	Reproduction factor
λ	Nuclear decay constant
ν	Fission neutron multiplicity
ρ	Core reactivity, Mass density
$\sigma_{a,th}$	Microscopic cross section for absorption of thermal neutrons
Σ_a	Macroscopic cross section for absorption
φ	Angular neutron flux
ϕ	Neutron flux
$\hat{\Omega}$	Angular direction
A	Atomic mass number
AGR	Advanced Gas-cooled Reactor
AS	Alpha Spectroscopy
b	Barn
BA	Burnable neutron Absorber
BFR	Burnable Fuel Rod
BOL	Beginning-of-Life
BU	Burnup
BWR	Boiling light Water Reactor
CANDU	Canadian Deuterium Uranium Reactor
CR	Control Rod
DOD	Day of Discharge
E	Energy
EGADSNF	Expert Group on Assay Data of Spent Nuclear Fuel
EOL	End-of-Life
eV	Electronvolt
f	Thermal neutron utilisation factor
FA	Fuel Assembly
FIMA	Fissions per Initial Metal Atom
FP	Fission Product
FR	Fuel Rod
g	Spatial self-shielding factor
GS	Gamma Spectroscopy
GWd/t_{HM}	Gigawatt-day per metric tonne of heavy metal
HEU	Highly Enriched Uranium
IAEA	International Atomic Energy Agency
IDMS	Isotope Dilution Mass Spectrometry
J	Joule
JAERI	Japan Atomic Energy Research Institute
K	Kelvin

k_{eff}	Effective neutron multiplication factor
KU Leuven	Catholic University of Leuven
LBTE	Linearised Boltzmann Transport Equation
LWR	Light Water Reactor
MA	Minor Actinide
MAGNOX	Magnesium Alloy Graphite-moderated Gas-cooled Uranium Oxide Reactor
MOX	Mixed Oxide fuels
MS	Mass Spectroscopy
MTC	Moderator Temperature Coefficient
n	Neutron density
N	Atom density
NEA	Nuclear Energy Agency
NTE	Neutron Transport Equation
ODE	Ordinary Differential Equation
OECD	Organisation for Economic Co-operation and Development
ORNL	Oak Ridge National Laboratory
p	Resonance escape probability
P	Power
P_{NL}	Non-leakage probability
pcm	Per Cent Mille
ppm	Parts Per Million
PWR	Pressurised light Water Reactor
$\vec{r}$	Spatial position
RBMK	Reaktor Bolshoy Moshchnosty Kanalny
RCA	Radiochemical Analysis
RR	Reaction Rate
s	Neutron source
S	Surface area
SCK CEN	Belgian Nuclear Research Centre
SFCOMPO	Spent Fuel Isotopic Composition
SI	International System of Units
SNF	Spent Nuclear Fuel
SD	Standard Deviation
t	Time
T	Temperature
$T_{1/2}$	Half-life value
TD	Theoretical mass Density
UHasselt	University of Hasselt
v	Neutron velocity
V	Volume
VTT	Technical Research Centre of Finland
VVER	Vodo-Vodyanoi Energetichesky Reaktor
wt%	Weight percent
WREBUS	Water Reactor Fuel Extended Burnup Study
Zry-4	Zircaloy-4

Abstract

The degree of enrichment in uranium dioxide (UO_2) nuclear fuels has evolved to the extent that the associated excess reactivity at reactor start-up requires additional compensation through the addition of gadolinium(III) oxide (Gd_2O_3). However, due to the increasing presence of Gd_2O_3, the accurate prediction of the isotopic evolution and power throughout irradiation cycles has a more significant impact on the fuel performance. Nevertheless, to date there have been no studies that have assessed the predictive capabilities of the SERPENT-2 fuel depletion code for low-doped UO_2-Gd_2O_3 fuel samples. Therefore, this master's thesis models selected UO_2-Gd_2O_3 Spent Nuclear Fuel (SNF) samples and compares them with experimental results from destructive radiochemical analyses in order to assess the predictive capabilities of SERPENT-2. The simulation models incorporate fuel sample design data and reactor operational histories from the Spent Fuel Isotopic Composition 2.0 database, which was developed by the Organisation for Economic Co-operation and Development: Nuclear Energy Agency. The eight selected SNF samples originate from the Japanese Pressurised Water Reactors (PWRs) Takahama-3 and Ohi-2. After running the simulations, the nuclide inventory predictions were compared utilising the 'C/E-1' representation. For both PWRs, the calculated results were in good agreement with the experimental results. Therefore, in the scope of validating PWR samples in which Gd_2O_3 is more prevalent, the SERPENT-2 fuel depletion code can be utilised.

Abstract (in Dutch)

De graad van verrijking in uraniumdioxide (UO_2)-kernbrandstoffen is zodanig geëvolueerd dat de bijhorende overreactiviteit bij het opstarten van de reactor extra compensatie vereist door toevoeging van gadolinium(III)oxide (Gd_2O_3). Door de toenemende aanwezigheid van Gd_2O_3 heeft de nauwkeurige voorspelling van de isotopenevolutie en het vermogen gedurende de bestralingscycli echter een grotere invloed op de brandstofprestaties. Desondanks zijn er tot op heden geen studies verricht die de voorspellingsmogelijkheden van de SERPENT-2-brandstofdepletiecode voor laaggedoteerde UO_2-Gd_2O_3-brandstofmonsters hebben beoordeeld. Daarom modelleert deze masterproef geselecteerde UO_2-Gd_2O_3-monsters van verbruikte kernbrandstof (SNF) en vergelijkt ze met experimentele resultaten van radio-chemische analyses om de voorspellingscapaciteit van SERPENT-2 te beoordelen. De simulatiemodellen bevatten gegevens over het ontwerp van het splijtstofmonster en de operationele geschiedenis van de reactoren opgehaald uit de Spent Fuel Isotopic Composition 2.0 databank, die is ontwikkeld door de OESO/NEA. De acht geselecteerde SNF-monsters zijn afkomstig van de Japanse drukwaterreactoren (PWR's) Takahama-3 en Ohi-2. Na het uitvoeren van de simulaties werden de nuclide-inventarissen vergeleken met behulp van de C/E-1-weergave. Voor beide PWR's kwamen de berekende resultaten goed overeen met de experimentele resultaten. In het kader van de validatie van PWR-monsters waarin Gd_2O_3 meer voorkomt, kan de SERPENT-2-brandstofdepletiecode dan ook worden gebruikt.

1 General

1.1 Introduction

Since the early days of commercial utilisation of nuclear energy, there has been a sustained and continuous effort to optimise fission reactor technology concepts. As a result, in the scope of improving the performance of commercial fission reactors and reducing the associated nuclear fuel costs – *i.e.* an economic incentive – a number of reactor operating modifications have already been implemented. The modifications include an increase in the irradiation time in the reactor – which improves fuel utilisation – and fuel cycle prolongation, which results in higher fuel depletion (*i.e.* fuel burnup) [1]. An increase in burnup (BU) affects various stages of the fuel cycle, including enrichment and fabrication, assembly configuration, performance, as well as back-end processes such as Spent Nuclear Fuel (SNF) handling, treatment, and storage [1]. The beneficial potential of extended BU on the fuel cycle was identified on an international scale during the 'Water Reactor Fuel Extended Burnup Study' (WREBUS), conducted by the International Atomic Energy Agency (IAEA) – beginning in 1988 and completed in 1991 [2].

In order to accommodate the aforementioned reactor operating modifications, it is necessary – in all international reactor technology types – to evolve the isotopic compositions of the nuclear fuels towards higher initial fissile isotope concentrations [3]. This isotopic evolution ensures the presence of sufficient fissile material throughout the extended timeframes (*e.g.* uranium-235 enrichment in uranium dioxide (UO_2) fuels or plutonium-239 enrichment in the case of mixed oxide (MOX) fuels). As a result, the elevated presence of the fissile isotopes has a significant impact on the core reactivity at the reactor's Beginning-of-Life (BOL), to the extent that the excess core reactivity cannot solely be compensated for by soluble neutron absorbers and by mechanical control rod elements [4]. It was therefore proposed that solid-state burnable neutron absorbers (BAs) be introduced as a homogeneous mixture into, or alternatively as a coating around, the UO_2 or MOX fuel pellets as a potential solution [5].

BAs are non-fissile atomic nuclei with a relatively large thermal neutron absorption cross section, whose isotopic concentrations decrease – in parallel with the evolution of excess reactivity – over the course of the nuclear reactor's operational fuel cycle. The most routinely utilised BA on an industrial energy-producing scale is currently gadolinium(III) oxide (*i.e.* gadolinia, Gd_2O_3) [6]. Moreover, the nuclear energy industry has conducted extensive research over the past decennia, with ongoing developments, resulting in the accumulation of significant reactor-related experience. In light of the aforementioned observations, it is evident that gadolinia-doped nuclear fission fuels represent the focus of this research.

1.2 Outline of the Work

The fuel assembly (FA) designs include the integration of burnable fuel rods (BFRs) at specific positions within the FA, as opposed to the uniform distribution of the BA throughout all the fuel rods (FRs). The appropriate spatial positioning of the BFRs in the assembly, allows for the control of local power peaking (*i.e.* power distribution control) [7]. Previously, these BFRs were processed with natural or low-enriched UO_2 mixed with typically 2 up to 6 weight percent (wt%) of natural gadolinia [8]. However, in the most recent FA designs, the progressive development of the gadolinia content is up to 10 wt%, with the uranium content comparable to that of the surrounding FRs [4], [9]. As a result, the accurate prediction of the nuclide inventories and power distributions throughout the entire irradiation period has a more significant impact on the performance of UO_2 or MOX fuels associated with the latest designs.

The accurate prediction of nuclide inventories is achieved through the utilisation of nuclear depletion calculation codes, as the performance of destructive analyses for multiple SNF samples from each irradiated assembly is impractical and financially uninteresting. The aforementioned codes simulate the interactional behaviour of neutrons and the physical operating conditions within the nuclear fission reactor, and subsequently calculate the expected nuclide inventories utilising the 'Bateman' equations.

In order to guarantee the isotopic accuracy of the calculated nuclide inventory results, it is essential to verify and validate the nuclear depletion calculation codes. A code validation process for the three-dimensional continuous-energy Monte Carlo neutron and photon transport code, SERPENT-2, has yet to be performed in the context of gadolinia-doped PWR-SNF samples. Therefore, the general objective of this master's thesis is to model eight selected SNF samples of PWR-UO_2-Gd_2O_3 nature with a relatively low doping degree of natural gadolinia – *i.e.* earlier PWR assembly designs – and subsequently analyse them with concentrations obtained by destructive radiochemical analyses (RCAs). Moreover, the nuclide inventories simulated by SERPENT-2 will be evaluated in comparison to those obtained through alternative nuclear depletion calculation codes. The selected PWR-SNF samples are sourced from the Japanese Kansai Electric Power Co. Takahama Reactor No. 3 Nuclear Power Station, and the Kansai Electric Power Co. Ohi Reactor No. 2 Nuclear Power Station. The reported operating data has been compiled by the Japan Atomic Energy Research Institute (JAERI). Following the comparative analyses, a final statement can be postulated regarding the predictive capabilities of SERPENT-2.

1.3 Outline of the Report

The master's thesis is structured into multiple chapters, each of which focuses on a specific aspect of the research. The initial chapter, entitled "Theoretical Framework", attempts to explain the required fundamental information and concepts essential for comprehending neutron and in-core reactor physics relevant to the implementation of gadolinia. Therefore, the objective of this chapter is not to provide an exhaustive explanation of all theoretical concepts, but rather to introduce them in a concise manner.

The subsequent chapter, entitled "Sample Descriptions", provides a detailed account of the geometrical assembly configurations, initial isotopic compositions, and specific operating histories of the modelled PWR-UO_2-Gd_2O_3 SNF samples. The thesis examines five samples obtained from the Takahama Reactor No. 3 – identified as "SF96-1" through "SF96-5" – and which are all sourced from assembly "NT3G23". In addition, three samples from the Ohi Reactor No. 2 are examined, specifically from rods "C5" and "O13", both of which are sourced from assembly "17G" – labelled as "89G01", "89G03", and "89G05".

Following the simulations, all calculated nuclide inventories are presented in the chapter entitled "Results by SERPENT-2". The format 'C/E-1' is utilised to present the percentage deviation between the calculated and the experimentally determined concentrations – including the sample-average and the standard deviation (SD). All experimental measurements were conducted at the 'JAERI post-irradiation fuel examination facility'. The chapter entitled "Discussion" presents a summary of the most relevant observations and remarks regarding the sample-average and sample-specific calculated concentrations.

In the final chapter, entitled "Conclusion", a concluding statement regarding the predictive capabilities of the SERPENT-2 depletion calculation code is postulated. Moreover, the concluding chapter provides a series of suggestions and recommendations for future Gd_2O_3-doped SNF characterisation assignments.

2 Theoretical Framework

2.1 Neutron Physics Concepts

2.1.1 Nuclear Fission Process

The ability of nuclear fission to occur – from an energy perspective – can be clarified by briefly explaining the concepts of 'binding energy' and 'critical energy'. The total binding energy, E_b, is defined as the energy that holds the nucleus together, and therefore is the energy which is required to separate the nucleus into its constituent nucleons (*i.e.* protons and neutrons) [10]. Nuclei with a high binding energy per nucleon are particularly stable or tightly bound, and require a relatively large amount of energy to break them apart. Figure 1 illustrates the average binding energy per nucleon as a function of the atomic mass number (*A*) [10]. It is important to note that the binding energy per nucleon curve attains its maximum value at '*A'* equal to 56 (*i.e.*iron-56) and decreases in a steady manner thereafter [11]. The behaviour of the curve is important in the identification of potential sources of nuclear energy [10].

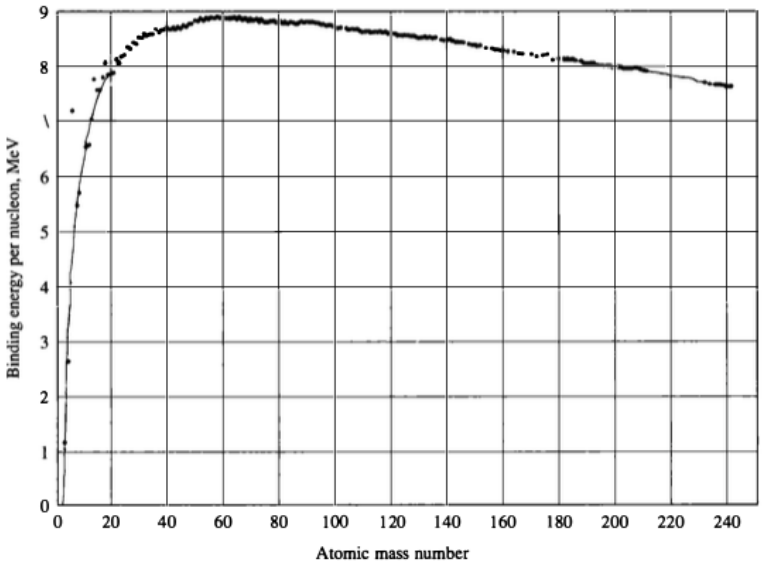

Figure 1: Binding energy per nucleon as a function of the atomic mass number [10, p. 31]

Figure 1 additionally indicates that heavy nuclei (*i.e.* $A > 56$) can achieve a more stable configuration of nucleons when they are split into two lighter separate nuclei, *i.e.* undergo fission [12]. As the nuclei become heavier, they become increasingly unstable, which consequently increases the potential for spontaneous fission. However, the spontaneous fission processes occur with insufficient frequency to be of any considerable significance in nuclear fission reactors [13]. In order to facilitate the fission processes, and overcome the attractive forces acting between the nucleons, energy must be supplied to the nucleus under consideration [13]. This energy quantity is referred to as the 'critical energy', E_c, which is the energy required to deform the nucleus to the extent that it can be fissioned.

In consideration of the aforementioned energy concepts, it can be concluded that if the binding energy of an additional neutron to the nucleus is greater than the critical energy (*i.e.* $E_b > E_c$), an incident neutron will induce fission [12], [14]. The most frequently utilised nuclides that satisfy this criterion are uranium-233, uranium-235, and plutonium-239, which are collectively referred to as 'fissile' nuclides.

In opposition to the ‘fissile’ nuclides, are the ‘fertile’ nuclides. Examples of ‘fertile’ nuclides include thorium-232, uranium-238, and plutonium-240 [14]. In this particular classification of nuclides, it is necessary to provide additional kinetic energy to the incident neutron in order to induce fissions. An additional possibility is induced fission after the nuclide has been transmuted – into a fissile nuclide. Transmutation is defined as the nuclear reaction process in which an incident neutron is captured by a heavy nucleus, resulting in the transformation of the nucleus under consideration to another isotope. To illustrate, in the case of fertile uranium-238, uranium-239 will be formed via radiative neutron capture, which is then followed by radioactive beta (β) decay to form neptunium-239. This, in turn, will decay via β decay, resulting in the formation of fissile plutonium-239 – this particular series of formation processes is referred to as ‘nuclear fuel breeding’ [15]. As posited by [16], nuclides with an odd *A* are more likely to absorb a neutron and subsequently undergo fission than nuclides with an even *A*.

Following the event of a fission, three distinct entities are released: energy (*E*), fission products (FPs), and prompt neutrons. Prompt neutrons are defined as neutrons that are born immediately (*i.e.* time $t < 10^{-17}$ s) and typically amount to between two and three neutrons per fission event [12]. The multiplicity of fission neutrons, denoted by the symbol υ, depends on the nuclide undergoing fission and the energy of the incident neutron [12]. It is these types of neutrons that require moderation and thermalisation – which is the dissipation of their energy through scattering with light atomic nuclei – in order to reach the thermal energy region and induce further fission (*i.e.* a chain reaction). More interesting are the FPs, which are the two lighter atomic nuclei that are formed when a heavy nucleus is split. Figure 2 illustrates the asymmetric fission product yield distribution of various heavy nuclei [17]. The fission product yield curve is dependent on both the fissioned nuclide and the energy of the incident neutron (second order dependence) [14]. The energy released per thermal fission is released in a variety of energy forms, not all of which are of recoverable nature. The majority of the released energy is transferred to the produced FPs and their associated decay processes, including β decay, gamma (γ) decay, and neutrino emission. However, it is not possible to recover the fraction of energy released in the form of neutrino emission.

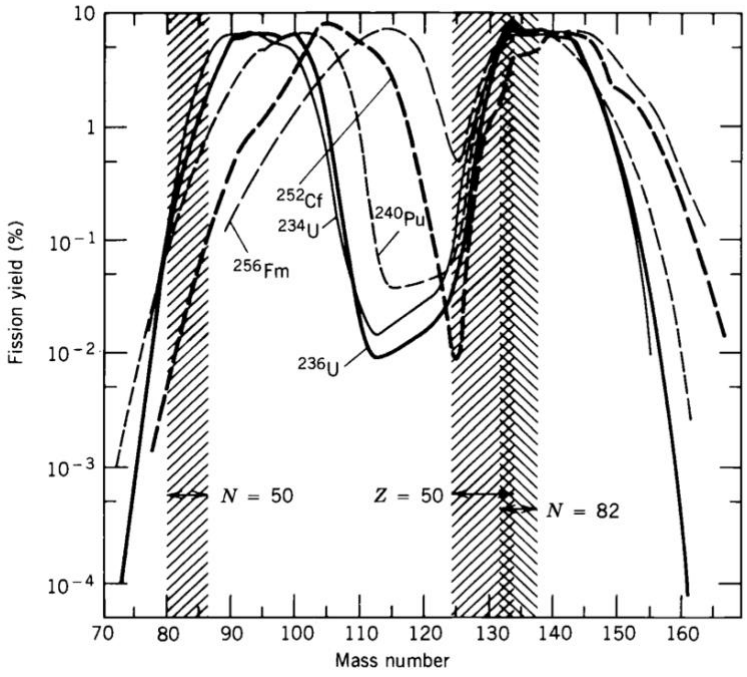

Figure 2: Fission yield distribution as a function of the atomic mass number [17, p. 232]

2.1.2 Microscopic Cross Section

The microscopic cross section, denoted as σ, is a measure of the relative probability that a given incident particle – in the context of a nuclear fission reactor, primarily a neutron – will induce a specific nuclear reaction, such as fission, radiative capture, inelastic or elastic scattering, *etc*. with a certain target atomic nucleus [18]. The microscopic cross section is a property intrinsic to the atomic nucleus and is defined for each type of nuclear interaction [14]. The physical quantity exhibits an energy dependence of the incident particle – due to the structure of the atomic nucleus [19]. It is therefore indicated in conjunction with the energetic state of the concerned incident particle (*e.g.* 'thermal', 'epithermal', and 'fast' state).

Given that both light water reactor (LWR) technology types "PWR" and "BWR" are thermal fission reactors, it can be stated that the nuclear fission processes are sustained by thermal neutrons. This implies that free-moving neutrons are in thermal equilibrium with their surrounding environment – following the 'Maxwell-Boltzmann' distribution [20] – and possess a most probable kinetic energy of 0.0253 electronvolts (eV, which is equal to 1.60218E-19 Joules) [21]. It is therefore evident that the thermal energy region of the microscopic cross section (σ_{th}) for specific neutron interactions represents the most relevant segment/region of the quantity. The standard unit for quantifying the microscopic cross section in terms of the characteristic target area – where a larger characteristic area implies a higher probability of nuclear interaction – is the barn (b). Moreover, the microscopic cross section can be expressed in accordance with the *International System of Units* (SI), where 1 b is equivalent to 1.0E-28 m^2 [22]. Figure 3 illustrates the total (σ_t, top line) and fission (σ_f, bottom line) microscopic cross sections of uranium-235 as a function of the incident neutron energy [23].

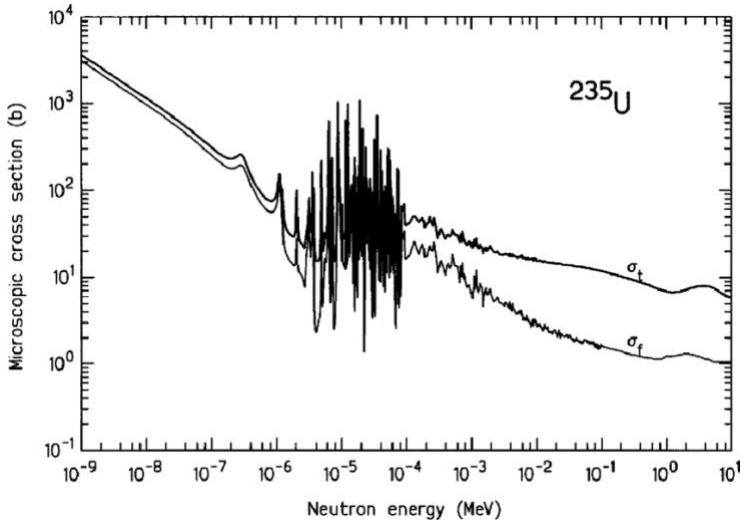

Figure 3: Total and fission microscopic cross section of uranium-235 as a function of the incident neutron energy [23, p. 201]

2.1.3 Neutron Flux and Reaction Rate

In order to clarify the following two quantities, a monoenergetic neutron beam is assumed to impinge on a target. The neutron flux, denoted as ϕ, is defined as a measure of the intensity with which a neutron beam strikes a target nuclide over a one-second time interval [24]. The quantity is the product of the neutron density (n) and the neutron velocity (v), and is expressed in neutrons/($cm^2 * s$) [14]. The reaction rate, *RR*, is an additional quantity and is the only one of the two that can be measured in a nuclear reactor.

The *RR* is defined as the product of the neutron flux (ϕ) and the macroscopic cross section (Σ) – which is the microscopic cross section (σ) multiplied by the atomic density (*N*) [14]. Consequently, the neutron flux – which exhibits an angular, axial, and radial dependence [25] – can be derived from the *RR* by utilising accurate cross section data available in evaluated nuclear data libraries (*vide infra*, p. 35).

Figure 4 illustrates a representative neutron flux spectrum of a commercial PWR core at BOL conditions [26]. It can be observed that the majority of the neutron flux is in the fast spectrum (*i.e.* $E > 0.1$ MeV) because of the prompt neutrons released during the fission processes. The relative increase in the magnitude of the neutron flux in the thermal energy region (*i.e.* $E < 0.0253$ eV) is a consequence of the moderation and thermalisation of the prompt neutrons. The relative magnitudes of the three distinct energy regions are contingent upon the specific operational parameters of the reactor in question [26].

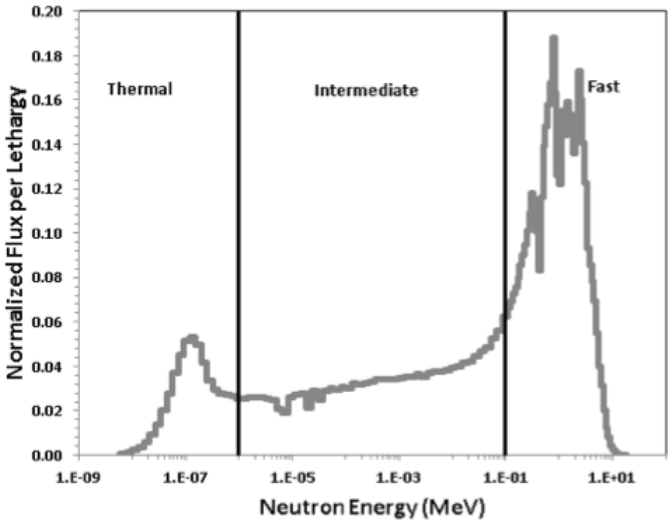

Figure 4: Normalised neutron flux as a function of the incident neutron energy [26, p. 473]

2.1.4 Neutron Transport Equation

The transport behaviour of neutrons in an arbitrary volume increment *V* can be described and simulated by utilising the 'linearised Boltzmann transport equation' (LBTE) [27]. The equation of continuity states that the variation rate of the number of neutrons (*i.e.* $\partial n / \partial t$) in an assumed volume is equal to the neutron generation rate in the assumed volume minus the neutron loss rate in the assumed volume [28]. There are seven independent variables present, including three for spatial positioning in the Cartesian coordinate system ($\vec{r}$(x, y, z)), two for the angular direction of motion ($\hat{\Omega}(\theta, \phi)$), and one each for energy (*E*) and time (*t*) [29]. Equation 1 presents the 'conservation of the neutron number' formula [29].

$$\frac{\partial n}{\partial t} = \text{Generation rate} - \text{Loss rate} \tag{1}$$

The total neutron population is governed by a variety of different generation and loss mechanisms. Potential generation mechanisms include any neutron sources present within the specified volume increment, about *E*, moving in the angular direction $\hat{\Omega}$, at time *t*. This mechanism is represented by the symbol $[s(\vec{r}, E, \hat{\Omega}, t)]$**,** and includes generation through induced fissions, neutron-producing reactions – *i.e.* (n, xn) – or the presence of independent neutron sources (*e.g.* americium-beryllium [30]).

A second potential generation mechanism is that neutrons may enter the specified volume increment through its defined surface *S*, which is represented by the term: $[v\,\nabla\cdot\hat{\Omega}\,n(\vec{r},E,\hat{\Omega},t)]$ [28]. In addition, neutrons may be subjected to scattering collisions, which transform their deviating energy and angular variables $(E',\hat{\Omega}')$ to those of interest $(E,\hat{\Omega})$. This particular generation mechanism is referred to as the 'in-scattering' term, and is represented by the following: $[v'\,\Sigma_s(\vec{r},E'\rightarrow E,\hat{\Omega}'\rightarrow\hat{\Omega})\,n(\vec{r},E',\hat{\Omega}',t)]$ [28]. Given that the leakage term – both leakage in and out – is a surface integral, 'Gauss's theorem' (*i.e.* the divergence theorem [31]) was employed to transform it into a volume integral [28]. Equation 2 presents the total neutron generation rate integrated over all angular directions (*i.e.* 4π) and energies.

$$\int_{4\pi}\mathrm{d}\hat{\Omega}'\int_0^{\infty}\mathrm{d}E'v'\,\Sigma_{\mathrm{s}}(\vec{r},E'\rightarrow E,\hat{\Omega}'\rightarrow\hat{\Omega})\,n(\vec{r},E',\hat{\Omega}',t)+s(\vec{r},E,\hat{\Omega},t) \tag{2}$$

At the opposite end of the continuity equation is the neutron loss rate, which consists of two distinct mechanisms. The first mechanism encompasses the streaming of neutrons out of the assumed volume increment through its defined surface. This mechanism is represented by the term: $[v\,\nabla\cdot\hat{\Omega}\,n(\vec{r},E,\hat{\Omega},t)]$ [28]. In addition, the loss of neutrons due to collisions within the volume increment – *i.e.* including both phenomena absorption and scattering by the atomic nucleus [29] – is represented by the following: $[v\,\Sigma_t(\vec{r},E)\,n(\vec{r},E,\hat{\Omega},\mathrm{t})]$ [28]. Equation 3 presents the total neutron loss rate.

$$\frac{\partial}{\partial\mathrm{t}}\,n(\vec{r},E,\hat{\Omega},t)+v\,\hat{\Omega}\cdot\nabla\,n(\vec{r},E,\hat{\Omega},t)+v\,\Sigma_{\mathrm{t}}(\vec{r},E)\,n(\vec{r},E,\hat{\Omega},t) \tag{3}$$

It is a common practice to rewrite Equations 2 and 3 by utilising the angular neutron flux ($\varphi(\vec{r},E,\hat{\Omega},t)$), which is equivalent to the term: $[v\cdot n(\vec{r},E,\hat{\Omega},t)]$ [28]. Equation 4 is a linear 'integro-differential' equation that presents the substituted versions of the neutron generation and loss rate terms [28]. However, in order to solve the 'LBTE', it is necessary to define appropriate problem-specific boundary conditions – *e.g.* interface boundary – and the initial conditions – *e.g.* neutron flux should be finite and non-negative real numbers – that the unique solution must satisfy [29].

$$\frac{1}{v}\frac{\partial}{\partial t}\,\varphi(\vec{r},E,\hat{\Omega},t)+\hat{\Omega}\cdot\nabla\,\varphi(\vec{r},E,\hat{\Omega},t)+\Sigma_{\mathrm{t}}(\vec{r},E)\,\varphi(\vec{r},E,\hat{\Omega},t)$$

$$=\int_{4\pi}\mathrm{d}\hat{\Omega}\int_0^{\infty}\mathrm{d}E'\,\Sigma_{\mathrm{s}}(\vec{r},E'\rightarrow E,\hat{\Omega}'\rightarrow\hat{\Omega})\,\varphi(\vec{r},E',\hat{\Omega}',t)+s(\vec{r},E,\hat{\Omega},t) \tag{4}$$

In the context of this research application, it is permitted to simplify the neutron transport equation (NTE), as only the reactor exploitation at nominal power (*P*) is of interest – *i.e.* start-up and shutdown processes are not considered [32]. The assumed operational state of the nuclear system is referred to as the 'steady state' condition. This condition assumes that the number of neutrons in the specified volume increment remains constant – *i.e.* neutron variation rate being equal to zero – and that $\lim_{t\rightarrow\infty}(\varphi\,(\vec{r},E,\hat{\Omega},t))$ is equal to zero (*i.e.* no time dependence is assumed in the nuclear system under consideration) [29]. Equation 5 presents the 'steady state NTE', which comprises six independent variables (*i.e.* no time *t*).

$$\hat{\Omega}\cdot\nabla\,\varphi(\vec{r},E,\hat{\Omega})+\Sigma_{\mathrm{t}}(\vec{r},E)\,\varphi(\vec{r},E,\hat{\Omega})$$

$$=\int_{4\pi}\mathrm{d}\hat{\Omega}\int_0^{\infty}\mathrm{d}E'\,\Sigma_{\mathrm{s}}(\vec{r},E'\rightarrow E,\hat{\Omega}'\rightarrow\hat{\Omega})\,\varphi(\vec{r},E',\hat{\Omega}')+s(\vec{r},E,\hat{\Omega}) \tag{5}$$

2.2 Reactor Physics Concepts

2.2.1 Effective Neutron Multiplication Factor

The effective neutron multiplication factor, denoted as k_{eff}, is defined as the ratio of the total number of neutrons resulting from fission in the current neutron generation to the total number of neutrons lost through absorption and leakage in the preceding neutron generation [33]. The aforementioned quantity is the driving factor of nuclear reactor kinetics and provides a quantitative description of the nuclear fission chain reaction. The effective neutron multiplication factor can be calculated using Equation 6. The equation is referred to as the 'neutron life cycle balance' equation. There are five independent fuel and reactor-related parameters present, which are the following: the fast fission factor (ε), the resonance escape probability (p), the thermal neutron utilisation factor (f), the reproduction factor (η), and the geometric non-leakage probability (P_{NL}) [34].

$$k_{eff} = \varepsilon * p * f * \eta * P_{NL} \tag{6}$$

The initial parameter of the neutron life cycle balance equation is the fast fission factor, denoted ε. This specific fuel-dependent parameter indicates the contribution to the total neutron multiplication factor by induced fissions that resulted from incident neutron energies higher than the thermal energy region [34] (*i.e.* fast/prompt induced fissions by incident neutrons which energetic state is the 'fast/prompt' state). The 'fast fission' factor is defined as the ratio of the total number of neutrons released as a result of all-energy induced fissions – *i.e.* thermal and fast/prompt – to the total number of neutrons released as a result of sole thermal-energy induced fissions. Moreover, the factor is dependent on the physical characteristics of the active fuel rod, the light atomic nuclei moderator, and the number of fertile nuclides present in the nuclear fuel [34] (as they are capable of undergoing fission by the assumed more energetic incident neutrons, as detailed in §2.1.1 Nuclear Fission Process. *e.g.* uranium-238 in UO_2 and MOX). The second parameter is the resonance escape probability, denoted as p, which describes the probability that a fast/prompt neutron will successfully be moderated from its energy level to the thermal energy region, *i.e.*, thereby avoiding radiative capture in the sterile resonance region (*i.e.* the energy region between 1.0 eV and 10E+4 eV) [34]. The parameter is contingent upon the atom density (N) of fissile uranium-238, the scattering characteristics of the light atomic nuclei moderator – *i.e.* macroscopic cross section – and the average energy transferred from the fast/prompt neutron to the moderator per collision. Subsequently, the thermal neutron utilisation factor, denoted f, is defined as the fraction of the thermal-energy neutrons that are effectively absorbed – *i.e.* utilised – in the nuclear fuel [34]. The factor depends on the physical pin/rod and assembly dimensions – *i.e.* diameter, length, and rod pitch – as well as the absorption characteristics of the nuclear fuel and all surrounding materials (*e.g.* cladding, vessel, *etc*.). The second to last parameter is the reproduction factor (η) which represents the average number of neutrons released per thermal-energy neutron absorbed in a fuel nucleus [34]. The aforementioned parameter is dependent upon the nuclide under consideration, the degree of fissile enrichment in the isotopic composition of the nuclear fuel, and the amount of occurred depletion (*i.e.* the degree to which the nuclear fuel has been utilised). Lastly, in order to account for the finite nature of practical nuclear fission reactors – *i.e.* the potential for all-energy neutrons to leak out of the reactor core and subsequently be lost – the non-leakage probability (P_{NL}) parameter is introduced. The non-leakage parameter can be further subdivided into two distinct fractions: one for thermal-energy neutrons lost and another for fast/prompt neutrons lost. The estimation of both, however, is performed in a slightly different manner.

The value of k_{eff} is indicative of the operational status of the nuclear system. In the event that the value of k_{eff} is less than one – *i.e.* $k_{eff} < 1.0$ – the number of total induced fissions in the fissile nuclei – and thereby the total number of fission neutrons released – from one neutron generation will decrease over time, thereby preventing the maintenance of a constant neutron chain reaction [35]. This system state is referred to as 'subcritical'. In the event that the value of k_{eff} is greater than one – *i.e.* $k_{eff} > 1.0$ – the number of total fission neutrons will increase from neutron generation to neutron generation [35]. Consequently, the neutron population – and the reactor power output level – will increase exponentially, and this condition is referred to as 'supercritical' [36]. Lastly, in the desired 'critical' state – wherein the value of k_{eff} is precisely equal to one – *i.e.* $k_{eff} = 1.0$ – the neutron chain reaction proceeds at a constant rate and the neutron population is stable over time [35]. Moreover, a stable neutron population will result in a constant reactor power output level (which is directly proportional to the thermal neutron flux) [37]. Figure 5 illustrates a schematic representation of a supercritical nuclear fission chain reaction, specifically illustrating the particular value of k_{eff} as two.

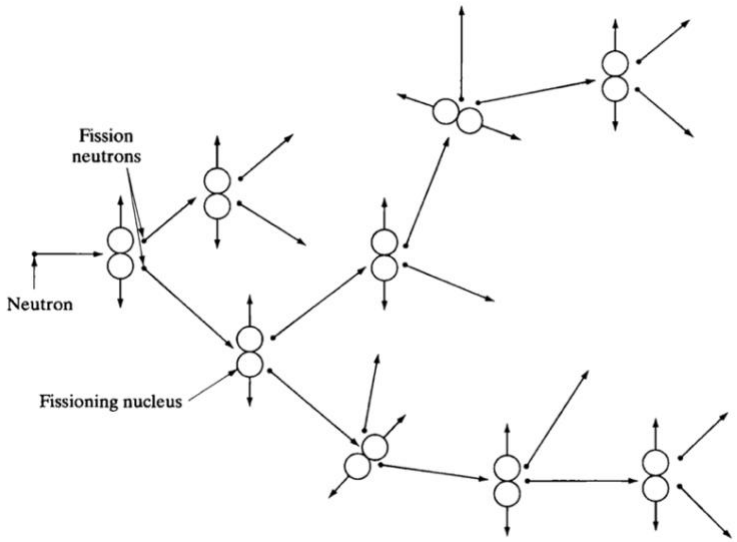

Figure 5: Schematic representation of a supercritical nuclear chain reaction [35, p. 118]

2.2.2 Core Reactivity

When discussing changes in the neutron population in a controlled nuclear reactor, the most convenient manner to forecast the evolution of the neutron population over time, is to describe how the system diverges from its critical state (*i.e.* $k_{eff} = 1.0$). The core reactivity, denoted as ρ, is a direct indicator of this relative deviation (Δ) per neutron generation and is expressed in per cent mille (pcm, and equal to 1.0E-05) or in dollars ($) [34], [37]. The relative magnitude of the core reactivity, whether positive ($+$) or negative ($-$), directly determines the rate at which the neutron population – and the reactor power output level – increase or decrease over time [37]. In other words, strict criticality is maintained when the core reactivity is equal to zero. In other instances, when the core reactivity is positive, the nuclear reactor becomes supercritical; vice versa when the core reactivity is negative, the nuclear reactor becomes subcritical. Equation 7 presents the formula for calculating the core reactivity of a finite reactor.

$$\rho = \frac{k_{eff} - 1}{k_{eff}} \tag{7}$$

2.2.3 Reactivity Effects

A number of physical phenomena may occur during the exploitation of a nuclear reactor, resulting in a change in core reactivity ($\Delta\rho$). Such phenomena are referred to as 'reactivity effects' and are categorised according to the underlying trigger. Examples of the aforementioned reactivity triggers include the fuel temperature (T_F), moderator temperature (T_{Mod}), steam void fraction, fuel depletion or burnup (BU), and FP poisons [37], [38]. An alternative method of categorising reactivity effects is according to the time of impact, which can be either direct/immediate or indirect/long-term [38]. Furthermore, the immediate reactivity coefficients (α) – which are associated to the direct/immediate reactivity effects – which represent the anticipated change in core reactivity per unit change in the reactor parameter under consideration, must remain negative at all times during exploitation in the context of reactor safety [38].

The initial prompt/immediate reactivity effect relates to the change in resonance escape probability (p) in response to an increase in T_F. This immediate reactivity effect is associated with the nuclear Doppler effect – which is also known as 'Doppler broadening' [39]. The Doppler broadening of the resonance capture cross sections ($\sigma_{c,res}$) is caused by the change in thermal motion of the fuel nuclei, which results in an increase in sterile absorptions within the resonance region (*i.e.* 1 eV < E < 300 eV) [37]. However, it is important to note that the intrinsic nuclear properties of the atomic nucleus are not affected, therefore the total neutron absorption probability – represented by the area under the curvature – is unaltered [37]. This aforementioned phenomenon can be described as a significant negative reactivity effect (α_D), which provides a safety feedback loop in the event of a reactivity-initiated accident (*i.e.* an accident wherein the fuel temperature continuously increases as a result of the exponentially increasing number of fissions) [40]. Figure 6 illustrates the Doppler broadening phenomenon in uranium-238 at the particular 6.67 eV resonance peak for fuel temperatures of 0 °C, 20 °C, and 1000 °C, respectively [40].

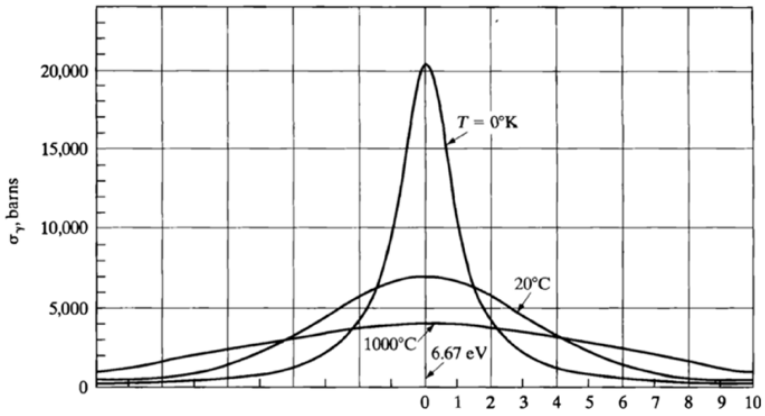

Figure 6: Nuclear Doppler effect in uranium-238 at the 6.67 eV resonance peak [40, p. 368]

The second prompt/immediate temperature reactivity effect is a consequence of an increase in T_{Mod}. There are two competing parameters of the neutron life cycle balance equation that are affected. The initial parameter is the thermal neutron utilisation factor – f – which will increase due to the reduction in the number of moderator atoms present, resulting in a relative increase in neutron absorptions within the fuel pins/rods [38]. The second parameter that is affected is the resonance escape probability (p). The aforementioned parameter will decrease as a consequence of the reduction in neutron moderation, and which will therefore increase the probability of neutrons being absorbed into the sterile resonance region [38]. These effects are relatively gradual, allowing sufficient time for a response to be made.

The steam void fraction reactivity effect represents an extreme case of the moderator temperature effect [41]. This prompt/immediate reactivity effect is a consequence of the presence of voids (*i.e.* bubbles and vapour regions) in the nuclear reactor core, which are caused by excessive moderator and/or coolant medium temperatures [41]. The mass density of bubbles and steam vapour is significantly less than that of the moderator and/or the coolant medium in their respective liquid state [40]. As a result, the average mass density of the liquid-vapour mixture is subject to alteration. It is therefore evident that a reduction in average mass density has a negative impact on the core reactivity, as all neutrons are able to traverse through the produced voids and bubbles without interacting, thereby increasing relative neutron leakage.

The final category of reactivity effects is characterised by changes in the isotopic composition of the reactor environment, which is a function of exploitation time (*i.e.* nuclear depletion). The long-term reactivity change is caused by the accumulation of poisonous FPs with a significantly large thermal cross section for neutron absorption ($\sigma_{a,th}$), which are also referred to as 'FP poisons' [40]. The most noteworthy neutron poison is xenon-135, which has a thermal absorption cross section of 2.65E+06 b [41]. Xenon-135 is formed both directly as a FP and as a decay daughter product of iodine-135 [40]. A second noteworthy neutron poison is samarium-149, which has a thermal absorption cross section of 56E+03 b [41]. The production path of samarium-149 differs from that of xenon-135, as it can only be formed as a decay daughter product of promethium-149, which is the decay daughter product of the direct FP neodymium-149 [40]. The presence of accumulated poisonous FPs will result in a reduction in the number of induced fissions in the fissile nuclei, thereby negatively affecting the chain reaction. Figure 7 illustrates the accumulation of poisonous FPs as a function of the irradiation time for various neutron fluxes [42].

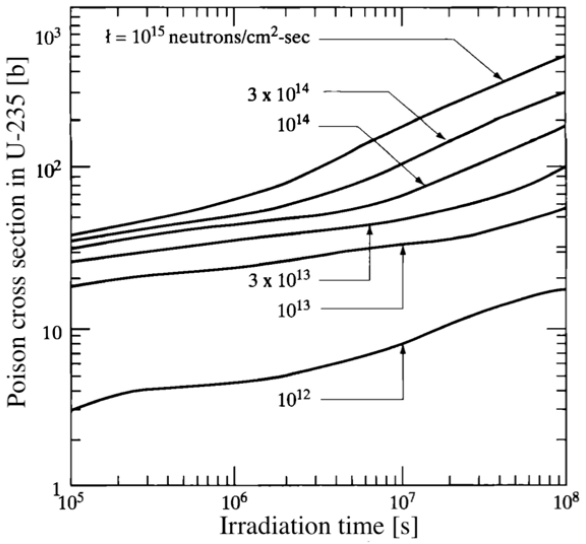

Figure 7: Accumulation of poisonous FPs as a function of the irradiation time [42, p. 404]

2.2.4 Nuclear Fuel Depletion

The irradiation of fresh nuclear fuel with neutrons in a nuclear fission reactor results in the consumption of the initially present atoms, consequently inducing a relative change in the isotopic composition of the fuel. These processes are collectively referred to as 'fuel depletion' or 'burnup' (BU) [43]. The BU can be expressed as the number of fissions that have occurred per initial heavy metal atom present (FIMA).

Alternatively, BU can be expressed in the more frequently utilised unit – in practice – of gigawatt-day per metric tonne of heavy metal (GWd/t_{HM}), which represents the thermal energy released up to a certain point in time per tonne of heavy metal initially present in the reactor core [43]. In Belgium, the maximum permissible BU for uranium dioxide (UO_2) fuels is 55.00 GWd/t_{HM} [43] Equation 8 presents the formula for calculating the BU of a fuel sample with a mass (m_0) over a time (t) with specific power (P) [32].

$$\mathrm{BU} = \frac{1}{m_0} * \int_0^t P(t)\,\mathrm{d}t \tag{8}$$

The degree of depletion will influence reactor-related parameters, such as the neutron flux spectrum – due to the induced relative changes in the nuclide inventory – and thereby implicitly the microscopic cross sections, as they are average values derived over specific energy intervals [44]. Moreover, the effective neutron multiplication factor will also be affected, which will consequently impact the reactor core's reactivity [44]. This impact on the core reactivity is due to the decrease in the number of fissile atomic nuclei over time (as they are consumed). However, while the fissile nuclei can also be accumulated via the transmutation process – *i.e.* fuel breeding – in the case of highly enriched uranium (HEU) nuclear fuels, this specific process of fissile nuclei production – *e.g.* fissile plutonium-239 via radiative neutron capture in fertile uranium-238 – is deemed insufficient to counter the core reactivity loss experienced due to the destruction of uranium-235 by induced thermal fissions [43]. Moreover, the extent of depletion will impact the parameters of SNF, including the decay heat, neutron and/or gamma emission rates, and radiotoxicity (*i.e.* biological impact) [32]. It is of significant importance to accurately quantify these radiation characteristics for subsequent operations, such as handling, transportation, and storage [32]. Figure 8 illustrates the evolution series of actinide transmutation post uranium-235 [45].

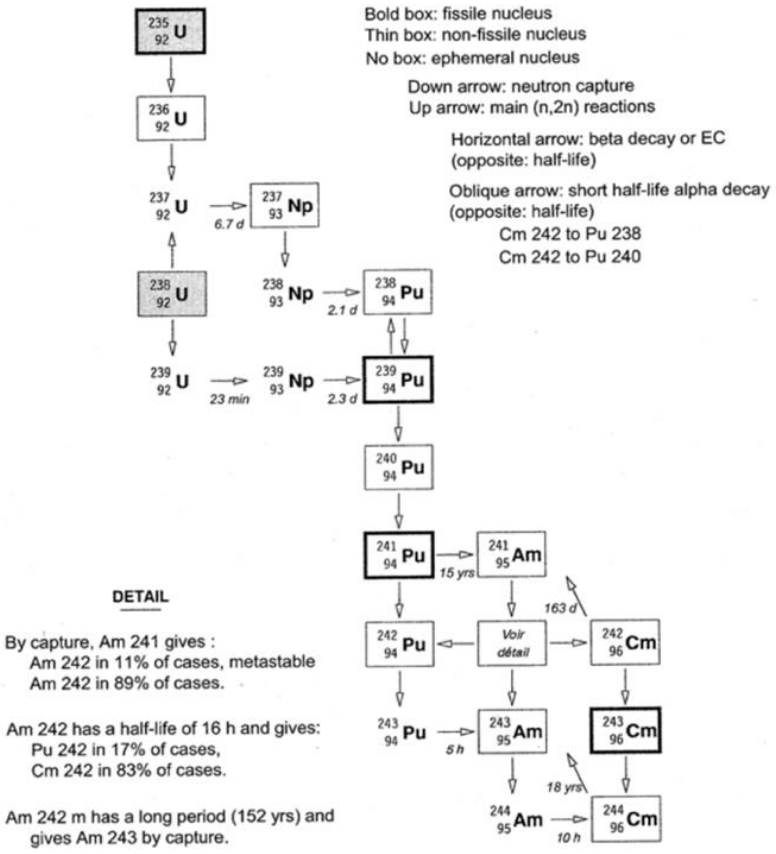

Figure 8: Actinide transmutation evolution series post uranium-235 [45, p. 317]

In 1910, Harry Bateman provided an analytical solution to the mathematical model – which had been formulated by Ernest Rutherford [46] – that can describe the time evolution of nuclide concentrations undergoing a serial or linear decay chain [47]. Consequently, the coupled set of homogeneous ordinary differential equations (ODEs) is referred to as the 'Bateman equations'. The coupled set of ODEs is implemented in nuclear depletion codes, which allow for the numerical prediction of the time evolution of complex nuclear transmutation and decay problems. The equations are dependent upon the utilisation of accurate nuclear data, including decay data, cross sections, branching ratios, fission yields, *etc*. [32]. Equation 9 presents a generic equation that describes the evolution of (radio)nuclide 'i' over time.

$$\frac{\mathrm{d}}{\mathrm{d}t}N_i(t) = \text{Production rate of } N_i - \text{Destruction rate of } N_i \tag{9}$$

Nuclear decay – also referred to as radioactive decay – is a physical phenomenon that occurs in unbalanced or unstable nuclides. This phenomenon concerns the spontaneous emission of energy in the form of ionising radiation [48]. The specific type of radionuclide determines the particles (*e.g.* alpha or beta particles) and/or gamma rays that can be emitted. Moreover, radionuclides are characterised by their radioactive half-life, which is denoted as $T_{1/2}$. This quantity represents the theoretical time required for a radionuclide to lose half of its current radioactive activity – which is equivalent to the number of disintegrations per second. Alternatively, radionuclides can be characterised by their radioactive decay constant, denoted as λ. The relationship between $T_{1/2}$ and λ is presented in Equation 10.

$$T_{1/2} = \ln(2)/\lambda \tag{10}$$

All radionuclides are subject to a number of atomic transformations – the majority of which involve a single decay process step – until they reach a stable non-radioactive ground state. In the event that radionuclides experience more than one decay process step, they are referred to as 'series radionuclides' [48]. Three distinct decay chains occur naturally: those of thorium-232, uranium-235, and uranium-238. Figure 9 illustrates the natural decay chain of uranium-238, proceeding to stable lead-206 [49].

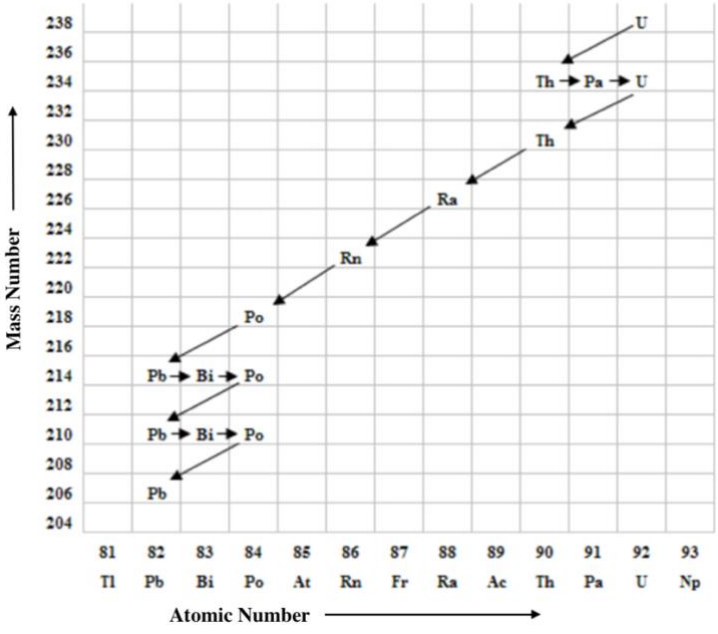

Figure 9: Natural decay chain of uranium-238 [49]

The production rate path of (radio)nuclide '*i*' – from Equation 9 – consists of a multitude of potential contribution terms. These contribution terms include the production of (radio)nuclide '*i*' through the incoming radioactive decay of radionuclide '*j*', the production via neutron-induced processes – *i.e.* radiative neutron capture, neutron-producing reactions (x, xn), neutron induced fission, *etc*. – as well as the production of FP nuclides [43]. The respective contributions are given by Equations 11, 12, and 13.

$$\frac{\mathrm{d}}{\mathrm{d}t}N_i(t) = \sum_{j \neq i}[b_{j \to i} * \lambda_{j \to i} * N_j(t)] \tag{11}$$

$$\frac{\mathrm{d}}{\mathrm{d}t}N_i(t) = \sum_{j \neq i}[N_j(t) * \int_0^{\infty} \sigma_{j \to i}(E) * \phi(E)\ \mathrm{d}E] \tag{12}$$

$$\frac{\mathrm{d}}{\mathrm{d}t}N_i(t) = \sum_{j \neq i}[N_j(t) * \int_0^{\infty} \gamma_{j \to i}(E) * \sigma_{f,j}(E) * \phi(E)\ \mathrm{d}E] \tag{13}$$

In Equation 11, $[b_{j \to i}]$ represents the branching ratio, which is defined as the fraction of radionuclide '*j*' that decays via a specific decay mode to form (radio)nuclide '*i*' [50]. The term $[\lambda_{j \to i}]$ represents the decay rate at which radionuclide '*j*' decays into (radio)nuclide '*i*'. In Equation 12, $[\sigma_{j \to i}]$ represents the microscopic cross section of radiative neutron capture in radionuclide '*j*', resulting in the transformation into (radio)nuclide '*i*', and $[\phi]$ represents the neutron flux. Lastly, in Equation 13, $[\gamma_{j \to i}]$ represents the cumulative fission product yield, while the term $[\sigma_{f,j}]$ represents the microscopic cross section of neutron-induced fission in radionuclide '*j*'. In all production contribution terms, the quantities $[N_i]$ and $[N_j]$ refer to the number of atoms present of the respective (radio)nuclides '*i*' and '*j*'. It is important to note, however, that the microscopic cross section is averaged over a single energy group, and that the *RR* is assumed to be constant over the course of a single integration time-step [43]. This significant assumption allows for less complex calculations. However, this simplified approach does not account for the spectral shift that is caused by boron depletion, FP poisons, and control rod movement [43].

At the opposite end of the generic equation – Equation 9 – is the rate of destruction of (radio)nuclide '*i*'. The destruction of the (radio)nuclide can be attributed to two distinct mechanisms. The first contributor is the potential radioactive decay of radionuclide '*i*', while the second contributor is due to the potential neutron-induced processes that could occur in (radio)nuclide '*i*' [43]. The aforementioned contributions are given by Equations 14 and 15, respectively [43].

$$\frac{\mathrm{d}}{\mathrm{d}t}N_i(t) = -\lambda_i * N_i \tag{14}$$

$$\frac{\mathrm{d}}{\mathrm{d}t}N_i(t) = -N_i(t) * \int_0^{\infty} \sigma_{a,i}(E) * \phi(E)\ \mathrm{d}E \tag{15}$$

The general equation for the production and destruction of (radio)nuclide '*i*' is given by Equation 16 [43]. It is important to note, however, that the production and destruction contribution terms are dependent upon the specific nuclide under consideration. Accordingly, certain production and/or destruction mechanisms may be inapplicable to the concerned (radio)nuclide '*i*'.

$$\frac{\mathrm{d}}{\mathrm{d}t}N_i(t) = \sum_{j \neq i}\left\{\lambda_{j \to i} + \int_0^{\infty} \sigma_{j \to i}(E) * \phi(E)\ \mathrm{d}E + \int_0^{\infty} \lambda_{j \to i} * \sigma_{f,j}(E) * \phi(E)\ \mathrm{d}E\right\} * N_j(t)$$

$$-\left\{\lambda_i + \int_0^{\infty} \sigma_{a,i}(E) * \phi(E)\ \mathrm{d}E\right\} * N_i(t) \tag{16}$$

Figure 10 illustrates the mass evolution of the main uranium and plutonium isotopes as a function of the fuel depletion in a PWR system [45]. It can be observed that the decreasing gradient in uranium-235's mass is approximately linear – with both axes being logarithmic – as a result of the thermal-neutron induced fissions. In contrast, the gradient in uranium-238's mass decreases marginally slow due to the relatively low proportion of fast/prompt induced fissions and the nuclear transmutation process to fissile plutonium-239. All other uranium and plutonium isotopes demonstrate growth at later stages, ultimately reaching an equilibrium concentration at which the rate of isotope production and destruction is equal.

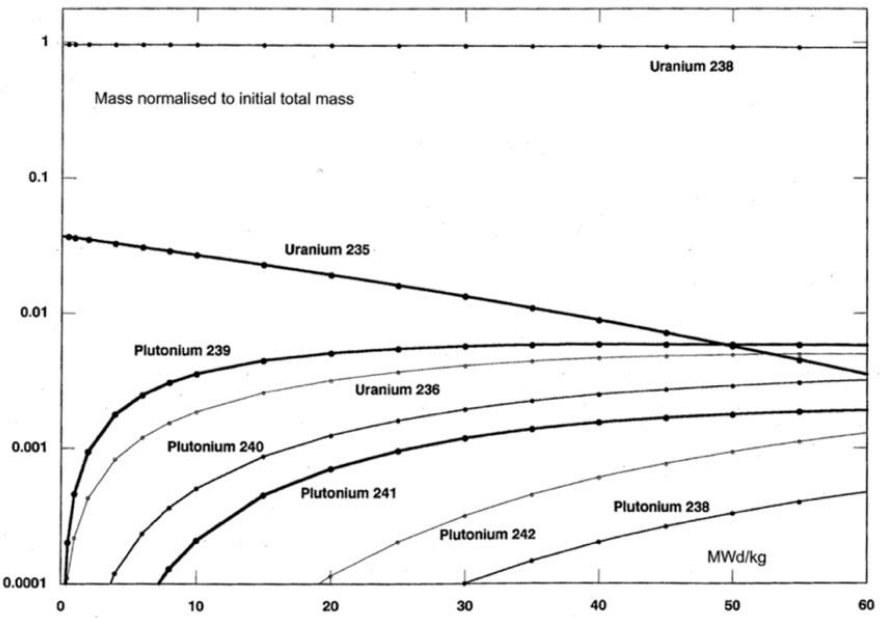

Figure 10: Evolution of main uranium and plutonium isotopes as a function of the fuel depletion [45, p. 324]

2.2.5 Experimental Burnup Monitor – Neodymium-148

The extent of nuclear depletion in irradiated SNF can be experimentally determined by measuring the accumulated isotopic concentration of neodymium-148, which is a non-radioactive refractory FP [51], [52]. The initial proposal for the measurement of the indicator nuclide was made in 1961 with the objective of determining whether a nuclear fuel had released an economically viable amount of energy [53]. It has since been demonstrated to be an effective BU monitor due to its favourable chemical and neutron-physical properties [52]. The isotope is stable – *i.e.* requiring no natural decay corrections – is non-volatile, has a relatively high fission yield – 1.675% in thermal fissions of uranium-235 [54] – and it is unlikely to be formed from adjacent mass chains [51]. The most widely accepted method for determining neodymium-148 concentrations is based on a chemical separation and mass spectrometric procedure, which was authored by the *American Society for Testing and Materials* (ASTM) [55]. The ASTM standard, "E 321-96", provides the definitive methodology for this procedure [56]. The isotope dilution mass spectrometry (IDMS) method yields results with a 0.9% uncertainty margin [57].

Accordingly, in this master's thesis each modelled sample will be normalised – following the completion of a preliminary SERPENT-2 simulation – by modifying the specific power history with the objective of reproducing the measured isotopic concentration of neodymium-148. Consequently, the calculated-to-experimental ratio should be approximately equal to one (*i.e.* "C/E*"* ≈ 1.000000) post-normalisation.

2.3 Reactivity Control Measures

2.3.1 Reactor Control Rods

Reactor control elements/rods (CRs) are a mechanical reactivity control mechanism composed of solid-state materials with high thermal neutron absorption capabilities, whose axial motions provide direct/immediate regulation over the neutron population [58]. The most frequently utilised absorbing materials are currently boron – in the form of ceramic boron carbide (B_4C) – the complex ternary alloy, silver-indium-cadmium (AIC) – with a relative ratio of 80-15-5 wt% – or hafnium [59]. The objective of employing CRs is to alter the relative fraction of thermal neutrons absorbed into the fissile fuel nuclei, thereby modifying the thermal neutron utilisation factor (f) – and consequently k_{eff} and the core reactivity [58]. In high-power reactors, which operate at high power densities and high temperatures, it is imperative to maintain a spatially uniform distribution of the thermal neutron flux throughout the reactor core [60]. Therefore, it is evident that high-power reactors contain a considerable number of control rod guide tubes (*e.g.* 24 CRs per FA, with the PWR nuclear fission reactor core totalling 120 to 200 FAs). The reactivity control mechanism can be actively regulated by human reactor operators – specifically an electrically interconnected group of cluster control rods, referred to as a 'control bank' – when an increase or decrease in the reactor power output level (P) is desired, or to maintain strict criticality by compensating for changes in the characteristics of the reactor that occur over its operational lifetime. CRs are categorised according to their compensating capacity – *i.e.* control rod worth – defined as the magnitude of change in k_{eff} that can be compensated for by the particular control rod [60]. The rods with a relatively large rod worth are designated 'control rods'. Rods with a lower rod worth are designated 'fine adjustment rods' and are consequently deployed for smaller desired reactivity increases or decreases (*i.e.* fine-tuning). The rod worth is dependent upon the spatial positioning of the rod in relation to the centre of the reactor core – at the periphery of the reactor core, the rod is considered to have the lowest worth, whereas near the centre, it is assigned the highest worth [58]. Moreover, the rod worth can be simulated through the utilisation of a three-dimensional in-core flux mapping monitoring system [61]. Furthermore, a final category of CRs is designed for safety purposes and is operated exclusively in the event of an emergency scram reactor shutdown. It is important to note, that when multiple CRs or control banks are deployed simultaneously, their collective influence/disturbance on the thermal neutron flux profile is not merely the summation of their individual contributions/rod worths – this phenomenon is referred to as the 'nuclear shadowing effect' [58], [62]. Figure 11 illustrates the suppression of the axial thermal neutron flux distribution as a function of the control rod insertion height [63].

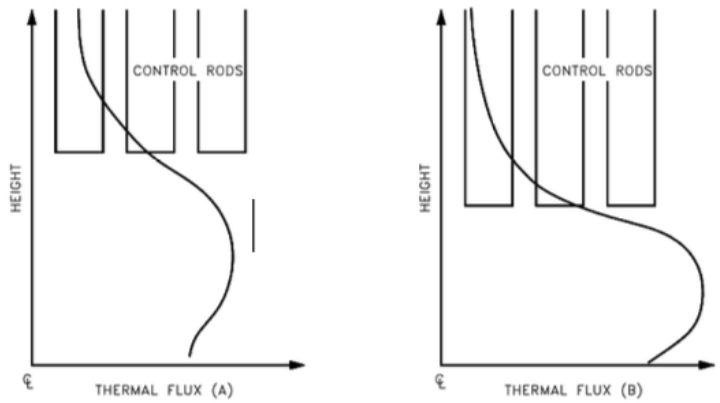

Figure 11: Thermal neutron flux distribution as a function of the control rod insertion height [63, p. 26]

2.3.2 Boric Acid – H_3BO_3

Boric acid – chemical formula: H_3BO_3 – is a solid-state soluble indirect/long-term reactivity control mechanism that is routinely introduced into the primary coolant system and/or moderator medium of a PWR – media: light water/light water – to provide uniform negative reactivity over the course of the nuclear reactor's operational fuel cycle [5]. The introduction of chemical shim is a consequence of the fact that CRs should not be utilised exhaustively to offset the excess core reactivity – which attains its maximum value at the reactor's BOC, because nuclear fuel depletion and the accumulation of poisonous FPs has not yet occurred – as inserting them deeper into the reactor's core would result in an increasingly non-uniform thermal neutron flux and power distribution [5]. Moreover, the deployment of a CR in this manner would result in a reduction in the effective control rod lifetime. It is therefore necessary to introduce one part of natural boron – or alternatively, enriched boron-10, which has a thermal cross section for neutron absorption of 3.85E+03 b [65] – per million parts of light water (ppm, which is equal to 1.0E-06) into the primary coolant system and/or moderator medium for approximately every ten pcm of excess core reactivity, in addition to the presence of the mechanical CRs [58]. As a result, the uniform introduction of chemical shim allows for the maintenance of strict criticality during xenon transients, as well as the compensation for nuclear fuel depletion and the accumulation of poisonous FPs [60], [64]. At the reactor's End-of-Cycle (EOC), the concentration of boric acid is approximately zero ppm, and the nuclear system requires boron refuelling [66]. The regulation of boric acid concentration is performed remotely and automatically by the reactor's computational "Chemical and Volume Control System" (CVCS), which introduces non-borated light water – H_2O – in proportion to the loss of excess core reactivity [61]. It is important to note, however, that the utilisation of boric acid is limited – 2,000 ppm – due to the fact that higher concentrations may have adverse effects, such as a positive MTC [67].

2.3.3 Gadolinium(III) Oxide – Gd_2O_3

Gadolinium(III) oxide – *i.e.* gadolinia, chemical formula: Gd_2O_3 – is a long-term burnable neutron absorber/poison that is routinely incorporated into the nuclear fuel composition of commercial LWRs – including both nuclear fuel types UO_2 and MOX – in order to prevent potential power mismatches between fresh unirradiated FAs and partially irradiated FAs [4], [68]. The particular BA was initially introduced in the Dresden Reactor No. 2 Nuclear Power Station – located in Morris, IL, USA – and implemented by *General Electric* in 1967 [4]. Of particular interest are the isotopes gadolinium-155 and gadolinium-157, which have the highest thermal neutron absorption cross sections of any naturally occurring element, with 60,700 b and 254,000 b, respectively [69]. Subsequent to the neutron absorption reaction, the aforementioned nuclides are transformed into nuclides with a comparatively low thermal neutron absorption cross section (gadolinium-156 and gadolinium-158, respectively). The incorporation of natural gadolinia into nuclear fuels is justified by the observation that excess core reactivity in the most recent FA designs is significantly greater than that which can be compensated for by soluble boric acid and CRs – when maintaining sufficient reactor safety margins – thereby necessitating its utilisation.

The depletion of the fissile fuel nuclei is accompanied by a corresponding depletion of the gadolinia. It is optimal that the two compounds deplete at an equivalent rate, thereby maintaining a constant core reactivity over time [5]. However, this is typically not feasible, as local spectral effects will affect the relative depletions. BAs may be incorporated into the nuclear fuel pellets as a homogeneous mixture or alternatively, as a coating around them. Figure 12 illustrates the methods of BA incorporation [5].

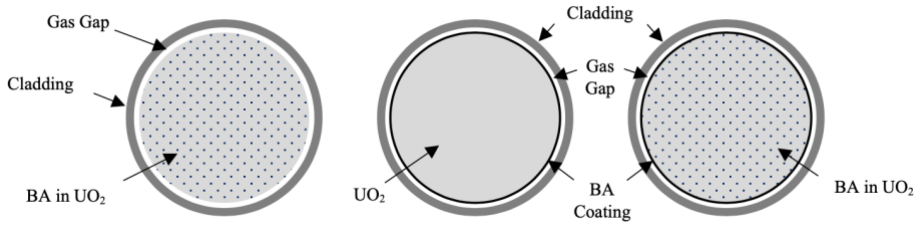

Figure 12: Three common nuclear fuel-BA designs for commercial nuclear fission reactors [5, p. 19]

The conventional PWR nuclear fuel management scheme – which does not incorporate BFRs – involves the loading of fresh, unirradiated FAs at the reactor core periphery and subsequently transferring them towards the reactor core centre after the initial cycle (*i.e.* 'out-in' management) [4]. However, at present, an alternative nuclear fuel management scheme – which incorporates BFRs – is in use. This scheme entails the loading of fresh FAs at the reactor core centre, which are subsequently relocated to the reactor core periphery for their final cycle (*i.e.* 'in-out' management, or 'low leakage loading pattern') [4]. While BAs do present certain challenges in terms of FA designs and reactor core management, they do facilitate highly uniform fuel depletion and power distributions [68]. Moreover, the incorporation of gadolinia into the nuclear fuel composition has the beneficial effect of reducing the number of control rods and the necessary boric acid concentration required for reactor control. In addition, a reduction in boric acid concentration guarantees that the MTC will remain negative (must). Figure 13 illustrates the evolution in boric acid concentration when including or excluding BAs as a function of the time [68].

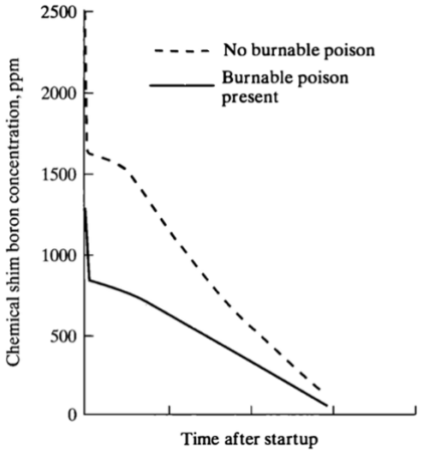

Figure 13: Boric acid concentration when including or excluding BAs as a function of the time [68, p. 396]

The phenomenon of spatial self-shielding has been observed in neutron absorber-containing fuel pellets, wherein the outer geometric layer of the absorber acts as a neutron shield for the inner geometric layer, thereby limiting its relative exposure to the neutron flux [70]. In order to quantify this effect, a spatial self-shielding factor, denoted as *g*, is introduced. This quantity is defined as the ratio of the neutron flux within the absorber region to the neutron flux that would be observed in the absence of the absorber [5]. Therefore, a highly effective neutron absorber will result in a localised depression in the neutron flux within the absorber (*i.e.* g < 1.00) [5]. The spatial self-shielding factor is presented in Equation 17.

$$g(\vec{r},E) = \frac{\phi_{BA}(\vec{r},E)}{\phi_{nBA}(E)} \tag{17}$$

2.4 Simulation Tools and Resources

2.4.1 SERPENT-2 Nuclear Depletion Code

The evolution in the nuclide inventories of the modelled PWR-UO_2-Gd_2O_3 SNF samples is simulated and calculated through the utilisation of the SERPENT-2 – version 2.2.1– three-dimensional continuous-energy Monte Carlo nuclear depletion code [71]. The nuclear depletion calculation code was developed at the Technical Research Centre of Finland (VTT) – since 2004, but under the preceding title of 'Probabilistic Scattering Game' – with its primary objective of performing complex three-dimensional neutron, photon, and coupled neutron-photon simulations within a lattice physics context [72]. Therefore, potential applications include the generation of homogenised multi-group constants for deterministic reactor calculations, assembly-level reactor physics calculations – including both thermal and fast-spectrum capabilities – and the validation of deterministic lattice transport codes [72]. However, the scope of applicability has been significantly expanded over time [72]. To illustrate, by October 2008, the source code had been entirely rewritten and significant effort had been invested in incorporating new functionalities, including self-contained, integrated depletion calculation subroutines. In addition, the working title was also modified to the current designated name of "SERPENT" (*i.e.* SERPENT-1) [71].

In order to simulate the depletion of nuclear fuels, it is necessary to calculate the isotopic one-group transmutation cross sections for each burnable material at each defined depletion time-step. This is accomplished by collapsing the continuous-energy cross sections with flux spectra that have been collected separately for each burnable material (*i.e.* the 'spectrum collapse' method) [71], [72], [73]. Consequently, the data is automatically combined with the present nuclei's radioactive decay constants, energy-dependent fission yields, and isomeric branching ratios for neutron reactions – which are read in from standard 'ENDF' format libraries – thereby obviating the need for additional user input [71], [72]. The self-contained, built-in depletion calculation subroutines – *i.e.* independent of external nuclear depletion solvers or pre-generated datasets – employ, by default, an advanced matrix exponential algorithm based on the 'Chebyshev Rational Approximation Method' (CRAM) [74] to solve the 'Bateman depletion equations' [72]. The method has been demonstrated to be both accurate and efficient in the calculation of depletion problems containing a significant number of (radio)nuclides – typically between 1,200 and 1,600 nuclear concentrations – and various depletion zones, without the utilisation of approximations [75]. Furthermore, SERPENT-2 provides a variety of advanced time integration techniques for the iterations between the neutronics and the depletion solutions. These include the 'Euler' and 'predictor-corrector' methods with linear interpolation, as well as higher-order methods based on combinations of linear and quadratic interpolation, together with sub-step solutions [76], [77].

Lastly, in order to achieve an acceptable overall running time on the depletion calculation problems – given the excessive computational cost of the Monte Carlo method – it may be necessary to utilise a computer cluster (*i.e.* parallel computing). Therefore, SERPENT-2 features a hybrid Message Passing Interface (MPI)/OpenMP methodology, which is a shared-memory parallelisation technique, operating at both the central processing unit (CPU) core and the cluster node levels [71], [72]. The implementation of parallelisation entails the partitioning of the neutron population between parallel tasks, with the results subsequently combined after the neutron transport cycle is completed. Moreover, the SERPENT-2 code is available free of charge for non-commercial research and educational purposes and is publicly distributed by two data centres: the OECD/NEA Data Bank and the Radiation Safety Information Computational Centre (RSICC) – for distribution in the United States [72].

2.4.2 Spent Fuel Isotopic Composition (SFCOMPO-2.0) Database

In order to evaluate the predictive capabilities of nuclear depletion calculation codes, it is essential to have access to accurately measured experimental nuclide concentrations – with estimated uncertainties – and accurate design specifications and operating data for the nuclear reactor being modelled [78]. In response to this necessity, a second international effort was initiated, namely the "Spent Fuel Isotopic Composition 2.0" (SFCOMPO-2.0) database. The "SFCOMPO-2.0" database is a well-documented, freely accessible, open-source repository of experimental assay data on SNF – released online in June 2017 as a downloadable Java application – which was developed by the Organisation for Economic Co-operation and Development Nuclear Energy Agency (OECD/NEA) in close collaboration with Oak Ridge National Laboratory (ORNL), and under the purview of the Expert Group on Assay Data of Spent Nuclear Fuel (EGADSNF), a multidisciplinary panel of international experts on RCA, nuclear waste management, reactor physics, and criticality safety, which develops guidelines for the review and evaluation of experiments and is part of the NEA Working Party on Nuclear Criticality Safety [79], [80].

The reviewed experimental assay datasets comprise accurate nuclide concentration measurements – derived from (non)-destructive RCA – design information regarding the nuclear fission reactor, FA, and FR from which the sample under consideration was taken, as well as other relevant information on reactor operational histories (e.g. boric acid concentration, sample-specific irradiation history, *etc*.) [78]. The "SFCOMPO-2.0" database includes isotopic assay data from 44 distinct nuclear fission reactors utilising eight different international technologies, namely the "Advanced Gas-cooled Reactor" (AGR), BWR, "Canadian Deuterium Uranium Reactor" (CANDU), "Magnesium Alloy Graphite-moderated Gas-cooled Uranium Oxide Reactor" (MAGNOX), PWR, "Reaktor Bolshoy Moshchnosty Kanalny" (RBMK), and "Vodo-Vodyanoi Energetichesky Reaktor" which has two possible concepts depending on the electric power, represented by "VVER-440" and "VVER-1000". In total, the aforementioned 44 reactors encompass 750 samples of SNF [78]. Furthermore, the database is structured in a vertical, hierarchical format comprising four levels of descriptive detail, as follows: (1) Reactor identifier, (2) Fuel assembly identifier, (3) Fuel rod identifier, and (4) Fuel sample identifier [78]. Figure 14 provides an illustration of the hierarchical system of descriptive detail within the "SFCOMPO-2.0" database [81].

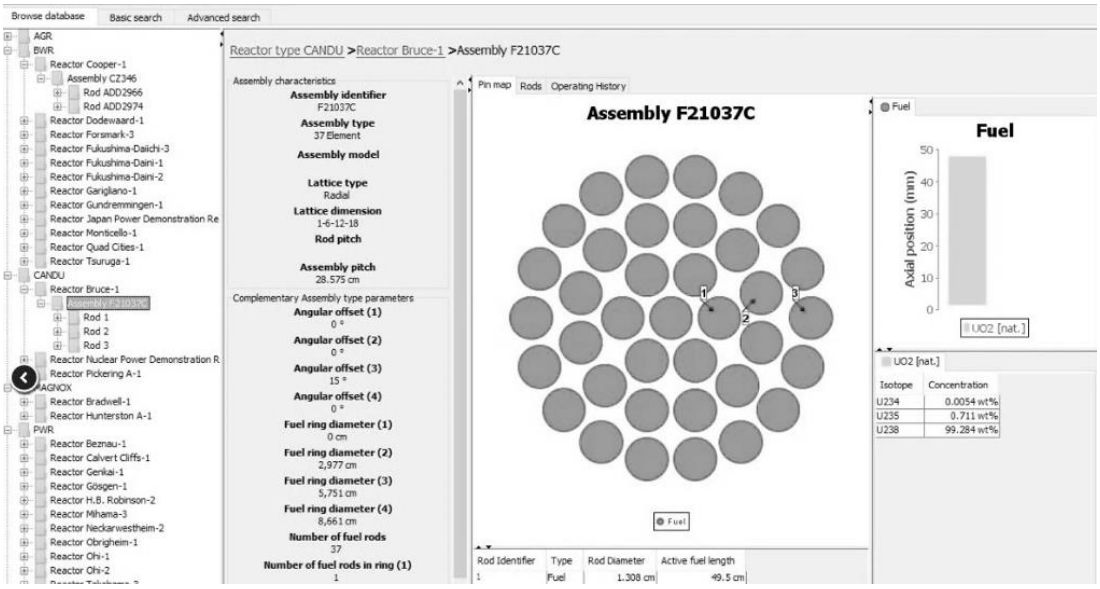

Figure 14: Hierarchical system of descriptive detail within the "SFCOMPO-2.0" database [81]

At the aforementioned initial (1) level of descriptive detail, designated “Reactor identifier”, the general and complementary characteristics of the selected nuclear fission reactor are displayed. These characteristics include the official nuclear reactor name and that of the operating company, the coolant and moderator media, the nominal power – both thermal and electric – the active physical dimensions, the country in which it is located, and the design model (*i.e.* manufacturer and the number of ‘loops’). At the subsequent (2) level of the hierarchical structure, designated “Fuel assembly identifier”, the corresponding FA design characteristics are provided. These characteristics include the lattice type, lattice dimensions, number of rods of the various types – *i.e.* FRs, BFRs, guide tubes – as well as pitches (for both the rods and the FA). Moreover, a visual assembly pin map is provided, which depicts the spatial positioning of the rods within the reactor core. At the third (3) level of descriptive detail, designated “Fuel rod identifier”, the geometry – specifically, the inner and outer diameter of the fuel pellets and the active and total length of the rods – and other material specifications, such as the isotopic compositions and respective enrichments, are provided. Furthermore, the axial zoning/positioning of the selected SNF sample is indicated on a cross-sectional slice of the reactor core. At the final (4) level of the hierarchical structure, designated “Sample identifier”, the SNF measurement data are reported. This includes the measured (radio)nuclides, concentrations, and associated reported uncertainties; the measuring method, laboratory, and date of measurement; experiment-based estimates of fuel depletion; and cycle-dependent operating information (*e.g.* boric acid concentration, and sample-specific power).

In addition, the “SFCOMPO-2.0” database provides open-source bibliographical references for all displayed information, including original documentation such as experimental laboratory reports, journal articles, and evaluation reports. This allows for complete traceability of all displayed data [82].

2.4.3 ENDF/B-VII.1 Evaluated Nuclear Data Library

In the field of advanced nuclear science – nuclear theory, modelling, simulation, and experimentation – and technology applications, one of the most utilised low-energy nuclear data library in particle transport codes is the “Evaluated Nuclear Data File Version B”, designated “ENDF/B.VII.1” [83]. This evaluated nuclear data library represents the second to last iteration of the “ENDF” library – with the previous iteration being “ENDF/B.VII.0” [84] and released in 2006. It is a cooperative repository of nuclear data and interactional information that is made available by the U.S. Cross Section Evaluation Working Group (CSWEG) since 2011. However, as of 2018, a new iteration of the ENDF library has become available, namely “ENDF/B.VIII.0”. Nevertheless, the older iteration – ENDF/B.VII.1 – is regarded as a reference library by the isotopic depletion calculation community. Moreover, to ensure the successful development of the nuclear data library, the CSWEG has been engaged in close collaboration with parallel evaluation projects in Europe, Japan, and South Korea (JEFF and JENDL libraries). A comparison of the integral validation testing results between the two latest iterations of “ENDF” revealed that the latest iteration demonstrated comparable – *i.e.* preserved – performance in the area of nuclear criticality. The results were found to be generally adequate across a wide range of “Monte Carlo N-Particle Transport Code” simulations of criticality benchmarks, with enhanced performance resulting from the incorporation of new structural material evaluations [83]. The ”ENDF/B-VII.1” library is comprised of 14 sub-libraries – ordered according to their identification number – including those dedicated to the following nuclear processes/phenomena: ‘Photonuclear’, ‘Photo-atomic‘, ‘Radioactive decay’, ‘Spontaneous fission yields’, ‘Atomic relaxation’, ‘Neutron’, ‘Neutron fission yields’, ‘Thermal scattering’, ‘Standards’, ‘Electro-atomic’, ‘Proton’, ‘Deuteron’, ‘Triton’, and ‘^{3}He’ [83].

3 Sample Descriptions

3.1 Takahama Reactor No. 3 Nuclear Power Station

3.1.1 General Data

The Kansai Electric Power Co. (Ltd.) Takahama Reactor No. 3 Nuclear Power Station is a ‘Mitsubishi Heavy Industries M 3-loop’ modelled PWR, located in the town of Takahama, Fukui Prefecture, Japan (geographical coordinates expressed in ‘DMS’: 35° 31’ 19.17” N; 135° 30’ 14.24” E) [85], [86]. The nuclear power station began commercial operations on 17 January 1985, with a thermal and electric power capacity of 2,660 MW and 870 MW, respectively [86]. Therefore, the nuclear power station will have reached Japan’s nominal operating period of 40 years in January 2025. However, the Japanese Nuclear Regulation Authority has granted regulatory approval for an additional twenty-year extension.

Table 1 presents the main core characteristics of the Takahama Reactor No. 3 Nuclear Power Station, from which the assembly designated “NT3G23” and consequently the BFR “SF96” – consisting of five SNF samples that have been subjected to destructive RCA, identified as “SF96-1” through “SF96-5” – data were obtained. Table 2 presents the main assembly characteristics of the “NT3G23” assembly [85].

Table 1: Main core characteristics of the Takahama Reactor No. 3 Nuclear Power Station [85, p. 361]

Reactor Core Data	
Number of Loops	3
Coolant Medium	Light Water
Moderator Medium	Light Water
Thermal Power [MW]	2,660
Electric Power [MW]	870
Active Core Height [m]	3.66
Active Core Diameter [m]	3.04
Uranium Weight [metric tonne]	~ 72
Coolant Inlet Temperature [°C]	284
Coolant Outlet Temperature [°C]	321
Coolant Pressure [MPa]	16.0

Table 2: Main assembly characteristics of the "NT3G23" assembly [85, p. 361]

Fuel Assembly Data	
Assembly Type	17 x 17
Number of Assemblies	157
Uranium Weight [kg]	~ 460
Rod Pitch [mm]	12.6
Assembly Pitch [mm]	214.0 ±0.5%
Number of Fuel Rods	264
Number of Guide Rods	24 + 1
Total Rod Length [mm]	4,035.5
Active Rod Length [mm]	3,648.0
Cladding Material	Zircaloy-4

Table 3 presents the initial isotopic compositions of the regular PWR-UO_2 fuel rods – *e.g.* "SF95" – and the gadolinia-containing PWR-UO_2-Gd_2O_3 fuel rods (*e.g.* "SF96") [85]. The mass density is reported in the official documentation to be approximately 95 percent (*i.e.* ~ 95%) of the theoretical mass density (TD) of UO_2 – *i.e.* 10.970 g/cm^3 at a temperature of 273 Kelvin (K) [87] – which equates to a numerical value of 10.412 g/cm^3. It is important to note that in the initial nuclide inventory of the PWR-UO_2-Gd_2O_3 fuel rods, the gadolinium content is characterised as exhibiting a 'natural' distribution. Therefore, the isotopic abundances of gadolinium are obtained through the utilisation of evaluated nuclear structure data files [88]. It is also of interest to note that the uranium isotopes present in the PWR-UO_2-Gd_2O_3 fuel rods do not summate to 100.00 wt% (*i.e.* 99.90 wt%). A review of the official documentation [85], [89], and [90] did not yield any clarifying insights or comments regarding this noteworthy occurrence.

Table 3: Initial isotopic compositions of the "SF95" and "SF96" fuel rods [85, p. 377]

Fuel Rod Data	**SF95 (UO_2)**	**SF96 (UO_2-Gd_2O_3)**
Mass Density [g/cm^3]	~ 95% TD	~ 95% TD
U-234 [wt%]	0.04	0.02
U-235 [wt%]	4.11	2.63
U-238 [wt%]	95.85	97.25
Gd (natural) [wt%]	N.A.	6.00
Gd-152 [wt%]	N.A.	0.20
Gd-154 [wt%]	N.A.	2.18
Gd-155 [wt%]	N.A.	14.80
Gd-156 [wt%]	N.A.	20.47
Gd-157 [wt%]	N.A.	15.65
Gd-158 [wt%]	N.A.	24.84
Gd-160 [wt%]	N.A.	21.86

Figure 15 provides an illustration of the fuel rod configuration present in the Takahama Reactor No. 3 "NT3G23" assembly [89]. The 17 x 17 square lattice configuration is compliant with the one-eighth symmetry in regard to the spatial positioning of the 250 PWR-UO_2 FRs, 14 PWR-UO_2-Gd_2O_3 BFRs, 24 control rod guide tubes, and central instrumentation thimble. The displayed arrows indicate the assembly positions of the rods that were subjected to destructive RCA (*i.e.* holding the PWR-SNF samples). The configuration is indexed in an alphabetical order, from left to right and top to bottom, corresponding to the letters A to Q. Therefore, "SF95" and "SF96" are located at positions 'A-Q' and 'C-M', respectively.

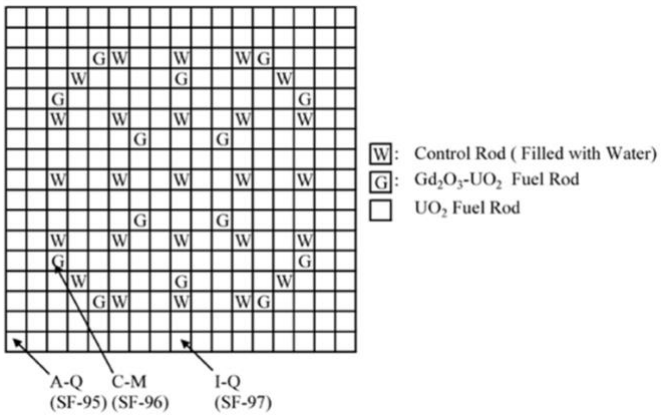

Figure 15: Fuel rod configuration in the Takahama Reactor No. 3 "NT3G23" assembly [89, p. 114]

3.1.2 Code Accuracy Evaluation

In order to evaluate the isotopic accuracy of the calculated nuclide inventory results simulated by SERPENT-2, the sample-specific calculated concentrations are compared against the experimental data (*i.e.* 'C/E', wherein the letter "C" represents the calculated value, and the letter "E" the experimental value, with numerical values of both quantities expressed in grams of the nuclide under consideration per gram of initial fuel (*i.e.* g/g_{fuel})). However, an alternative representation is utilised in the chapter entitled "Results by SERPENT-2". In particular, the 'percentage deviation' format, which can be calculated utilising Equation 18. Moreover, the sample-average 'C/E' and the standard deviation (SD) – which quantifies the expected variation of a given statistical population relative to its sample-average – are additionally calculated. Equation 19 presents the statistical formula for calculating the SD, in which the variable "n" represents the number of independent data points for the nuclide under consideration.

$$\text{Percentage deviation} = \left(\frac{C}{E} - 1\right) * 100\% \tag{18}$$

$$SD = \sqrt{\frac{1}{n-1} * \sum_{i=1}^{n}\left(\left(\frac{C}{E}\right)_i - \left(\frac{C}{E}\right)_{average}\right)^2} \tag{19}$$

3.1.3 Cell Configuration – Burnable Fuel Rod "SF96"

A single two-dimensional lattice geometry cell – *i.e.* an infinite 2D square lattice – is defined for the SERPENT-2 simulations. The geometrical description is based on a 'constructive solid geometry' methodology, in which homogeneous material cells are defined utilising a combination of elementary and derived surface types [91]. The adopted model comprises three nested annular (*R*) material regions (Table 4). The primary annular region – *i.e.* $R \leq 0.4025$ cm – represents either a UO_2 or UO_2-Gd_2O_3 fuel pellet (depending on the fuel rod being modelled). Bounding the "Fuel Pellet" region and the "Inner Cladding" region is a void – *i.e.* $0.4025 \text{ cm} < R \leq 0.4110$ cm – which in practice is filled with a helium gas mixture. However, [92] suggests that the assumption of a void is deemed sufficient. Subsequently, the specific cladding 'Zircaloy-4' (Zry-4) [93] is delineated by its inner and outer radii, represented by "Inner Cladding" and "Outer Cladding", respectively (*i.e.* $0.4110 \text{ cm} < R \leq 0.4750$ cm). To complete the pin cell structure, the annular region of the coolant medium is defined (*i.e.* $0.4750 \text{ cm} < R$). It is important to note, however, that this outermost region does not require explicit boundary definitions, as it is by default radially infinite [94] (detailed in the SERPENT-2 input code in §Appendix A). Moreover, the specular reflective boundary condition is assumed at the geometry's outer boundary surface – *i.e.* a square boundary surface around the PWR assembly – which results in an axially infinite nuclear system.

To ensure the compositional accuracy of the UO_2-Gd_2O_3 fuel pellets during the depletion simulations, it is necessary to implement a multitude of radial material subdivisions. The independent depletion zones guarantee a better approximation of absorber burn-out. Accordingly, ten subdivisions have been defined.

Table 4: Annular cell geometry of the "SF95" and "SF96" fuel rods [85, p. 363]

Region	Radius [cm]
Fuel Pellet	~ 0.4025
Inner Cladding	~ 0.4110
Outer Cladding	~ 0.4750

3.1.4 Temperature and Axial Cutting Positioning

Throughout the entirety of the SERPENT-2 simulation, it is assumed that the temperatures within the PWR-UO_2 and PWR-UO_2-Gd_2O_3 fuel pellets remain constant at 900.0 K, whereas the Zry-4 cladding region is held constant at 600.0 K [85]. The aforementioned temperatures are considered to be reasonable assumptions based on the analyses of conventional UO_2 fuel pellet temperature distributions observed in commercial LWRs [95]. With regard to the reported temperatures of the coolant region, a calculation is performed through the utilisation of Equation 20, wherein it is assumed that an incremental increase in the coolant temperature is directly proportional to the integrated power from the lower boundary of the active PWR-UO_2 or PWR-UO_2-Gd_2O_3 fuel stack to each sample cutting position in the axial direction, and assuming the additional hypothesis that the axial power distribution is cosine-shaped [96]. The thermodynamic equation is comprised of a series of in-core reactor parameters, including: the reactor coolant inlet temperature (T_{inlet}); the active rod length of the PWR-UO_2 or PWR-UO_2-Gd_2O_3 fuel stack (H); the temperature gradient between reactor coolant inlet and outlet (ΔT); and the cutting position of the sample in the axial direction (z), which is measured relatively in reference to the lower boundary of the active PWR-UO_2 or PWR-UO_2-Gd_2O_3 fuel stack [85].

$$T(z) = T_{inlet} + \frac{\pi * \Delta T}{2 * H} * \int_0^z \cos\left(\frac{\pi}{2 * H} * z\right) \mathrm{dz} \tag{20}$$

In conjunction with the aforementioned formula for determining the temperatures of the coolant region, the data related to the axial cutting positions of the PWR-SNF samples – detailed in Table 5 – are integrated in order to obtain sample-specific coolant temperatures. Table 6 presents an overview of the reported sample-specific coolant temperatures [85]. Moreover, as the temperature of the coolant region is sample-specific, the intrinsic thermal scattering properties of the coolant medium likewise exhibit sample-specific variations, contingent upon the PWR-SNF sample under consideration. It is therefore necessary – in the SERPENT-2 input code – to interpolate between the implemented datasets of thermal scattering libraries associated with hydrogen in light water (based on ENDF/B.VII.1). Furthermore, the mass density of the coolant must also be interpolated on the basis of its temperature and pressure [97].

Table 5: Axial cutting positions of the "SF96" samples [85, p. 379]

Sample ID	From Bottom of Active Stack [mm]	From Top [mm]
SF96-1	3,631	176
SF96-2	3,471	336
SF96-3	2,951	856
SF96-4	1,671	2,136
SF96-5	271	3,536

Table 6: Coolant temperatures of the "SF96" samples [85, p. 149]

Sample ID	Coolant Temperature [K]
SF96-1	593.05
SF96-2	592.82
SF96-3	589.62
SF96-4	570.82
SF96-5	554.28

3.1.5 Specific Power History

The “SF96” SNF samples were irradiated in two distinct cycles, designated “Cycle 5” and “Cycle 6”, respectively. The date-related details of these operational cycles are outlined in Table 7 [85]. Moreover, Table 8 presents the irradiation histories as disclosed to JAERI by the Kansai Electric Power Co. [85].

Table 7: Operating history of the Takahama Reactor No. 3 Nuclear Power Station [85, p. 378]

Start Date [dd/mm/yyyy]	**Stop Date [dd/mm/yyyy]**	**Days [d]**	**Status**
26/01/1990	15/02/1991	385	Burnup
15/02/1991	14/05/1991	88	Cooling
14/05/1991	19/06/1992	402	Burnup

Table 8: Irradiation histories of the “SF96” samples [85, p. 382]

Days [d]	**Power [MW/t_{HM}]**				
	SF96-1	SF96-2	SF96-3	SF96-4	SF96-5
12	0.99	2.09	3.59	3.68	3.08
8	3.97	8.37	14.37	14.73	12.32
27	4.21	8.88	15.24	15.62	13.07
35	4.47	9.44	16.19	16.60	13.89
28	5.04	10.64	18.25	18.70	15.65
21	5.64	11.90	20.42	20.93	17.52
35	6.39	13.48	23.13	23.71	19.84
35	7.97	16.82	28.85	29.57	24.75
28	8.90	18.78	32.21	33.02	27.63
27	9.84	20.76	35.61	36.50	30.55
49	10.71	22.59	38.75	39.72	33.24
15	11.42	24.10	41.34	42.37	35.46
37	12.13	25.59	43.90	44.99	37.66
19	12.34	26.04	44.68	45.79	38.32
9	12.61	26.59	45.62	46.76	39.14
88	0.00	0.00	0.00	0.00	0.00
10	5.61	11.84	20.32	20.83	17.43
11	11.30	23.84	40.90	41.92	35.08
20	11.45	24.16	41.45	42.48	35.55
23	11.57	24.41	41.88	42.93	35.93
28	11.64	24.56	42.13	43.18	36.14
28	11.71	24.70	42.37	43.43	36.35
28	11.78	24.86	42.64	43.71	36.58
35	11.86	25.01	42.91	43.99	36.81
28	11.93	25.16	43.16	44.24	37.02
34	11.99	25.29	43.38	44.46	37.21
43	12.06	25.44	43.65	44.74	37.44
28	12.06	25.44	43.65	44.74	37.44
28	12.04	25.40	43.57	44.66	37.48
35	12.07	25.45	43.67	44.76	37.46
15	12.08	25.48	43.72	44.81	37.50
8	12.09	25.50	43.74	44.83	37.52

3.1.6 Boric Acid Concentration History

Tables 9 and 10 present the date-specific histories of boric acid concentration for the two operational cycles under consideration, designated “Cycle 5” and “Cycle 6”, respectively. The aforementioned operational data were disclosed to JAERI by the Kansai Electric Power Co. [89]. It is important to note, however, that the reported boron concentrations were obtained once the equilibrium state of the poisonous FP, xenon-135, had been reached. Nevertheless, despite the availability of this date-specific data, it was not specifically defined in this dynamic manner (in the SERPENT-2 input code). Instead, the overall cycle-averages of the boron concentrations were utilised, as it has been demonstrated to yield equivalent results in the context of isotopic depletion calculations [79]. Moreover, it is also important to note that the initial boron concentrations reported at the beginning of each cycle – *i.e.* zero days elapsed – were not included in the calculation of the respective cycle averages.

Table 9: Boric acid concentration history of the Takahama Reactor No. 3 – Cycle 5 [89, p. 116]

Cumulative Elapsed Days [d]	Boron Concentration [ppm]
0	1,154
106	894
205	651
306	404
385	210

Table 10: Boric acid concentration history of the Takahama Reactor No. 3 – Cycle 6 [89, p. 116]

Cumulative Elapsed Days [d]	Boron Concentration [ppm]
0	1,132
119	864
231	613
344	358
402	228

3.2 Ohi Reactor No. 2 Nuclear Power Station

3.2.1 General Data

The Kansai Electric Power Co. (Ltd.) Ohi Reactor No. 2 Nuclear Power Station is a 'Westinghouse Mitsubishi Heavy Industries W 4-loop' modelled PWR, located in the town of Ohi, Fukui Prefecture, Japan (geographical coordinates expressed in 'DMS': 35° 32' 26.25" N; 135° 39' 7.32" E) [96], [98]. The nuclear power station began commercial operations on 5 December 1979, with a thermal and electric power capacity of 3,423 MW and 1,120 MW, respectively [98]. However, the nuclear power station has been permanently shut down since 1 March 2018 [98]. The decision to cease operations was motivated by the fact that the reactor had almost reached Japan's nominal operating period of 40 years, as well as the technical challenges associated with efforts to comply with Japan's updated reactor safety regulations (as part of the regulatory approval process for an additional twenty-year licence extension).

Table 11 presents the main core characteristics of the Ohi Reactor No. 2 Nuclear Power Station, from which the assembly designated "17G" and consequently the BFRs "C5" and "O13" – consisting of three UO_2-Gd_2O_3 SNF samples that have been subjected to destructive RCA experiments and identified as "C5-89G01", "C5-89G03", and "O13-89G05", respectively – data were obtained. In addition, Table 12 presents the main assembly characteristics of the "17G" assembly [96].

Table 11: Main core characteristics of the Ohi Reactor No. 2 Nuclear Power Station [96, p. 931]

Reactor Core Data	
Number of Loops	4
Coolant Medium	Light Water
Moderator Medium	Light Water
Thermal Power [MW]	3,423
Electric Power [MW]	1,120
Active Core Height [m]	3.66
Active Core Diameter [m]	3.37
Uranium Weight [metric tonne]	~ 87
Coolant Inlet Temperature [°C]	289
Coolant Outlet Temperature [°C]	325
Coolant Pressure [MPa]	15.5

Table 12: Main assembly characteristics of the "17G" assembly [96, p. 931]

Fuel Assembly Data	
Assembly Type	17 x 17
Number of Assemblies	193
Uranium Weight [kg]	~ 460
Rod Pitch [mm]	12.6
Assembly Pitch [mm]	214.0 ±0.5%
Number of Fuel Rods	264
Number of Guide Rods	24 + 1
Total Rod Length [mm]	3,865.0
Active Rod Length [mm]	3,816.0
Cladding Material	Zircaloy-4

Table 13 presents the initial isotopic compositions of the regular PWR-UO_2 fuel rods – *e.g.* "F4" – and the gadolinia-containing PWR-UO_2-Gd_2O_3 fuel rods (*e.g.* "C5" and "O13") [99]. The mass density is reported in the official documentation [99] to be approximately 95 percent (*i.e.* ~ 95%) of the theoretical mass density (TD) of UO_2 – *i.e.* 10.970 g/cm^3 at a temperature of 273 Kelvin (K) [87] – which equates to a numerical value of 10.412 g/cm^3. It is important to note that the initial nuclide inventory of the PWR-UO_2-Gd_2O_3 fuel rods includes a detailed description of the isotopic abundances of gadolinium. The reported isotopic abundances are consistent with the observed distribution in natural gadolinium.

Table 13: Initial isotopic compositions of the "C5", "F4", and "O13" fuel rods [99, p. 1121]

Fuel Rod Data	**F4 (UO_2)**	**C5 and O13 (UO_2-Gd_2O_3)**
Mass Density [g/cm^3]	~ 95% TD	~ 95% TD
U-234 [wt%]	0.0281	0.0141
U-235 [wt%]	3.2000	1.6874
U-236 [wt%]	0.0020	0.0008
U-238 [wt%]	96.7699	98.2977
Gd (natural) [wt%]	N.A.	6.00
Gd-152 [wt%]	N.A.	0.19
Gd-154 [wt%]	N.A.	2.13
Gd-155 [wt%]	N.A.	14.58
Gd-156 [wt%]	N.A.	20.30
Gd-157 [wt%]	N.A.	15.62
Gd-158 [wt%]	N.A.	24.95
Gd-160 [wt%]	N.A.	22.23

Figure 16 provides an illustration of the fuel rod configuration present in the Ohi Reactor No. 2 "17G" assembly [99]. The 17 x 17 square lattice configuration is compliant with the one-eighth symmetry in regard to the spatial positioning of the 248 PWR-UO_2 FRs, 16 PWR-UO_2-Gd_2O_3 BFRs, 24 control rod guide tubes, and a single central instrumentation thimble. The displayed arrows indicate the assembly positions of the fuel rods that were subjected to destructive RCA (*i.e.* holding the PWR-SNF samples). The configuration is indexed in a numerical and alphabetical order, from left to right and from top to bottom, respectively, corresponding to the numbers 1 to 17, and the letters A to Q. Therefore, the PWR-UO_2-Gd_2O_3 rods are located at positions 'C-5' and 'O-13', while the PWR-UO_2 rod is located at 'F-4'.

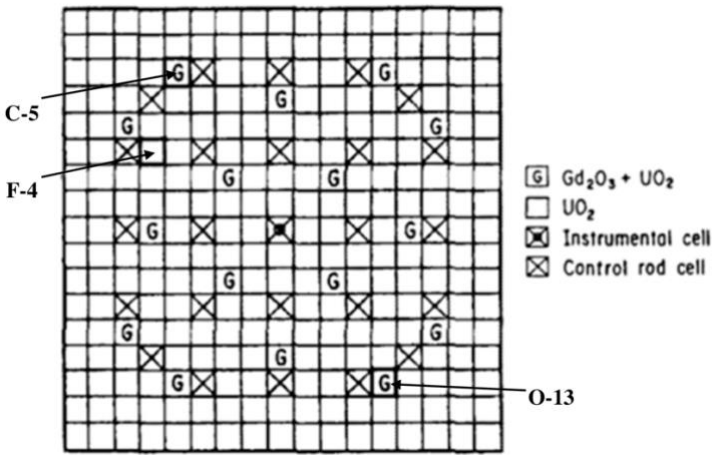

Figure 16: Fuel rod configuration in the Ohi Reactor No. 2 "17G" assembly [99, p. 1120]

3.2.2 Code Accuracy Evaluation

In order to evaluate the isotopic accuracy of the calculated nuclide inventory results simulated by SERPENT-2, the sample-specific calculated concentrations are compared against the experimental data (*i.e.* 'C/E', wherein the letter "C" represents the calculated value, and the letter "E" the experimental value, with numerical values of both quantities expressed in grams of the nuclide under consideration per gram of initial fuel (*i.e.* g/g_{fuel}). However, an alternative representation is utilised in the chapter entitled "Results by SERPENT-2". In particular, the 'percentage deviation' format, which can be calculated utilising Equation 18. Moreover, the sample-average 'C/E' and the standard deviation (SD) – which quantifies the expected variation of a given statistical population relative to its sample-average – are additionally included. Equation 19 presents the statistical formula for calculating the SD.

3.2.3 Cell Configuration – Burnable Fuel Rods "C5" and "O13"

A single two-dimensional lattice geometry cell – *i.e.* an infinite 2D square lattice – is defined for the SERPENT-2 simulations. The geometrical description is based on a 'constructive solid geometry' methodology, in which homogeneous material cells are defined utilising a combination of elementary and derived surface types [91]. The adopted model comprises three nested annular (R) material regions. The primary annular region – *i.e.* $R \leq 0.4025$ cm – represents either a solid UO_2 or UO_2-Gd_2O_3 fuel pellet (depending on the fuel rod being modelled). Bounding the "Fuel Pellet" region and the "Inner Cladding" region is a void – *i.e.* $0.4025 \text{ cm} < R \leq 0.4110 \text{ cm}$ – which in practice is filled with a helium gas mixture. However, [92] suggests that the assumption of a void is deemed sufficient. Subsequently, the specific cladding 'Zircaloy-4' (Zry-4) [93] is delineated by its inner and outer radii, represented by "Inner Cladding" and "Outer Cladding", respectively (*i.e.* $0.4110 \text{ cm} < R \leq 0.4750 \text{ cm}$). To complete the pin cell structure, the annular region of the coolant medium is defined (*i.e.* $0.4750 \text{ cm} < R$). It is important to note, however, that this outermost region does not require explicit boundary definitions, as it is by default radially infinite [94] (detailed in the SERPENT-2 input code in §Appendix A). Moreover, the specular reflective boundary condition is assumed at the geometry's outer boundary surface – *i.e.* a square boundary surface around the PWR assembly – which results in an axially infinite nuclear system. Table 14 presents the modelled annular cell geometry of the PWR-UO_2 and PWR-UO_2-Gd_2O_3 fuel rods.

It is a typical design characteristic of a PWR assembly that the control rod guide tubes and the central instrumentation thimble have larger radial dimensions than the UO_2 or UO_2-Gd_2O_3 fuel rods. Therefore, an additional annular cell geometry is defined. It should be noted, however, that these aforementioned tubes are assumed to be empty (for the SERPENT-2 simulation processes). The primary annular region – *i.e.* $R \leq 0.5625$ cm – represents the assumed empty volume and is filled with coolant medium. The Zry-4 cladding region – *i.e.* $0.5625 \text{ cm} < R \leq 0.6025 \text{ cm}$ – is located adjacent to the void/coolant region. To complete the second pin cell structure, the outermost coolant region is defined (*i.e.* $0.6025 \text{ cm} < R$). Table 15 presents the modelled annular cell geometry of the control rod guide tubes.

Table 14: Annular cell geometry of the "C5", "F4", and "O13" fuel rods [96, p. 931]

Region	Radius [cm]
Fuel Pellet	0.4025
Inner Cladding	0.4110
Outer Cladding	0.4750

Table 15: Annular cell geometry of the control rod guide tubes [96, p. 931]

Region	Radius [cm]
Guide Inner	0.5625
Guide Outer	0.6025

To ensure the compositional accuracy of the UO_2-Gd_2O_3 fuel pellets during the depletion simulations, it is necessary to implement a multitude of radial material subdivisions. The independent depletion zones guarantee a more accurate approximation of absorber burn-out. Accordingly, four independent radial subdivisions have been defined for the UO_2 pellets and ten subdivisions for the UO_2-Gd_2O_3 pellets.

3.2.4 Temperature and Axial Cutting Positioning

Throughout the entirety of the SERPENT-2 simulation, it is assumed that the temperatures within the PWR-UO_2 and PWR-UO_2-Gd_2O_3 fuel pellets remain constant at 968.8 K, whereas the Zry-4 cladding region is held constant at 600.0 K [96]. The aforementioned temperatures are considered to be reasonable assumptions based on an international 'burnup credit criticality' benchmark [100]. With regard to the reported temperatures of the coolant region, a calculation is performed through the utilisation of Equation 20, wherein it is assumed that an incremental increase in the coolant temperature is directly proportional to the integrated power from the lower boundary of the active PWR-UO_2 or PWR-UO_2-Gd_2O_3 fuel stack to each sample cutting position in the axial direction, and assuming the additional hypothesis that the axial power distribution is described by a cosine function [96].

In conjunction with Equation 20, the data related to the axial cutting positions of the PWR-SNF samples – which are detailed in Table 16 – are integrated in order to obtain sample-specific coolant temperatures. Table 17 presents an overview of the calculated sample-specific coolant temperatures. Moreover, as the temperature of the coolant region is sample-specific, the intrinsic thermal scattering properties of the coolant medium likewise exhibit sample-specific variations, contingent upon the PWR-SNF sample under consideration. It is therefore necessary – in the SERPENT-2 input code – to interpolate between the implemented datasets of thermal scattering libraries associated with hydrogen in light water (based on ENDF/B.VII.1). Furthermore, the mass density of the coolant must also be interpolated on the basis of its temperature and pressure [97].

Table 16: Axial cutting positions of the "C5" and "O13" samples [99, p. 1120]

Sample ID	From Bottom of Active Stack [mm]	From Top [mm]
C5-89G01	267	3,393
C5-89G03	737	2,923
O13-89G05	733	2,927

Table 17: Coolant temperatures of the "C5" and "O13" samples

Sample ID	Coolant Temperature [K]
C5-89G01	559.05
C5-89G03	564.65
O13-89G05	564.62

3.2.5 Specific Power History

The UO_2-Gd_2O_3 PWR-SNF samples identified as “C5-89G01”, “C5-8903”, and ‘O13-89G05’ were subjected to irradiation in two distinct cycles, designated “Cycle 5” and “Cycle 6”, respectively. The date-related specifications of these operational cycles – *i.e.* the initial and final dates – are not available on a cycle-specific basis. The only information available regarding their operational status is that they collectively covered the period between July 1984 and February 1987. However, the duration of each individual cycle, in contrast, is reported in the official documentation [99], with “Cycle 5” covering 410 operational days and “Cycle 6” covering 427 operational days. The cooling period between the two operational cycles lasted for a total of 88 days. Table 18 presents the irradiation histories as disclosed to JAERI by the Kansai Electric Power Co. [96].

Table 18: Irradiation histories of the “C5” and “O13” samples [96, p. 934]

Days [d]	**Power [MW/t_{HM}]**		
	C5-89G01	C5-89G03	O13-89G05
17	5.2713	7.0522	4.9558
29	5.3752	7.1909	4.8717
29	8.6538	11.5775	7.4757
34	10.5425	14.1044	9.0156
28	12.4725	16.6859	10.4147
33	15.3365	20.5177	12.4871
30	18.5945	24.8760	14.6983
28	22.1015	29.5683	17.1644
29	26.0241	34.8155	20.2423
36	29.3654	39.2851	23.8536
54	31.7315	42.4508	29.0331
35	31.9805	42.7829	31.9448
16	31.9178	42.7008	31.8608
11	25.8998	34.6494	27.0730
1	25.8998	34.6494	27.0730
104	0.0000	0.0000	0.0000
23	20.8979	27.9577	27.3535
29	29.3860	39.3134	38.5528
28	29.9261	40.0353	39.4762
32	30.5073	40.8128	40.6526
30	31.6688	42.3678	42.6116
29	29.6350	39.6465	40.2041
32	30.8386	41.2572	41.9961
31	32.3539	43.2839	44.1798
27	32.8313	43.9218	44.9078
35	33.0596	44.2275	45.2996
33	32.9763	44.1161	45.3562
23	33.0185	44.1718	45.5517
37	32.3333	43.2556	44.6840
14	33.0596	44.2275	45.6816
12	25.6506	34.3154	35.4447
12	25.6506	34.3154	35.4447

3.2.6 Boric Acid Concentration History

Tables 19 and 20 present the date-specific histories of boric acid concentration for the two operational cycles under consideration, designated “Cycle 5” and “Cycle 6”, respectively. The aforementioned operational data were disclosed to JAERI by the Kansai Electric Power Co. [96]. It is important to note, however, that the reported boron concentrations were obtained once the equilibrium state of the poisonous FP, xenon-135, had been reached. Nevertheless, despite the availability of this date-specific data, it was not specifically defined in this dynamic manner (in the SERPENT-2 input code). Instead, the overall cycle-averages of the boron concentrations were utilised, as it has been demonstrated to yield equivalent results in the context of isotopic depletion calculations [79]. Moreover, it is also important to note that the initial boron concentrations reported at the beginning of each cycle – *i.e.* 17 and 23 days elapsed, respectively – were not included in the calculation of the respective cycle averages.

Table 19: Boric acid concentration history of the Ohi Reactor No. 2 – Cycle 5 [96, p. 934]

Cumulative Elapsed Days [d]	Boron Concentration [ppm]
17	1,078.2
46	1,019.3
75	945.1
109	864.4
137	785.0
170	706.9
200	626.2
228	552.0
257	479.0
293	395.7
347	280.5
382	166.5
398	101.2
411	51.3

Table 20: Boric acid concentration history of the Ohi Reactor No. 2 – Cycle 6 [96, p. 934]

Cumulative Elapsed Days [d]	Boron Concentration [ppm]
23	1,071.7
52	1,007.8
80	937.7
112	863.9
142	787.7
171	715.2
203	640.2
234	562.7
296	415.2
329	331.6
352	262.7
389	188.9
403	126.2
415	94.3
427	64.8

4 Results by SERPENT-2

4.1 Takahama Reactor No. 3 Nuclear Power Station

The selected nuclides in the simulated nuclide inventory, which were subjected to a comparative analysis and derived from the UO_2-Gd_2O_3 SNF samples retrieved from the Takahama Reactor No. 3 Nuclear Power Station – identified as "SF96-1" to "SF96-5", were characterised by nuclear depletion levels between 7.79 GWd/t_{HM} and 28.91 GWd/t_{HM} – included: uranium, *i.e.* U-234, U-235, U-236, and U-238; neptunium, *i.e.* Np-237; plutonium, *i.e.* Pu-238, Pu-239, Pu-240, Pu-241, and Pu-242; americium, *i.e.* Am-241, Am-242m, and Am-243; curium, *i.e.* Cm-242 and Cm-244; and a variety of FP nuclides, beginning with caesium and neodymium (Ru-106, Sb-125, Ce-144, and Eu-154 additionally included). Subsequently, the sample-specific calculated nuclide concentrations were evaluated in comparison with the reported experimental concentrations – detailed in §Appendix B – utilising the 'C/E' representation. The data reported by JAERI from the destructive analyses were previously normalised to the appropriate day of discharge (DOD), thereby eliminating the necessity to consider the cooling period – 4.161 years for both the actinides and FP nuclides [89] – between DOD and the date of performed chemical analysis. The preliminary SERPENT-2 simulations were performed with 250 active and 50 inactive calculation cycles, each comprising 10,000 neutrons per neutron transport cycle. Subsequently, the sample-specific calculated nuclide inventories were processed utilising a Python script and executed within the Microsoft Visual Studio Code editor environment. The processing of the SERPENT-2 depletion output files was made possible through the utilisation of the free and publicly available Python package, 'serpentTools'. Moreover, during processing of the sample-specific 'C/E' results, particular interest was directed towards the isotopic concentrations of neodymium-148, which has been demonstrated to be an effective experimental burnup monitor (as detailed in §2.2.5 Experimental Burnup Monitor – Neodymium-148). Accordingly, the JAERI-reported sample-specific irradiation histories were modified in order to align the calculated concentrations with the measured concentrations of neodymium-148. Once the aforementioned adjustments had been completed, a definitive SERPENT-2 simulation was performed, comprising 250 active and 50 inactive calculation cycles, each with 100,000 neutrons in the neutron transport cycle. The implementation of this specific neutron population size was intended to reduce the statistical uncertainties. Furthermore, the utilised depletion-step length is determined by a consideration between the impact (due to linearisation) on the simulated nuclide inventory, *i.e.* isotopic accuracy, and the associated computational running time. In addition, the calculated nuclide inventories of SERPENT-2 were evaluated in comparison with those simulated by alternative depletion calculation codes, with the objective of ascertaining the relative isotopic accuracy of the performed SERPENT-2 simulations. The depletion calculation codes included in the official documentation [85] were the "Step-Wise Burnup Analysis Code System", or "SWAT" [101] (§Appendix C) and ORNL's ORIGEN2.1 (§Appendix D) [102]. The nuclear data libraries utilised in both referenced alternative depletion codes are based on the Japanese evaluated nuclear data library, JENDL-3.2 (released in June 1994) [103]. For ORIGEN2.1, the specific 'PWR41J32' library of the 'ORLIBJ32' package was utilised [104]. It is important to note that the simulated nuclide inventory results by SERPENT-2 for the primary sample, identified as "SF96-1", could not be compared relatively to the alternative depletion calculation codes, as the official documentation [85] excluded this particular sample with the aim of solely analysing samples irradiated with the assembly's average neutron spectra. In other words, samples obtained from axial cutting positions in close proximity to the upper or lower boundaries of the active PWR-UO_2 or PWR-UO_2-Gd_2O_3 fuel stack were not included in the objects subjected to code accuracy evaluation [85].

4.1.1 ‘C/E-1’ Results for Sample “SF96-1”

The primary UO_2-Gd_2O_3 PWR-SNF sample retrieved from the Takahama Reactor No. 3 Nuclear Power Station, identified as “SF96-1”, represents an extremity sample – *i.e.* located at an axial height of 17 mm in close proximity to the upper boundary of the active UO_2-Gd_2O_3 fuel stack – which was reported to exhibit an experimentally based depletion level of 7.79 GWd/t_{HM} [85]. However, the nuclear depletion achieved by the definitive SERPENT-2 simulation process – after normalisation of the neodymium-148 isotope concentration – was higher, reaching 7.85 GWd/t_{HM} (*i.e.* corresponding to the nuclear depletion excess of 0.725160462% reported by serpentTools). Figures 17 and 18 illustrate the calculated results of the nuclide inventory for sample “SF96-1” of the reported FPs and the actinide nuclides, respectively.

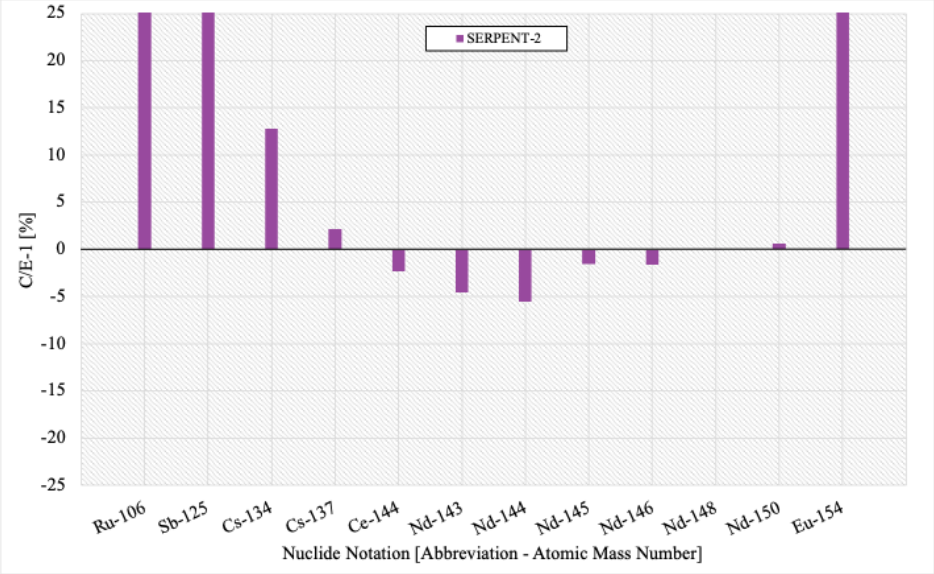

Figure 17: ‘C/E-1’ results of fission product nuclides for the "SF96-1" sample

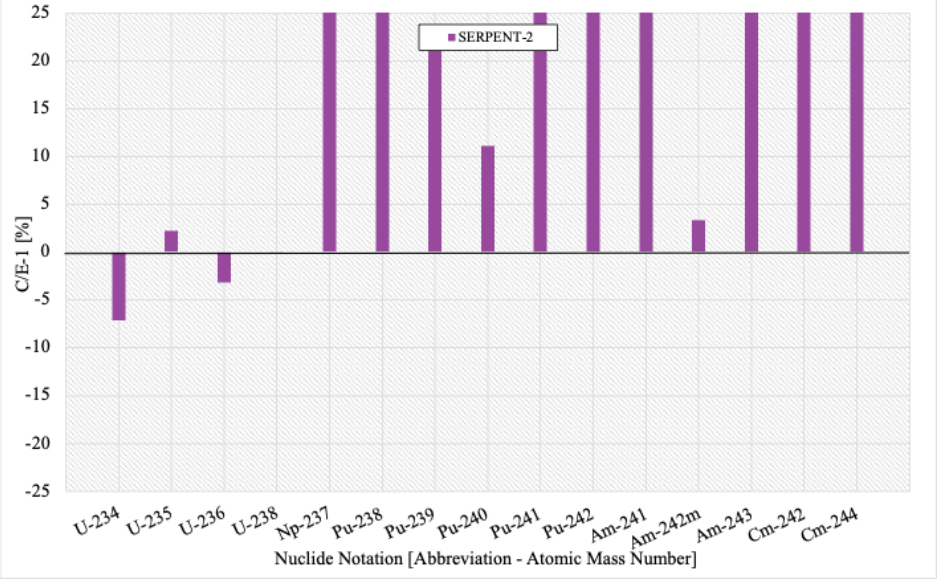

Figure 18: ‘C/E-1’ results of actinide nuclides for the "SF96-1" sample

4.1.2 ‘C/E-1’ Results for Sample “SF96-2”

The second UO_2-Gd_2O_3 PWR-SNF sample retrieved from the Takahama Reactor No. 3 Nuclear Power Station, identified as “SF96-2”, was reported to exhibit an experimentally determined nuclear depletion level of 16.44 GWd/t_{HM} [85]. However, the depletion achieved by the definitive SERPENT-2 simulation process – after the normalisation procedure of the neodymium-148 isotope concentration – was higher, reaching 16.59 GWd/t_{HM} (*i.e.* corresponding to the nuclear depletion excess of 0.919708029% reported by serpentTools). Figures 19 and 20 illustrate the calculated results of the nuclide inventory in terms of percentage deviations for sample “SF96-2” of the reported FPs and the actinide nuclides, respectively.

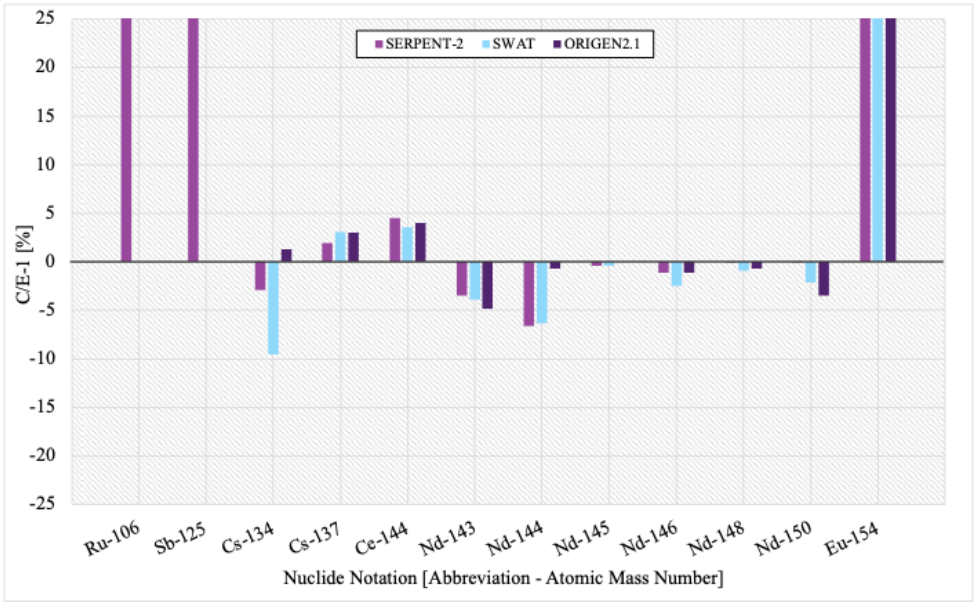

Figure 19: ‘C/E-1’ results of fission product nuclides for the "SF96-2" sample

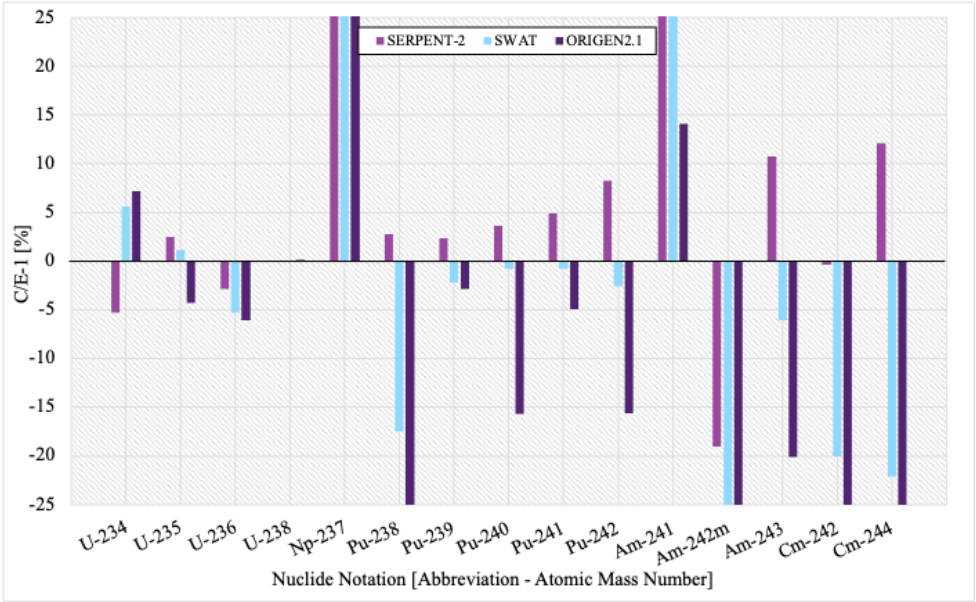

Figure 20: ‘C/E-1’ results of actinide nuclides for the "SF96-2" sample

4.1.3 ‘C/E-1’ Results for Sample “SF96-3”

The third UO_2-Gd_2O_3 PWR-SNF sample retrieved from the Takahama Reactor No. 3 Nuclear Power Station, identified as “SF96-3”, was reported to exhibit an experimentally determined nuclear depletion level of 28.20 GWd/t_{HM} [85]. However, the depletion achieved by the definitive SERPENT-2 simulation process – after the normalisation procedure of the neodymium-148 isotope concentration – was higher, reaching 28.60 GWd/t_{HM} (*i.e.* corresponding to the nuclear depletion excess of 1.427659574% reported by serpentTools). Figures 21 and 22 illustrate the calculated results of the nuclide inventory in terms of percentage deviations for sample “SF96-3” of the reported FPs and the actinide nuclides, respectively.

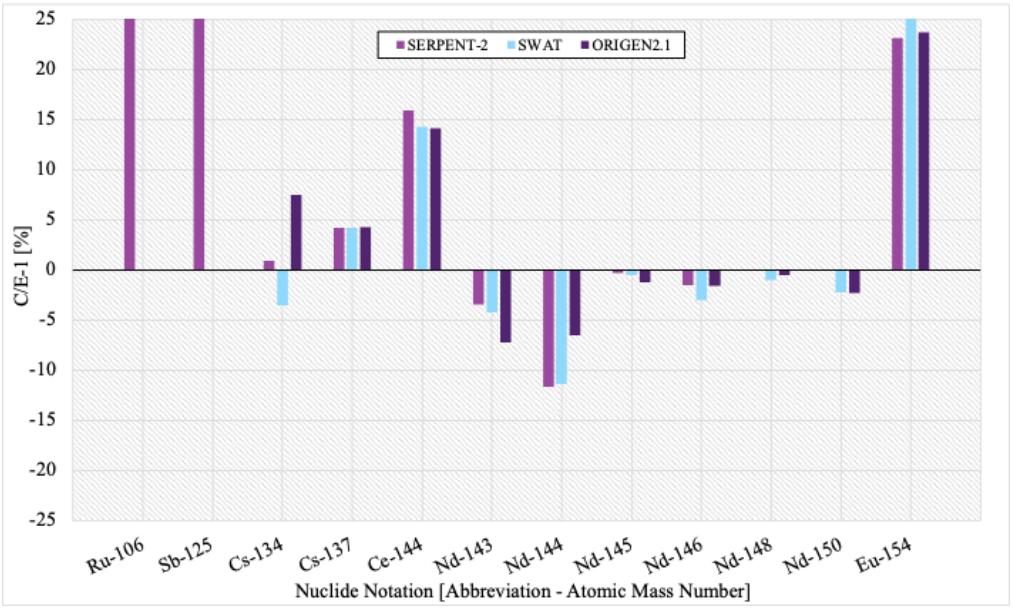

Figure 21: ‘C/E-1’ results of fission product nuclides for the "SF96-3" sample

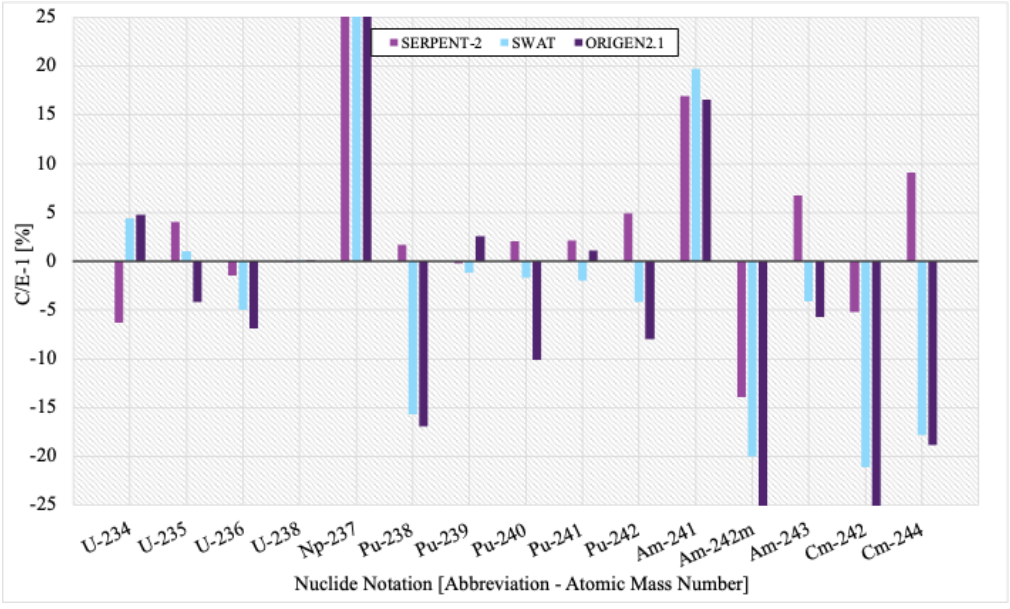

Figure 22: ‘C/E-1’ results of actinide nuclides for the "SF96-3" sample

4.1.4 ‘C/E-1’ Results for Sample “SF96-4”

The fourth UO_2-Gd_2O_3 PWR-SNF sample retrieved from the Takahama Reactor No. 3 Nuclear Power Station, identified as “SF96-4”, was reported to exhibit an experimentally determined nuclear depletion level of 28.91 GWd/t_{HM} [85]. However, the depletion achieved by the definitive SERPENT-2 simulation process – after the normalisation procedure of the neodymium-148 isotope concentration – was higher, reaching 29.32 GWd/t_{HM} (*i.e.* corresponding to the nuclear depletion excess of 1.425804219% reported by serpentTools). Figures 23 and 24 illustrate the calculated results of the nuclide inventory in terms of percentage deviations for sample “SF96-4” of the reported FPs and the actinide nuclides, respectively.

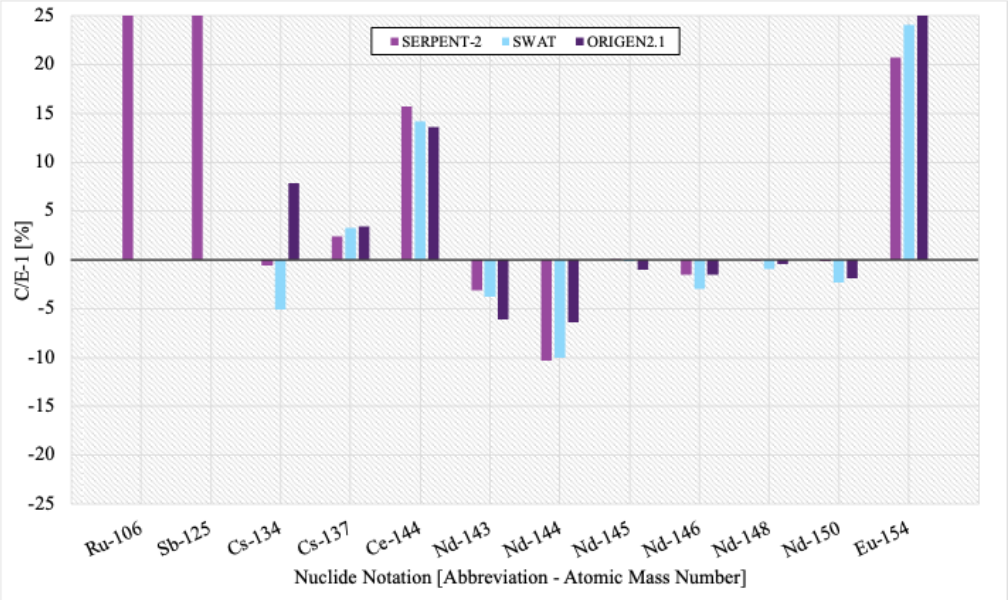

Figure 23: ‘C/E-1’ results of fission product nuclides for the "SF96-4" sample

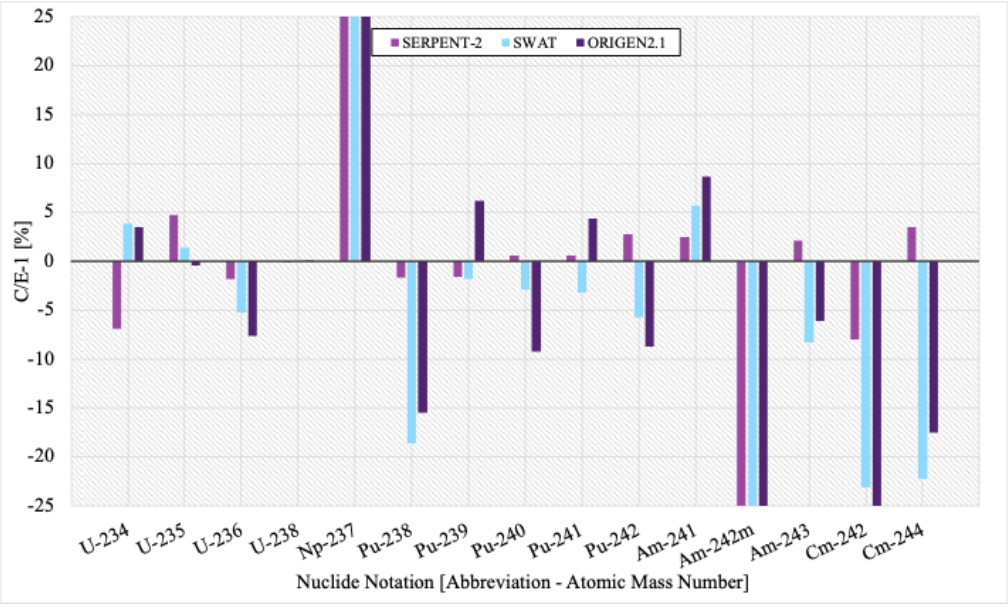

Figure 24: ‘C/E-1’ results of actinide nuclides for the "SF96-4" sample

4.1.5 ‘C/E-1’ Results for Sample “SF96-5”

The final UO_2-Gd_2O_3 PWR-SNF sample retrieved from the Takahama Reactor No. 3 Nuclear Power Station, identified as “SF96-5”, was reported to exhibit an experimentally determined nuclear depletion level of 24.19 GWd/t_{HM} [85]. However, the depletion achieved by the definitive SERPENT-2 simulation process – after the normalisation procedure of the neodymium-148 isotope concentration – was higher, reaching 24.48 GWd/t_{HM} (*i.e.* corresponding to the nuclear depletion excess of 1.216618437% reported by serpentTools). Figures 25 and 26 illustrate the calculated results of the nuclide inventory in terms of percentage deviations for sample “SF96-5” of the reported FPs and the actinide nuclides, respectively.

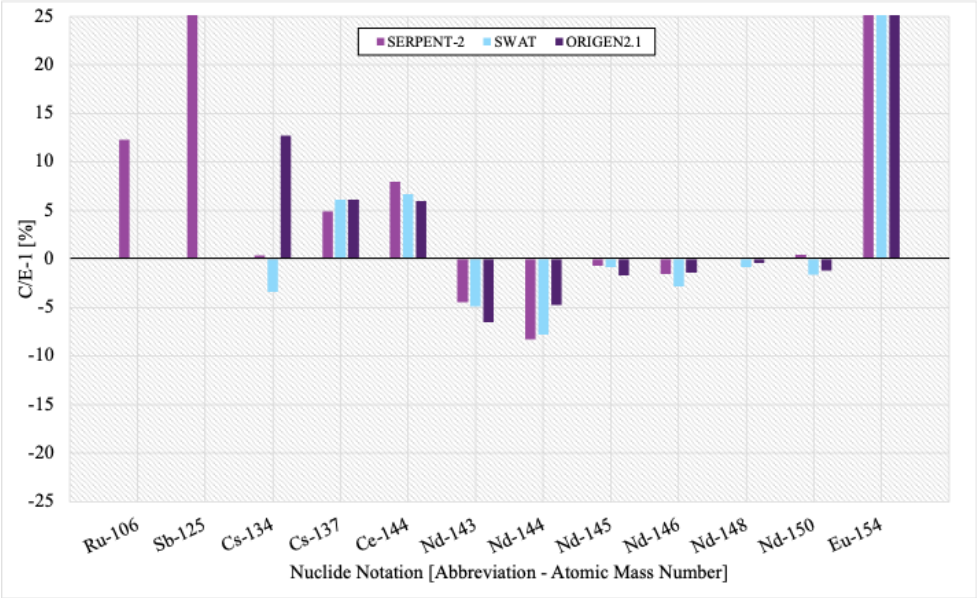

Figure 25: ‘C/E-1’ results of fission product nuclides for the "SF96-5" sample

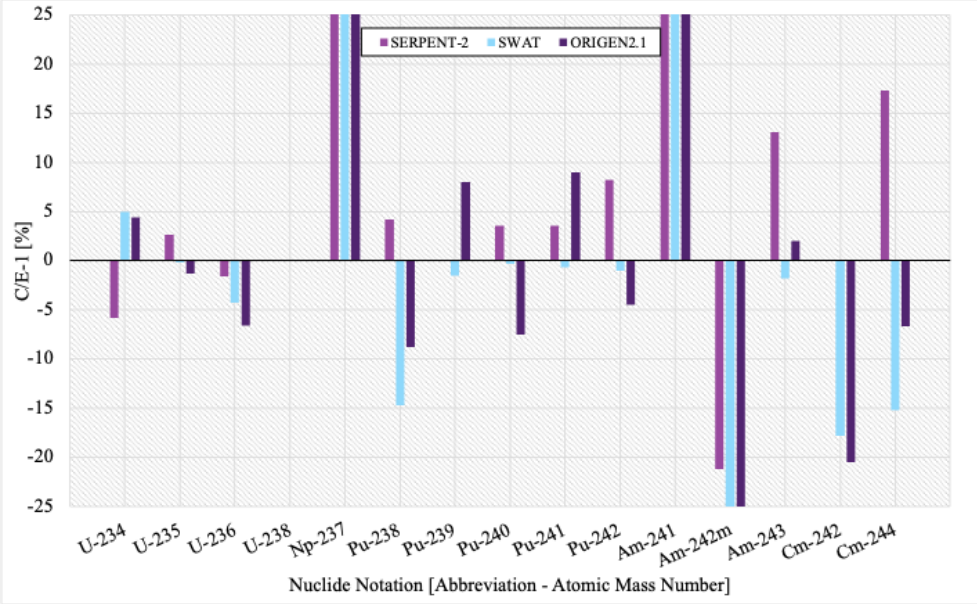

Figure 26: ‘C/E-1’ results of actinide nuclides for the "SF96-5” sample

4.1.6 Overview ‘C/E’ Results for “SF96” Samples

Table 21 provides a detailed overview of the sample-specific ‘C/E’ results for the selected nuclides investigated in the comparative analysis of UO_2-Gd_2O_3 PWR-SNF samples simulated by SERPENT-2 and retrieved from the Takahama Reactor No. 3 Nuclear Power Station. It should be noted, however, that the “Average” column does not include the weighted contribution of the extremity sample – *i.e.* “SF96-1”. This exclusion was performed in order to ensure that sample-average results could be evaluated in a uniform and consistent manner with those obtained by the alternative nuclear depletion calculation codes, which have excluded this specific PWR-SNF sample from their code accuracy evaluation (as detailed in §4.1 Takahama Reactor No. 3 Nuclear Power Station). Furthermore, the numerical sample-specific and sample-average ‘C/E’ results – including the SD – for the alternative depletion calculation codes SWAT and ORIGEN2.1 are provided in Appendices C and D, respectively.

Table 21: Overview ‘C/E’ results for the "SF96" samples

Nuclide	SF96-1	SF96-2	SF96-3	SF96-4	SF96-5	Average	SD
Ru-106	1.286725	1.534568	1.363639	1.510433	1.123023	1.38	0.19
Sb-125	1.945943	2.094788	2.879474	2.293718	2.353883	2.41	0.33
Cs-134	1.127711	0.971288	1.009062	0.994546	1.003773	0.99	0.02
Cs-137	1.021918	1.019306	1.042270	1.023783	1.049237	1.03	0.01
Ce-144	0.977179	1.045400	1.158837	1.156894	1.079655	1.11	0.06
Nd-143	0.954290	0.965046	0.965561	0.968920	0.955876	0.96	0.01
Nd-144	0.944590	0.933782	0.883354	0.896916	0.916883	0.91	0.02
Nd-145	0.984314	0.996207	0.997098	1.001123	0.992785	1.00	0.00
Nd-146	0.983665	0.989014	0.985159	0.984539	0.985761	0.99	0.00
Nd-148	0.999837	0.999979	1.000062	0.999966	1.000016	1.00	0.00
Nd-150	1.006129	0.999855	1.000046	0.998344	1.004414	1.00	0.00
Eu-154	1.639169	1.305136	1.231410	1.207551	1.291697	1.26	0.05
U-234	0.928529	0.947119	0.937336	0.931203	0.941953	0.94	0.01
U-235	1.022226	1.024932	1.040220	1.047417	1.026253	1.03	0.01
U-236	0.968057	0.971024	0.985261	0.981751	0.984073	0.98	0.01
U-238	0.998522	0.999352	0.999483	0.999667	0.999534	1.00	0.00
Np-237	1.416374	1.436256	1.603364	1.530373	1.477342	1.51	0.07
Pu-238	1.284670	1.027387	1.017141	0.983077	1.041922	1.02	0.03
Pu-239	1.220592	1.023416	0.997660	0.984344	1.001365	1.00	0.02
Pu-240	1.111549	1.035988	1.020401	1.006120	1.035854	1.02	0.01
Pu-241	1.334957	1.049111	1.021266	1.005686	1.035380	1.03	0.02
Pu-242	1.283483	1.082206	1.049055	1.027554	1.081882	1.06	0.03
Am-241	1.743636	1.415313	1.169026	1.024827	1.355873	1.24	0.18
Am-242m	1.033570	0.809566	0.861007	0.745360	0.787755	0.80	0.05
Am-243	1.561153	1.107445	1.067758	1.020935	1.130998	1.08	0.05
Cm-242	1.313369	0.996138	0.947809	0.920357	1.001291	0.97	0.04
Cm-244	1.762626	1.120653	1.090596	1.034694	1.173370	1.10	0.06

4.2 Ohi Reactor No. 2 Nuclear Power Station

The selected nuclides in the simulated nuclide inventory, which were subjected to a comparative analysis and derived from the UO_2-Gd_2O_3 SNF samples retrieved from the Ohi Reactor No. 2 Nuclear Power Station – identified as "C5-89G01", "C5-89G03", and "O13-89G05", and with nuclear depletion levels between 21.465 GWd/t_{HM} and 28.717 GWd/t_{HM} – included: uranium, *i.e.* U-232, U-234, U-235, U-236, and U-238; neptunium, *i.e.* Np-237; plutonium, *i.e.* Pu-236, Pu-238, Pu-239, Pu-240, Pu-241, Pu-242; americium, *i.e.* Am-241, (metastable) Am-242m, and Am-243; curium, *i.e.* Cm-242, Cm-243, Cm-244, Cm-245, Cm-246, and Cm-247; and a variety of FP nuclides, beginning with caesium and neodymium (Ru-106, (metastable) Ag-110m, Sb-125, Ce-144, and Eu-154 additionally included). Subsequently, the sample-specific calculated nuclide concentrations were evaluated in comparison with the experimental measurements performed by JAERI – as detailed in §Appendix E – utilising the 'C/E' representation. The data reported by JAERI from the destructive analyses of the actinide nuclides were previously normalised to the appropriate day of discharge (DOD), thereby eliminating the necessity to consider the cooling period between DOD and the date of performed chemical analysis. However, the reported data for the FP nuclides were not subjected to prior normalisation, which necessitated a correction of the calculated concentrations with respect to the cooling period, which was reported to be five years [96].

The preliminary SERPENT-2 simulations were performed with 250 active and 50 inactive calculation cycles, each comprising 10,000 neutrons per neutron transport cycle. Subsequently, the sample-specific calculated nuclide inventories were processed utilising a Python script and executed within the Microsoft Visual Studio Code editor environment. The processing of the SERPENT-2 depletion output files was made possible through the utilisation of the free and publicly available Python package, 'serpentTools'. Moreover, during processing of the sample-specific 'C/E' results, particular interest was directed towards the isotopic concentrations of neodymium-148, which has been demonstrated to be an effective experimental burnup monitor (as detailed in §2.2.5 Experimental Burnup Monitor – Neodymium-148). Accordingly, the JAERI-reported sample-specific irradiation histories were modified in order to align the calculated concentrations with the measured concentrations of neodymium-148. Once the aforementioned adjustments had been completed, a definitive SERPENT-2 simulation was performed, comprising 250 active and 50 inactive calculation cycles, each with 100,000 neutrons in the neutron transport cycle. The implementation of this specific neutron population size was intended to reduce the statistical uncertainties. Furthermore, the utilised depletion-step length is determined by a consideration between the impact (due to linearisation) on the simulated nuclide inventory, *i.e.* isotopic accuracy, and the associated computational running time. In addition, the calculated nuclide inventories of SERPENT-2 were evaluated in comparison with those simulated by an alternative depletion calculation code, with the objective of ascertaining the relative isotopic accuracy of the performed SERPENT-2 simulations. The depletion calculation code included in the official documentation [96] was the "Step-Wise Burnup Analysis Code System Version 2.1" or "SWAT2.1" (*i.e.* revised version of "SWAT") [105] (§Appendix F). The nuclear data library utilised in the referenced alternative depletion code is based on the Japanese evaluated nuclear data library, JENDL-3.3 (released in May 2002) [106].

4.2.1 ‘C/E-1’ Results for Sample “C5-89G01”

The primary UO_2-Gd_2O_3 PWR-SNF sample retrieved from the Ohi Reactor No. 2 Nuclear Power Station, identified as “C5-89G01”, was reported to have an experimentally determined nuclear depletion level of 21.465 GWd/t_{HM} [96]. However, the nuclear depletion achieved by the definitive SERPENT-2 simulation process – following the normalisation of the neodymium-148 isotope concentration – was lower, reaching 21.142 GWd/t_{HM} (*i.e.* corresponding to the depletion deficit of 1.50477522% reported by serpentTools). Figures 27 and 28 illustrate the calculated results of the nuclide inventory in terms of percentage deviations for sample “C5-89G01” of the reported FPs and actinide nuclides, respectively.

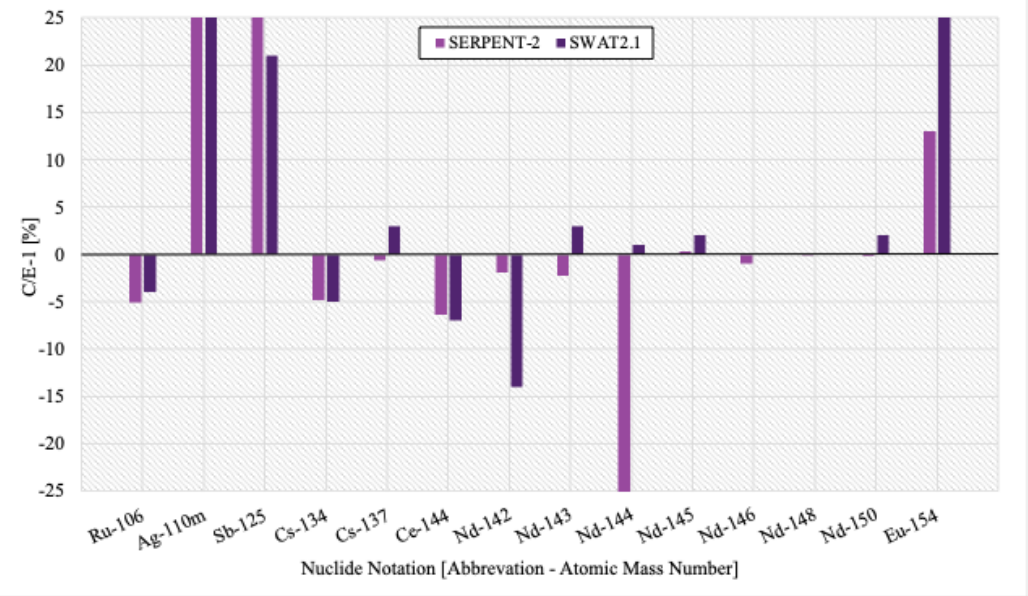

Figure 27: ‘C/E-1’ results of fission product nuclides for the "C5-89G01" sample

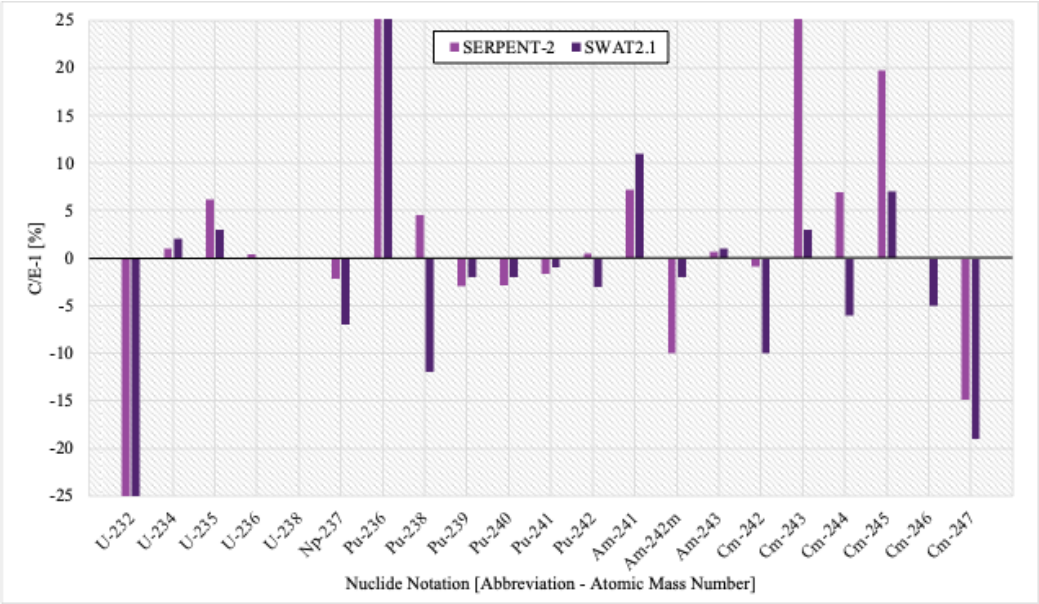

Figure 28: ‘C/E-1’ results of actinide nuclides for the "C5-89G01" sample

4.2.2 ‘C/E-1’ Results for Sample “C5-89G03”

The second UO_2-Gd_2O_3 PWR-SNF sample retrieved from the Ohi Reactor No. 2 Nuclear Power Station, identified as “C5-89G03”, was reported to have an experimentally determined nuclear depletion level of 28.717 GWd/t_{HM} [96]. However, the nuclear depletion achieved by the definitive SERPENT-2 simulation process – following the normalisation of the neodymium-148 isotope concentration – was lower, reaching 28.347 GWd/t_{HM} (*i.e.* corresponding to the depletion deficit of 1.28773897% reported by serpentTools). Figures 29 and 30 illustrate the calculated results of the nuclide inventory in terms of percentage deviations for sample “C5-89G03” of the reported FPs and actinide nuclides, respectively.

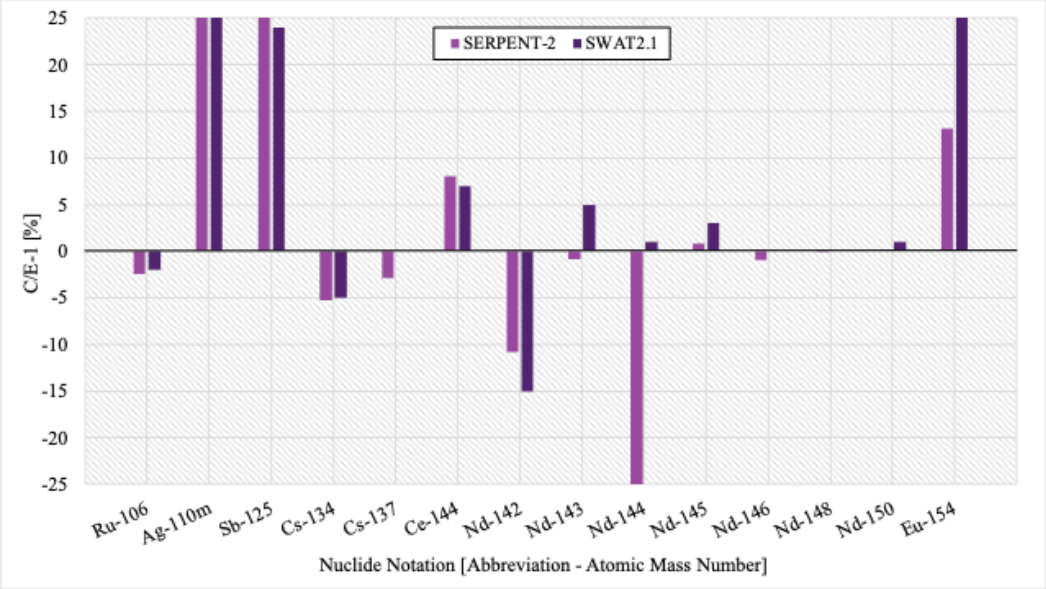

Figure 29: ‘C/E-1’ results of fission product nuclides for the "C5-89G03" sample

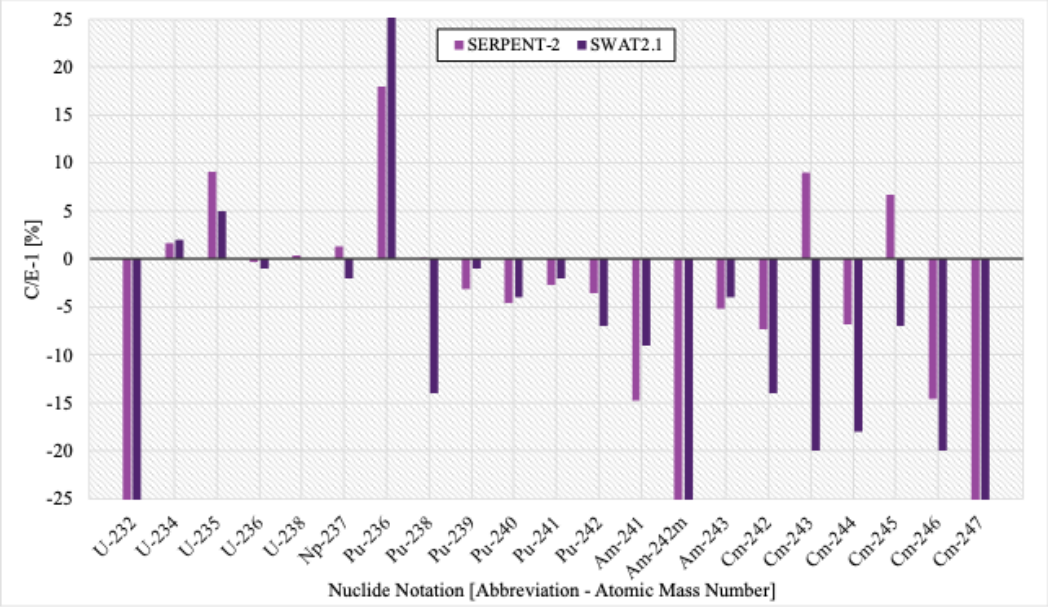

Figure 30: ‘C/E-1’ results of actinide nuclides for the "C5-89G03" sample

4.2.3 ‘C/E-1’ Results for Sample “O13-89G05”

The final UO_2-Gd_2O_3 PWR-SNF sample retrieved from the Ohi Reactor No. 2 Nuclear Power Station, identified as “O13-89G05”, was reported to have an experimentally determined nuclear depletion level of 25.137 GWd/t_{HM} [96]. However, the nuclear depletion achieved by the definitive SERPENT-2 simulation process – following the normalisation of the neodymium-148 isotope concentration – was lower, reaching 24.816 GWd/t_{HM} (*i.e.* corresponding to the depletion deficit of 1.27700203% reported by serpentTools). Figures 31 and 32 illustrate the calculated results of the nuclide inventory in terms of percentage deviations for sample “O13-89G05” of the reported FPs and actinide nuclides, respectively.

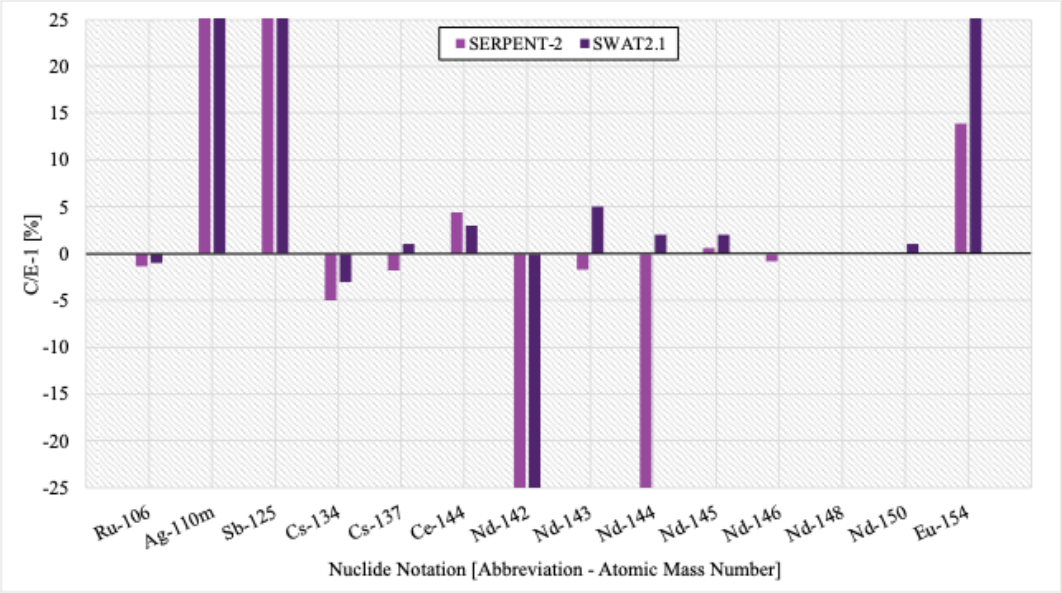

Figure 31: ‘C/E-1’ results of fission product nuclides for the "O13-89G05" sample

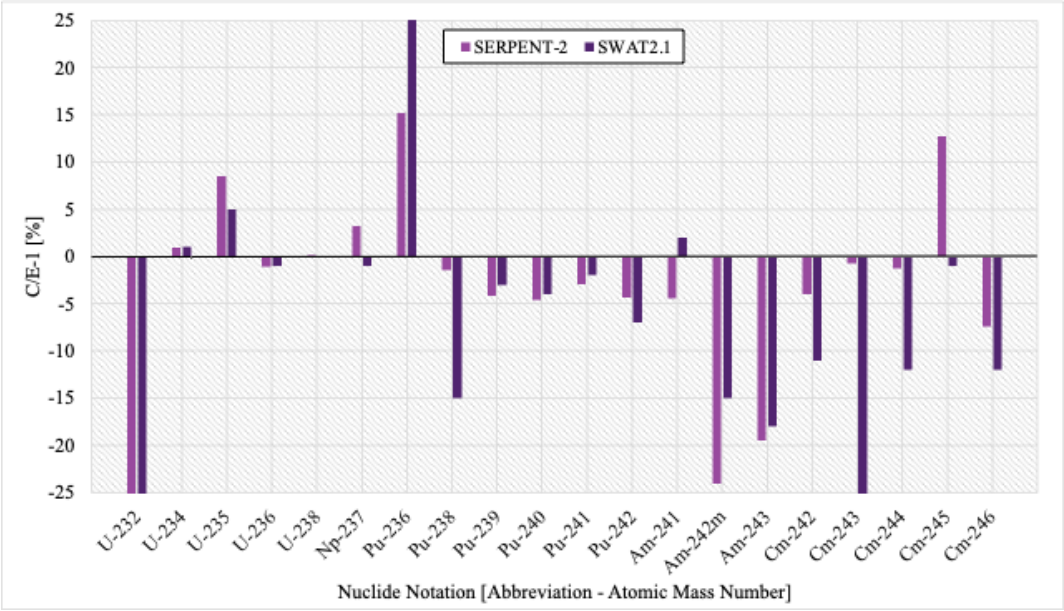

Figure 32: ‘C/E-1’ results of actinide nuclides for the "O13-89G05" sample

4.2.4 Overview ‘C/E’ Results for “C5” and “O13” Samples

Table 22 provides a detailed overview of the sample-specific ‘C/E’ results for the selected nuclides investigated in the comparative analysis of UO_2-Gd_2O_3 PWR-SNF samples simulated by SERPENT-2 and retrieved from the Ohi Reactor No. 2 Nuclear Power Station. Moreover, the numerical sample-specific and sample-average ‘C/E’ results – including the SD – for the alternative depletion calculation code SWAT2.1 are provided in Appendix F.

Table 22: Overview ‘C/E’ results for the "C5" and "O13" samples

Nuclide	C5-89G01	C5-89G03	O13-89G05	Average	SD
Ru-106	0.949354	0.975964	0.986551	0.97	0.02
Ag-110m	1.796986	2.081301	1.966173	1.95	0.14
Sb-125	1.520989	1.553123	1.651705	1.58	0.07
Cs-134	0.951301	0.947594	0.950170	0.95	0.00
Cs-137	0.993844	0.971307	0.981839	0.98	0.01
Ce-144	0.936604	1.080358	1.044128	1.02	0.07
Nd-142	0.980845	0.891884	0.655763	0.84	0.17
Nd-143	0.977298	0.991044	0.983229	0.98	0.01
Nd-144	0.631909	0.653205	0.613546	0.63	0.02
Nd-145	1.003087	1.008608	1.006030	1.01	0.00
Nd-146	0.990035	0.990950	0.991841	0.99	0.00
Nd-148	0.999884	0.999908	1.000360	1.00	0.00
Nd-150	0.998181	1.000196	1.000511	1.00	0.00
Eu-154	1.130222	1.131131	1.138769	1.13	0.00
U-232	0.120622	0.129903	0.123929	0.12	0.00
U-234	1.009971	1.016737	1.009262	1.01	0.00
U-235	1.061546	1.090758	1.085002	1.08	0.02
U-236	1.004273	0.996668	0.989486	1.00	0.01
U-238	1.000973	1.003982	1.001376	1.00	0.00
Np-237	0.978454	1.012903	1.032595	1.01	0.03
Pu-236	1.265517	1.179284	1.152066	1.20	0.06
Pu-238	1.045508	1.000941	0.985395	1.01	0.03
Pu-239	0.970219	0.968361	0.957963	0.97	0.01
Pu-240	0.971233	0.954016	0.953984	0.96	0.01
Pu-241	0.983234	0.972706	0.970485	0.98	0.01
Pu-242	1.004528	0.964214	0.956592	0.98	0.03
Am-241	1.071742	0.852415	0.955278	0.96	0.11
Am-242m	0.900466	0.580157	0.759241	0.75	0.16
Am-243	1.006360	0.948386	0.804960	0.92	0.10
Cm-242	0.990949	0.926701	0.960519	0.96	0.03
Cm-243	1.444482	1.089433	0.993009	1.18	0.24
Cm-244	1.068913	0.931834	0.987748	1.00	0.07
Cm-245	1.197262	1.066444	1.127336	1.13	0.07
Cm-246	0.999749	0.853897	0.925815	0.93	0.07
Cm-247	0.851133	0.714926	N.A.	0.78	0.10

5 Discussion

5.1 Takahama Reactor No. 3 Samples

5.1.1 Sample-average Nuclide Inventory

A sample-average comparative analysis of the calculated nuclide inventories of the UO_2-Gd_2O_3 samples originating from the Takahama Reactor No. 3 with the experimental concentrations, demonstrates that the SERPENT-2 nuclear depletion calculation code yields results that are within 6% of the main uranium – *i.e.* U-234 ('C/E' = 0.94), U-235 ('C/E' = 1.03), U-236 ('C/E' = 0.98), and U-238 ('C/E' = 1.00) – and plutonium reported results (*i.e.* Pu-238 ('C/E' = 1.02), Pu-239 ('C/E' = 1.00), Pu-240 ('C/E' = 1.02), Pu-241 ('C/E' = 1.03), and Pu-242 ('C/E' = 1.06)). It is imperative that the aforementioned actinides be included in the simulated nuclide inventories when introducing the concept of 'burnup credit' in nuclear criticality safety analyses of spent nuclear fuel [85]. Moreover, it is important to consider that should the radioisotopes U-234 and Pu-242 be excluded from the sample-average comparative analysis – of the uranium and plutonium nuclide inventories – the SERPENT-2 code would predict the main uranium and plutonium isotopes to be within 2 to 3% of the experimentally determined results. This suggested isotopic exclusion is based on the observation that the 'C/E' result of the U-234 isotope is considerably dependent on the achieved accuracy of the reported U-234 concentration and the determining method (IDMS) – *i.e.* 1% reported uncertainty margin – provided in the official nuclide inventories [85]. With regard to the suggested exclusion of the plutonium isotope, Pu-242, this specific isotope is considered a 'higher' actinide, which suggests the possibility of propagated uncertainties from the prior actinides being factored into its calculated sample-average isotopic concentration. Therefore, in consideration of the aforementioned obtained sample-average 'C/E' results and the two suggested isotopic exclusions, it can be concluded that the calculated main uranium and plutonium isotope concentrations are in excellent agreement with the experimental measurements. Furthermore, these sample-average calculated actinide concentrations are considerably more accurate than those obtained through the alternative nuclear depletion calculation codes, with a reported sample-average discrepancy for the main uranium and plutonium isotopes of 10% for both codes, SWAT and ORIGEN2.1. The sample-average 'C/E' results for the main uranium and plutonium isotopes of both are presented in §Appendix C and D, respectively.

Upon evaluation of the sample-average calculated nuclide concentrations for the minor actinides (MAs) – *i.e.* Np, Am, and Cm isotopes – it becomes apparent that the obtained concentration differences are more significant than those observed in the calculated concentrations of the main uranium and plutonium isotopes, with sample-average deviations exceeding 50% for neptunium – *i.e.* Np-237 ('C/E' = 1.51) – and 20% for both Am-241 and metastable Am-242m (*i.e.* 'C/E' = 1.24 and 'C/E' = 0.80, respectively). However, the curium isotopes – of which Cm-244 is the principal source of the short-term (t < 100 y) neutron-emitting properties of irradiated spent fuel [107] – demonstrate sample-average differences of less than 10% (3% and 10%, respectively). Moreover, the aforementioned significant MA deviations in the sample-average neptunium and americium concentrations are similarly reported in the SWAT and ORIGEN2.1 calculated nuclide inventories, with their respective sample-average deviations exceeding 40% and 25%. A further in-depth analysis is performed to identify the principal factors responsible for the significant sample-average concentration differences observed in the MAs' nuclide inventories. It is first important to note that the observed over-accumulation of Am-241 is a direct consequence of the radioactive β decay production path from the fissile plutonium isotope, Pu-241 (*i.e.* mother nuclide).

The calculated concentration of Pu-241, however, appears to be in close agreement with the anticipated value, *i.e.*, 3% over-accumulated. It may therefore be presumed that the utilised nuclear decay data specific to Pu-241 – and therefore the decay data of the production path to Am-241 – does not accurately reflect the physical decay process. However, this argument is rendered invalid by the well-documented and highly accurate nature of the specific nuclear decay data. An alternative and more reasonable explanation for the observed discrepancy is that an irregularity may have occurred during the destructive RCA experiments, as detailed in Table 23. This irregularity could potentially be attributable to the different analytical techniques employed for determining Pu-241 – *i.e.* Isotope Dilution Mass Spectrometry (IDMS) – and Am-241 concentrations (*i.e.* Mass Spectrometry (MS)). Nevertheless, the reported measuring uncertainties of both determining methods – *i.e.* 0.3% and 2%, respectively – are insufficient as a standalone argument to attribute the significant discrepancy to. It can therefore be concluded that a notable irregularity must have occurred during the concentration measurements. Furthermore, in consideration of the aforementioned sample-average discrepancy in the concentration of Am-241 (+24%) it is possible to elucidate the opposite tendency in Am-242m's (-20%) accumulation (*i.e.* over versus under-accumulation) by postulating that the Am-241's specific nuclear interaction data (*i.e.* radiative neutron capture) would appear to be erroneous. However, it is more plausible to suggest that the specific nuclear interaction data – of Am-241 – are accurate and that the aforementioned major measurement irregularity argument is valid. This identical justification based on the potential major irregularity that may have occurred during the determining measurements of Am-241 would suggest that the experimental concentrations of Am-241 should be greater, thereby reducing its corresponding 'C/E' value and perhaps even resulting in an under-accumulated 'C/E' value, similarly to the tendency observed in the metastable americium isotope, Am-242m. This irregularity justification would in addition provide an explanation for the noteworthy occurrence of the opposite accumulation tendencies. Lastly, the observed sample-average differences in the later MA, curium (maximum deviation of +10%), can be attributed to the accumulation of its isotopes – *i.e.* Cm-242 and Cm-244 – occurring at later stages in the depletion process of the UO_2-Gd_2O_3 nuclear fuel (*i.e.* the propagation of the prior MAs' relative discrepancies, and thereby the potential for factoring them into curium's calculated concentrations).

The isotopic evaluation of the sample-average calculated nuclide inventories for the reported FPs reveals that SERPENT-2 produces isotopic concentrations for the included caesium and neodymium isotopes, with an accuracy of 3% and 4%, respectively (with the exception of the neodymium isotope, Nd-144). Both mentioned chemical elements contain a number of 'depletion indicator' isotopes – *i.e.* Cs-134 ('C/E' = 0.99) and Cs-137 ('C/E' = 1.03), as well as Nd-148 (C/E = 1.00) – which are frequently utilised for the experimental determinations of nuclear fuel depletion (see §2.2.5 Experimental Burnup Monitor – Neodymium-148). In consideration of the aforementioned FP-specific concentration accuracies, and the reference to the presence of 'depletion indicators' – with a margin of uncertainty of 0.1% – it can be concluded that the complete sample-average calculated nuclide inventory by SERPENT-2 provides a reliable estimation of the physical depletion processes occurring in the PWR-UO_2-Gd_2O_3 nuclear fuels. It is important to acknowledge, however, that the specific FP nuclides, Ru-106, Sb-125, and Eu-154 diverge considerably from their anticipated concentrations, with sample-average discrepancies reaching +38%, +141%, and +26%, respectively. Following this notable observation, the official documentation [89] suggests that the significant sample-average discrepancies in these aforementioned FP nuclides can be attributed to their limited solubility in dissolution during the conducted destructive RCA experiments (*i.e.*, in comparison to the non-destructive measurements conducted by JAERI, the respective reported isotopic concentrations appeared to be consistently lower. However, these results were not disclosed).

5.1.2 Sample-specific Nuclide Inventory

Subsequent to the preceding sample-average analysis, a series of sample-specific comparative analyses of the calculated nuclide inventories for the five PWR-UO_2-Gd_2O_3 SNF samples retrieved from the Takahama Reactor No. 3 Nuclear Power Station were performed to investigate and potentially identify the axial cutting positioning dependency – *i.e.* the spatial and coolant temperature dependency – as well as the depletion/burnup (BU) dependency. In these sample-specific nuclide inventory analyses, both the relative 'boundary extremity' samples, namely "SF96-1" and "SF96-5" – *i.e.* sample "SF96-1" is located in close proximity to the top of the active PWR-UO_2-Gd_2O_3 fuel stack, and sample "SF96-5" is located in close proximity to the bottom, although it is relatively less of an extremity (detailed in Table 5) – are evaluated in comparison to the most central sample, "SF96-4" – *i.e.* located at 1,671 mm measured from the bottom of the total active fuel stack, which has a total length of 3,807 mm – and is additionally, also the most depleted UO_2-Gd_2O_3 sample among the five examined. Consequently, due to its central position within the axial direction, "SF96-4" was irradiated with the assembly's axial-average neutron spectrum.

The sample-specific analyses of the main uranium and plutonium isotopes demonstrate that all three aforementioned UO_2-Gd_2O_3 SNF samples exhibit comparable behaviour in regard to uranium isotope accumulation and destruction (sample-specific 'C/E' results are detailed in Table 21). In contrast, the calculated sample-specific plutonium concentrations demonstrate notable discrepancies, with only two out of the three considered samples , *i.e.*, "SF96-4" and "SF96-5", yielding comparable concentrations. It is therefore necessary to perform an additional investigation and comparison of the two 'boundary extremity' samples, specifically "SF96-1" and "SF96-5", in order to identify the factors that differentiate them and thereby ascertain the dependencies of the deviating isotopes. The plutonium isotope-interval 'C/E' results for sample "SF96-1" fall within the range of 1.11 to 1.33, whereas for sample "SF96-5", the 'C/E' results are between 1.00 and 1.08. It should be noted, however, that the determining method for the plutonium concentrations – IDMS – yields results with a margin of uncertainty of 0.3% to 0.5% (detailed in Table 23). Therefore, it can be concluded that no significant concentration discrepancies can be attributed to measurements made utilising this accurate determining method. Nevertheless, it is evident that the spatial positioning – with regard to the neutron spectrum 'softening' phenomenon – and therefore the observed temperature difference in the coolant medium – 593.05 K for "SF96-1" and 554.28 K for "SF96-5" – are unlikely to be the sole determining factors responsible for these significant sample-specific concentration discrepancies. Given that both aforementioned samples were irradiated with non-average neutron spectra due to their respective positioning, it can be assumed that additional factors/dependencies are involved. Moreover, the two 'boundary extremity' samples have experienced a significantly different level of nuclear depletion. In particular, sample "SF96-1" has been depleted to a relatively low level of 7.79 GWd/t_{HM}, whereas sample "SF96-5" has reached a significantly higher nuclear depletion level of 24.19 GWd/t_{HM}. In consideration of the aforementioned observations, it can be concluded that the degree of nuclear depletion of the sample, and by extension the duration for which the sample was subjected to its associated neutron spectrum, was insufficient for the destruction of all the accumulated plutonium isotopes. Consequently, the inability of sample "SF96-1" to deplete/burn the accumulated plutonium isotopes provides a reasonable explanation for the observed tendency of over-accumulation across all reported plutonium isotopes. Additionally, the observed discrepancies in the sample-specific calculated concentrations of the preceding plutonium isotopes will contribute/propagate to respective deviations in the subsequent plutonium isotopes and ultimately in the 'higher' actinides, such as Am and Cm. The "SF96-1" plutonium discrepancies are: +28%, +22%, +11%, +33%, and +28%.

Following an evaluation of the sample-specific calculated nuclide concentrations for the MAs, it can be concluded that – although a major irregularity is assumed to have occurred during the performed RCA experiments for the specific MA, americium-241 (detailed in §5.1.1 Sample-average Nuclide Inventory) – the two 'boundary extremity' samples, "SF96-1" and "SF96-5", demonstrate similar behaviour, *i.e.*, a significantly higher degree of over-accumulation of Am-241 in comparison to the most central sample (+74% and +36%, respectively, in contrast to a near-perfect accumulation of +2% for "SF96-4"). This sample-specific observation regarding the over-accumulation tendency in Am-241 indicates that the spatial positioning – specifically in the axial direction – and consequently the associated exposed neutron spectra, exert a significant influence on the respective accumulations. Moreover, a comparable trend is identified in an alternative americium isotope, Am-243, which suggests that this aforementioned over-accumulation tendency is consistent across all reported americium isotopes, albeit to a lesser extent (+56% and +13%, respectively, in contrast to a near-perfect accumulation of +2% in sample "SF96-4"). Furthermore, the later MA, curium and its isotopic concentrations demonstrate similar behaviour to that observed in the plutonium and americium concentrations, depending on the specific Cm isotope under consideration. To elaborate further, the sample-specific concentrations of Cm-242 appear to reflect the same tendencies observed in the plutonium isotopes, *i.e.*, an observed over-accumulation that is limited to the relatively low depleted sample, "SF96-1" (+31% in comparison to a perfect calculation, *i.e.*, +0%). It must be acknowledged that the margin of uncertainty in MS for Cm-242 is relatively high, at 10%. While the sample-specific concentrations of Cm-244 appear to align with the observed behaviour of the americium isotopes, *i.e.*, a significantly higher degree of over-accumulation in the 'boundary extremity' samples (+76% and +17%, respectively, in comparison to +3% in the most central sample, with a low MS uncertainty margin of 2%, indicating the considerable nature of the Cm-244 discrepancies). In light of these discrepancies and the associated MS accuracy, it is important to note that additional monitoring is advised for Cm-244, as it is the principal source of the short-term (t < 100 y) neutron-emitting properties of irradiated spent fuel [107]. The discrepancies in Np-237 are consistent across all samples.

5.2 Ohi Reactor No. 2 Samples

5.2.1 Sample-average Nuclide Inventory

The sample-average isotopic evaluation of the calculated nuclide inventories of the three UO_2-Gd_2O_3 samples retrieved from the Ohi Reactor No. 2 Nuclear Power Station indicates that the SERPENT-2 code yields sample-average 'C/E' results for the reported main uranium and plutonium isotopes with concentration accuracies of 8% and 4%, respectively. However, the aforementioned statement is reliant upon the isotopic exclusion of the challenging-to-measure and short-lived U-232 isotope (*i.e.* U-234 ('C/E' = 1.01), U-235 ('C/E' = 1.08), U-236 ('C/E' = 1.00), U-238 ('C/E' = 1.00); and for plutonium, Pu-238 ('C/E' = 1.01), Pu-239 ('C/E' = 0.97), Pu-240 ('C/E' = 0.96), Pu-241 ('C/E' = 0.98), and lastly Pu-242 ('C/E' = 0.98)). The aforementioned isotopic exclusion of U-232 becomes evident upon further analysis of the particular isotope's sample-average 'C/E' result, which is equal to 0.12 and is therefore considered to be unsuitable for additional uranium isotope analyses. However, it is important to consider that the alternative nuclear depletion calculation code, SWAT2.1, similarly reports a comparable low 'C/E' result of 0.14 [96] ('C/E' results detailed in §Appendix F). The justification for this significant sample-average discrepancy in U-232's concentration is that its occurrence may be attributed to the inherent challenging-to-measure nature of the specific U isotope. Additionally, given that the margin of uncertainty of IDMS is 1.6%, it can be concluded that the deviation cannot be attributed to the method.

Moreover, the maximum concentration discrepancy between the sample-average uranium isotopes, is observed in uranium-235. The slight elevation in the predicted uranium-235 concentration of 8% can be attributed to the sample-average depletion deficiency of approximately 1.35% – *i.e.* -1.35% – as reported by serpentTools. To further substantiate this deficiency-induced justification, the sample-average 'C/E' result of plutonium-239 is analysed, which reveals that plutonium-239 is slightly under accumulated (*i.e.* -3%). The accumulation of plutonium-239 is achieved through the radiative capture of thermal neutrons in fertile uranium-238, resulting in the formation of the daughter nuclide, *i.e.*, the short-lived neptunium-239, which in turn, decays via radioactive β decay to produce plutonium-239. In accordance with the aforementioned deficiency-induced justification, it was assumed that the nuclear depletion processes had concluded prematurely, which resulted in insufficient time for the further depletion of uranium-235 and the accumulation of fissile plutonium-239 (hence the under-accumulation tendency observed in Pu-239's sample-average concentrations). In addition, the aforementioned assumption of premature termination provides a plausible explanation for the under-accumulation tendency observed across all later plutonium isotopes, given that their respective accumulation deficiencies are propagated. Nevertheless, in consideration of the obtained uranium and plutonium concentration accuracies and the fact that the significantly divergent concentration of U-232 is independent of the employed depletion calculation code, it can be concluded that the calculated sample-average uranium and plutonium concentrations are in satisfactory agreement to the experimental data (with a 0.5% uncertainty margin).

Furthermore, a comparative analysis of the sample-average nuclide inventory results for the MAs with the experimentally determined concentrations reveals a satisfactory degree of correspondence between the simulated concentrations and the experimental data. To elaborate, the sample-average discrepancies in concentration for each MA element are summarised as follows: 1% for neptunium (*i.e.* ('C/E' = 1.01); 8% for both the non-isomeric americium isotopes (*i.e.* Am-241 ('C/E' = 0.96), Am-243 ('C/E' = 0.92)); and approximately 15% divergence for the curium isotopes. An additional relative analysis between the sample-average nuclide inventories simulated by SERPENT-2 and SWAT2.1 demonstrates that the alternative depletion calculation code produces comparable sample-average concentrations, with MA accuracies of 3%, 7%, and 15%, respectively [96]. The slight under-accumulation of the non-isomeric americium isotopes (-8%) can be attributed to the overall under-accumulation tendencies of the later plutonium isotopes. This under-accumulation tendency occurs because both Am-241 and Am-243 are formed directly through radioactive β decay in the plutonium isotopes, Pu-241 and Pu-243, respectively. It is important to note that the sample-average 'C/E' result for the metastable nuclear isomer, Am-242m, consistently yields a significant deviation of +25% in comparison with the anticipated concentration. However, this notable Am-241 observation is consistent with the sample-average 'C/E' results obtained for the UO_2-Gd_2O_3 samples retrieved from the Takahama Reactor No. 3 and with the reported results of the alternative depletion calculation code SWAT2.1 ('C/E' results detailed in §Appendix F). In order to conclude the sample-average analysis of the MAs, an investigation of the reported curium isotopes is presented. Overall, the curium isotopes are in excellent agreement with the experimental measurements, with Cm-242, Cm-244, and Cm-246 differing by -4%, +0%, and -7%, respectively. The highly accurate prediction of the aforementioned curium isotopes indicates that no further monitoring is necessary with regard to the neutron-emitting properties of irradiated spent fuel, in which Cm-244 is the principal source in the short term (t < 100 y) and Cm-246 in the medium term (t > 100 y). In contrast, Cm-243, Cm-245, and Cm-247's concentrations deviate significantly, amounting to +18%, +13%, and -22%, respectively. However, the margin of uncertainty associated with Cm-243 is considerable, reaching 19% for the MS method. Nevertheless, this is not the case for the other isotopes, with an uncertainty of 1.3% and 1.1%.

Lastly, in the comparative process of the calculated sample-average concentrations for the reported FP nuclides, the SERPENT-2 depletion calculation code produces caesium and neodymium results with an accuracy of 5% and 2%, respectively, when the neodymium isotopes, Nd-142 and Nd-144, are excluded. The excluded neodymium isotopes, however, exhibit significant deviations, with under-accumulation tendencies reaching -16% and -37%, respectively. It is important to note, however, that the alternative depletion calculation code, SWAT2.1, also exhibits a comparable discrepancy for the aforementioned excluded isotope, Nd-142 (*i.e.* 'C/E' = 0.78) [96]. In contrast, for the latter neodymium isotope, Nd-144, SWAT2.1 produces an excellent sample-average 'C/E' result of 1.01 (*i.e.* +1%), indicating the necessity for further investigation into this discrepancy in the SERPENT-2 nuclide inventory. With regard to the deviation of the neodymium-142 isotope, the IDMS determining method yields concentrations with a margin of uncertainty of 0.5%, and therefore cannot be held attributable for the notable discrepancy. However, given that SWAT2.1 also exhibits a significant deviation for Nd-142, it is plausible that an irregularity may have occurred during the experimental measurements (since Nd-142 is produced exclusively through induced fissions and the associated nuclear fission data is well-documented and highly accurate, this cannot be proposed as a potential explanation, thereby indicating another reason). Furthermore, the remaining FP nuclides, specifically Ru-106, Ag-110m, Sb-125, and Eu-154, yield significantly lower deviating sample-average concentrations in comparison to the previous sample-average discrepancies observed in the UO_2-Gd_2O_3 samples retrieved from the Takahama Reactor No. 3. The observed discrepancies amount to -3%, +95%, +58%, and +13%, in contrast to +38%, +141%, and +26%, respectively. It is important to note, however, that the metastable Ag110m (+95%) was not included in the analysis of Takahama Reactor No. 3 and therefore cannot be compared relatively.

5.2.2 Sample-specific Nuclide Inventory

Following the preceding sample-average analysis, a series of sample-specific comparative analyses of the calculated nuclide inventories for the three PWR-UO_2-Gd_2O_3 SNF samples retrieved from the Ohi Reactor No. 2 Nuclear Power Station were performed to investigate and potentially identify the axial cutting positioning dependency – *i.e.* the spatial and coolant temperature dependency – as well as the depletion/burnup (BU) dependency. It should be noted, however, that the obtained Ohi Reactor No. 2 SNF samples were axially located in close proximity to each other. As a result, no significant spatial dependencies can be identified. Additionally, the samples were also depleted to a comparable level, *i.e.*, with nuclear depletion levels varying between 21.465 GWd/t_{HM} and 28.347 GWd/t_{HM}. Nevertheless, there are sample-specific concentration discrepancies which require further investigation, particularly with regard to the nuclide inventories of the MAs. A comparison of the nuclide inventory of the least depleted sample, "C5-89G01", with that of the most depleted sample, "C5-89G03", reveals a significant sample-specific discrepancy with regard to Am-241. In particular, there is a notable over-accumulation tendency – "C5-89G01" – in comparison to an under-accumulation tendency ("C5-89G03"). A potential factor is the depletion level difference between the samples, although the respective plutonium-241 concentrations are accurate to within 2 and 3%, respectively. A similar discrepancy is observed in the sample-specific concentrations of Am-242m, and to a lesser degree in the concentrations of Am-243. This is a comparable observation as in Takahama Reactor No. 3's sample-specific nuclide inventories. With regard to the curium isotopes, they exhibit the same behaviour as americium, given that they are 'higher' actinides and therefore the prior actinides discrepancies are factored into their calculated concentrations. Lastly, it is noteworthy that for the reported FP nuclides, the significant sample-average discrepancy in Nd-142, is accurate for sample "C5-89G01', with a margin of uncertainty of 0.52%.

6 Conclusion

In conclusion, this master's thesis has investigated the predictive capabilities of the three-dimensional continuous-energy Monte Carlo neutron and photon transport code, SERPENT-2, in the context of relatively low-doped UO_2-Gd_2O_3 SNF samples, which was part of its validation and verification process. The increasing international adoption of depletion calculation codes to predict the nuclide inventories of irradiated commercial fuels, becomes evident from an economical, technical, and safety perspective. Moreover, with the latest technological developments in PWR assembly designs, the accurate prediction of the nuclide inventories and power distributions throughout the entire irradiation period has a more significant impact on the predicted fuel performance. It was therefore, that eight earlier design PWR UO_2-Gd_2O_3 SNF samples with a natural gadolinia enrichment of 6.00 wt% were selected and modelled utilising the SERPENT-2 depletion calculation code. Subsequently, the predicted nuclide inventories were analysed in comparison with JAERI-reported experimental data obtained through destructive RCA experiments. In addition, the calculated nuclide inventories by SERPENT-2 were compared relatively with alternative depletion calculation codes, *i.e.*, SWAT and ORIGEN2.1. Five UO_2-Gd_2O_3 samples were obtained from the Kansai Electric Power Co. Takahama Reactor No. 3 Nuclear Power Station, and three were sourced from the Kansai Electric Power Co. Ohi Reactor No. 2 Nuclear Power Station. The former nuclear power station, serving as an international benchmark provided well-available documents, in contrast to the relatively lesser-studied Ohi Reactor No. 2. Nevertheless, for both nuclear power stations, the geometrical assembly configurations, initial isotopic UO_2 fuel compositions, and cycle-specific operating histories are compiled in the publicly available "SFCOMPO-2.0" database.

The predicted nuclide inventories by SERPENT-2 for the PWR-UO_2-Gd_2O_3 SNF samples retrieved from the Takahama Reactor No. 3 demonstrated a satisfactory to excellent degree of correlation with the reported experimental concentrations, contingent upon the isotope under consideration. In the case of the main actinide nuclides, the SERPENT-2 code yielded more accurate results on average than both alternative depletion calculation codes. However, for the specific MA isotopes, Am-241 and its isomer Am-242m, SERPENT-2 yielded inconsistent concentrations, which are hypothesised to be due to a significant irregularity occurring during the MS analytical determining method. Moreover, with respect to the FP nuclides, an excellent correlation was observed, with the exception of Ru-106, Sb-125, and Eu-154. However, the official documentation stated that the concentrations determined through destructive RCA were not representative when compared with those obtained through non-destructive techniques. With regard to the predicted nuclide inventories by SERPENT-2 for the Ohi Reactor No. 2, a similar degree of correlation was observed with the reported experimental results, although this was contingent on the assumption of premature termination of the nuclear depletion processes, *i.e.*, depletion deficiency. Furthermore, the SERPENT-2 results exhibited a considerable degree of consistency for the main actinides, with the exception of the relatively short-lived uranium isotope, U-232. Nevertheless, SWAT2.1 reported a comparatively low concentration for U-232. With regard to the MAs, the calculated results were considered to be in satisfactory agreement, due to propagated deviations in prior isotopes. To conclude, the predicted FP nuclide inventory was in excellent agreement to the experimental data.

In consideration of the aforementioned conclusions regarding the predicted nuclide inventories and the isotopic accuracies, it can be postulated that the SERPENT-2 depletion calculation code is a reliable and consistent instrument, thereby justifying its potential employment in the context of simulating depletion processes in commercial PWR-UO_2-Gd_2O_3 fuels with a relatively low degree of natural gadolinia.

Upon completion of this master's thesis, a variety of recommendations for future consideration can be presented. Firstly, an additional characterisation assignment could entail the modelling and simulation of a different reactor technology type that utilises urania-gadolinia-doped fuels, *i.e.*, BWR-UO_2-Gd_2O_3. A second proposal is the prediction of the nuclide inventory for a MOX-Gd_2O_3 nuclear fuel composition. The final recommendation for additional investigation into the predictive capabilities of SERPENT-2, would be – once the requisite data becomes publicly available – to model more recent PWR assembly designs in which gadolinia is more prevalent, *i.e.*, nuclear fission fuels with an initial isotopic composition of more than 6.00 wt% of natural gadolinia, as was the standard in this performed research.

References

[1] P. Lang, "Impact of extended burnup on the nuclear fuel cycle," IAEA, Vienna, Austria, Tech. Rep. Ser. *IAEA-TECDOC-699*, Apr. 1993.

[2] O. Bernander, P. Duflou, R. von Jan, P. Lang, and F. Pazdera, "Water Reactor Fuel Extended Burnup Study," IAEA, Vienna, Austria, Tech. Rep. Ser. *IAEA-TECDOC-343*, Nov. 1992.

[3] M. Durazzo et al., "Sintering behavior of UO_2-Er_2O_3 mixed fuel," *J. Nucl. Mater*, vol. *510*, pp. *603-612*, Nov. 2018, doi: *10.1016/j.jnucmat.2018.08.051*.

[4] H. Bairiot, D. Farrant, and V. Onufriev, "Characteristics and use of Urania-gadolinia fuels," IAEA, Vienna, Austria, Tech. Rep. Ser. *IAEA-TECDOC-844*, Nov. 1995.

[5] J. A. Evans, D. D. Keiser Jr, M. D. DeHart, and K. D. Weaver, "Burnable Absorbers in Nuclear Reactors – A Review," INL, Idaho Falls, ID, USA, Rep. *INL/JOU-21-61443*, May 2022.

[6] E. H. Uguru, S. F. A. Sani, M. U. Khandaker, M. H. Rabir, and J. A. Karim, "A comparative study on the impact of Gd_2O_3 burnable neutron absorber in UO_2 and (U, Th)O_2 fuels," *Nucl. Eng. Technol*, vol. *52*, no. *6*, pp. *1099-1109*, June 2020, doi: *10.1016/j.net.2019.11.010*.

[7] M. Schlieck, H. D. Berger, and A. Neufert, "Optimized gadolinia concepts for advanced in-core fuel management in PWRs," *Nucl. Eng. Des*, vol. *205*, no. *2*, pp. *191-198*, Mar. 2001, doi: *10.1016/S0029-5493(00)00355-1*.

[8] R. Manzel and W. Dörr, "Manufacturing and irradiation experience with UO_2-Gd_2O_3 fuel," *Am. Ceram. Soc. Bull*, vol. *59*, no. *6*, pp. *601-603*, 1980.

[9] J. Eysermans et al., "REGAL International Program: Analysis of experimental data for depletion code validation," *Ann. Nucl. Energy*, vol. *172*, July 2022, Art. no. 109057, doi: *10.1016/j.anucene.2022.109057*.

[10] J. R. Lamarsh and A. J. Baratta, "Atomic and Nuclear Physics: Binding Energy," in *Introduction to Nuclear Engineering*, D. A. George, Ed., Upper Saddle River, NJ, USA: Prentice Hall, 2001, ch. *2*, pp. *29-33*.

[11] Boston University. (2024). Stability. [Online]. Available: http://physics.bu.edu/~duffy/sc546_notes10/stability.html.

[12] P. Baeten. (2022). Reactor Technology: Neutron Physics [PowerPoint slides]. Unpublished.

[13] J. R. Lamarsh and A. J. Baratta, "Interaction of Radiation with Matter: Fission," in *Introduction to Nuclear Engineering*, D. A. George, Ed., Upper Saddle River, NJ, USA: Prentice Hall, 2001, ch. *3*, pp. *74-90*.

[14] G. Van den Eynde. (2024). Reactor Physics: Introduction [PowerPoint slides]. Unpublished.

[15] K. Sahasrabuddhe. (2010). Nuclear Breeding. [Online]. Available: http://large.stanford.edu/courses/2010/ph240/sahasrabuddhe2.

[16] H. J. Krappe, and K. Pomorski, "Fission Dynamics," in *Theory of Nuclear Fission*. Berlin, Germany: Springer, 2021, ch. *5*, pp. *207-294*.

[17] A. C. Wahl, "Mass and Charge Distribution in Low-energy Fission." presented at the *Symp. on Physics and Chemistry of Fission*, Salzburg, Austria, Mar. 22-26, 1965, pp. *317-331*.

[18] K. S. Krane, "Nuclear Reactions: Reaction Cross Sections," in *Introductory Nuclear Physics*, R. McConnin, Ed., New York, NY, USA: Wiley, 1987, ch. *11*, pp. *392-395*.

[19] European Organization for Nuclear Research. (2023). The Cross-Section. [Online]. Available: https://indico.cern.ch/event/145296/contributions/1381140/attachments/136908/194248/lecture10.

[20] E. Musacchio-González et al., “Maxwell-Boltzmann-like neutron spectrum production for Maxwellian averaged cross sections measurements,” *NIM-A*, vol. *1063*, June 2024, Art. no. *169255*.

[21] K. S. Krane, “Basic Concepts: Units and Dimensions,” in *Introductory Nuclear Physics*, R. McConnin, Ed., New York, NY, USA: Wiley, 1987, ch. *1*, pp. *7-8*.

[22] International Bureau of Weights and Measures. “barn.” metricsystem.net. Accessed: Apr. 3, 2024. [Online]. Available: https://metricsystem.net/non-si-units/other-non-si-units/barn/.

[23] J. K. Shultis and R. E. Faw, “Radiation Interactions with Matter: Attenuation of Charged Particles,” in *Fundamentals of Nuclear Science and Engineering*, New York, NY, USA: Marcel Dekker, 2002, ch. *7*, pp. *199-210*.

[24] United States Nuclear Regulatory Commission. “Neutron flux.” nrc.gov. Accessed: Apr. 4, 2024. [Online]. Available: https://www.nrc.gov/reading-rm/basic-ref/glossary/neutron-flux.html.

[25] K. Khattab, H. Omar, and N. Ghazi, “The effect of temperature and control rod position on the spatial neutron flux distribution in the Syrian miniature neutron source reactor,” *Nucl. Eng. Des.*, vol. *236*, no. *23*, pp. *2419-2423*, Dec. 2006, doi: *10.1016/j.nucengdes.2006.03.003*.

[26] K. Burns, D. Wootan, R. Gates, B. Schmitt, and D. M. Asner, “How to Produce a Reactor Neutron Spectrum Using a Proton Accelerator,” *Phys. Procedia*, vol. *66*, 2015, doi: *10.1016/j.phpro.2015.05.060*.

[27] C. Syros, “The linear Boltzmann equation properties and solutions,” *Phys. Rep*, vol. *45*, no. *4*, pp. *211-300*, Sept. 1978, doi: *10.1016/0370-1573(78)90055-8*.

[28] G. Van den Eynde. (2024). Reactor Physics: The Neutron Transport Equation [PowerPoint slides]. Unpublished.

[29] L. Cao, “Neutron transport equation,” in *Deterministic Numerical methods for Unstructured-Mesh Neutron Transport Calculation*. Amsterdam, The Netherlands: Elsevier, 2021, ch. *1*, pp. *1-34*.

[30] H. Ito et al., “Analysing the neutron and gamma-ray emission properties of an americium-beryllium tagged neutron source,” *NIM-A*, vol. *1057*, Dec. 2023, Art. no. 168701, doi: *10.1016/j.nima.2023.168701*.

[31] Lehman College. (2018). Lecture 7: Gauss’ and Stokes’ Theorems. [Online]. Available: https://www.lehman.edu/faculty/anchordoqui/VC-4.pdf.

[32] L. Pollet, “Validation of ALEPH2 Burn-up Code using Benchmarks from SFCOMPO,” M.S. thesis, Dept. Nucl. Eng., UHasselt & KULeuven, Diepenbeek, Belgium, 2021. Available: http://hdl.handle.net/1942/35061.

[33] Massachusetts Institute of Technology. (2006). Reactor Physics - Lecture 13: Criticality Conditions. [Online]. Available: https://dspace.mit.edu/bitstream/handle/1721.1/74136/22-05-fall-2006/contents/lecture-notes/lecture13.pdf.

[34] G. Van den Eynde. (2024). Reactor Physics: The Six Factor Formula [PowerPoint slides]. Unpublished.

[35] J. R. Lamarsh and A. J. Baratta, “Nuclear Reactors and Nuclear Power: The Fission Chain Reaction,” in *Introduction to Nuclear Engineering*, D. A. George, Ed., Upper Saddle River, NJ, USA: Prentice Hall, 2001, ch. *4*, pp. *117-119*.

[36] K. W. Hesketh, “Burnable Poisons in Nuclear Fuels,” in *Encyclopaedia of Materials: Science and Technology*, 2nd., Amsterdam, The Netherlands: Elsevier, 2002, ch. *1*, pp. *1-8*.

[37] U.S. NRC, Rockville, MD, USA. *General Electric Systems Technology Manual*. (2011). Accessed: Apr. 5, 2024. [Online]. Available: https://www.nrc.gov/docs/ML1125/ML11258A296.pdf.

[38] P. Baeten. (2022). Reactor Technology: Reactivity Coefficients [PowerPoint slides]. Unpublished.

[39] L. Cao, H. Wu, Q. Zhang, Q. He, and T. Zu, "Resonance cross-section processing," in *Resonance Self-Shielding Calculation Methods in Nuclear Reactors*. Amsterdam, The Netherlands: Elsevier, 2023, ch. *2*, pp. *17-62*.

[40] J. R. Lamarsh and A. J. Baratta, "The Time-dependent Reactor: Temperature Effects on Reactivity," in *Introduction to Nuclear Engineering*, D. A. George, Ed., Upper Saddle River, NJ, USA: Prentice Hall, 2001, ch. *7*, pp. *365-376*.

[41] G. Van den Eynde. (2024). Reactor Physics: Dynamics [PowerPoint slides]. Unpublished.

[42] E. M. Pennington et al., "Reactor Physics Constants," ANL, Lemont, IL, USA, Tech. Rep. *ANL-5800*, 1963, Art. no. *4620873*, doi: *10.2172/4620873*.

[43] G. Van den Eynde. (2024). Reactor Physics: Isotopic Changes [PowerPoint slides]. Unpublished.

[44] P. Baeten. (2022). Reactor Technology: Burn up Conversion [PowerPoint slides]. Unpublished.

[45] P. Reuss, "Fuel evolution (heavy nuclei)," in *Neutron Physics*, Les Ulis, France: EDP Sciences, 2008, ch. *12*, pp. *317-336*.

[46] Nuclear Power. "Bateman Equations – Radioactive Decay." nuclear-power.com. Accessed: Apr. 10, 2024. [Online]. Available: https://www.nuclear-power.com/nuclear-power/reactor-physics/atomic-nuclear-physics/radioactive-decay/radioactive-equilibrium/bateman-equations/

[47] J. Cetnar, "General solution of Bateman equations for nuclear transmutations," *Ann. Nucl. Energy*, vol. *33*, no. *7*, pp. *640-645*, May 2006, doi: *10.1016/j.anucene.2006.02.004*.

[48] U.S. Environmental Protection Agency. "Radioactive Decay." epa.gov. Accessed: Apr. 10, 2024. [Online]. Available: https://www.epa.gov/radiation/radioactive-decay.

[49] G. Peetermans, "Dosisafhankelijke effecten van uranium op Arabidopsis thaliana bji pH 7,5," B.S. thesis, Dept. Chem., Katholieke Hogeschool Kempen, Geel, Belgium, 2011. Available: https://roma.sckcen.be/ws/portalfiles/portal/4536889/Dosisafhankelijke_effecten_van_uranium_op_Arabidopsis_thaliana_bij_pH_7_5.pdf.

[50] A. Tsilanizara and T. D. Huynh, "New feature of DARWIN/PEPIN2 inventory code; Propagation of nuclear data uncertainties to decay heat and nuclide density," *Ann. Nucl. Energy*, vol. *164*, Dec. 2021, Art. no. *108579*, doi: *10.1016/j.pnucene.2021.108579*.

[51] B. F. Rider, C. P. Ruiz, J. P. Peterson Jr, and F. R. Smith, "Determination of Neodymium-148 in irradiated Uranium and Plutonium as a Measure of Burnup," *GEAP*, Pleasanton, CA, USA, Rep. *GEAP-5354*, Oct. 30, 1967.

[52] C. Devida, M. Betti, P. Peerani, E. H. Toscano, and W. Goll, "Quantitative Burnup Determination: A Comparison of Different Experimental Methods," in *HOTLAB*, Halden, Norway, Sep. 06-08, 2004, pp. *106-113*.

[53] A. Fudge, J. Wood, and M. F. Banham, "The Determination of Burnup in Nuclear Fuel Test Specimens Using Stable Fission Product Isotopes and Isotopic Dilution," *USAEC*, Washington, DC, USA, Rep. *TID-7629*, Oct. 1961.

[54] B. F. Rider, C. P. Ruiz, J. P. Peterson Jr, and F. R. Smith, "Accurate Nuclear Fuel Burnup Analyses XVI," *GEAP*, Pleasanton, CA, USA, Rep. *GEAP-5060*, 1965.

[55] T. T. Vandergraaf, L. M. Carefoot, and D. G. Boase, “Burnup Determination of Nuclear Fuels using Neodymium-148,” *AECL*, Pinawa, MB, Canada, Rep. *AECL-5964*, June 1978.

[56] *Standard Test Method for Atom Percent Fission in Uranium and Plutonium Fuel (Neodymium-148 Method)*, ASTM E321–96, 2012. [Online]. Available: https://www.astm.org/e0321-96r12.html.

[57] B. F. Rider, C. P. Ruiz, J. P. Peterson Jr, and F. R. Smith, “Accurate Nuclear Fuel Burnup Analyses XX,” *GEAP*, Pleasanton, CA, USA, Rep. *GEAP-5403*, 1966.

[58] P. Baeten. (2022). Reactor Technology: Reactor Control [PowerPoint slides]. Unpublished.

[59] D. Gosset and B. Kryger, “Boron and Hafnium Base Absorbers for Advanced PWR Control Rods,” IAEA, Vienna, Austria, Tech. Rep. Ser. *IAEA-TECDOC-813*, July 1995.

[60] J. R. Lamarsh and A. J. Baratta, “The Time-dependent Reactor: Control Rods and Chemical Shim,” in *Introduction to Nuclear Engineering*, D. A. George, Ed., Upper Saddle River, NJ, USA: Prentice Hall, 2001, ch. *7*, pp. *348-365*.

[61] M. Eissa, M. Naguib, and A. Badawi, “PWR control rods position monitoring,” *Ann. Nucl. Energy*, vol. *81*, pp. *106-116*, July 2015, doi: *10.1016/j.anucene.2015.03.011*.

[62] H. K. Louis, R. M. Refeat, and M. I. Hassan, “Control rod shadowing effect in PWR core utilizing Urania-Gadolinia fuel,” *Prog. Nuclear Energy*, vol. *142*, Dec. 2021, Art. no. *103993*, doi: *10.1016/j.pnucene.2021.103993*.

[63] U.S. Department of Energy, “Module 4: Reactor Theory (Reactor Operations),” in *DOE Fundamentals Handbook: Nuclear Physics and Reactor Theory*, Springfield, VA, USA: DOE, 2015.

[64] M. A. Schultz, *Control of Nuclear Reactors and Power Plants*, New York, NY, USA: McGraw-Hill, 1961.

[65] H. W. Schmitt, R. C. Block, and R. L. Bailey, “Total neutron cross section of B-10 in the thermal neutron energy range,” *Nucl. Phys. A.*, vol. *17*, pp. *109-115*, July 1960, doi: *10.1016/0029-5582(60)90105-X*.

[66] Nuclear Power. “Boric Acid – Chemical Shim.” nuclear-power.com. Accessed: Apr. 13, 2024. [Online]. Available: https://www.nuclear-power.com/glossary/boron-10/boric-acid-chemical-shim/.

[67] Metrohm Applikon, “Nuclear Power Plants: Analysis of Boric Acid in cooling water PWRs,” Metrohm Applikon, Schiedam, The Netherlands, Rep. *AN-PAN-1013*. Accessed: 15 Apr. 2024. [Online]. Available: https://www.metrohm.com/an-p/an-pan-1013.

[68] J. R. Lamarsh and A. J. Baratta, “The Time-dependent Reactor: Core Properties during Lifetime,” in *Introduction to Nuclear Engineering*, D. A. George, Ed., Upper Saddle River, NJ, USA: Prentice Hall, 2001, ch. *7*, pp. *389-397*.

[69] G. Leinweber et al., “Neutron Capture and Total Cross Section Measurements and Resonance Parameters of Gadolinium,” *LMT*, Schenectady, NY, USA, Rep. *LM-05K106*, June 2005.

[70] P. Čudrnák and V. Nečas, “Optimized gadolinium fuel assemblies for light water reactors,” presented at the 10th Int. Sci. Conf. on Power Eng., Tatranské Matliare, High Tatras, Slovak Republic, June 7-9, 2011.

[71] J. Leppänen, “2.2 Serpent Monte Carlo Reactor Physics Code,” in 20th *Symp. On VVER Reactor Physics and Reactor Safety*, Espoo, Finland, Sept. 20-24, 2010.

[72] J. Leppänen, M. Pusa, T. Viitanen, V. Valtavirta, and T. Kaltiaisenaho, “The Serpent Monte Carlo code: Status, development and applications in 2013,” *Ann. Nucl. Energy*, vol. *82*, pp. *142-150*, Aug. 2015, doi: *10.1016/j.anucene.2014.08.024*.

[73] W. Haeck and B. Verboomen, "An optimum approach to Monte Carlo burnup," *NSE*, vol. *156*, no. *2*, pp. *180-196*, Jun. 2007, doi: *10.13182/NSE07-A2695*.

[74] O. Calvin, S. Schunert, and B. Ganapol, "Global error analysis of the Chebyshev rational approximation method," *Ann. Nucl. Energy*, vol. *150*, no. *7*, Aug. 2020, Art. no. *107828*, doi: *10.1016/j.anucene.2020.107828*.

[75] A. Isotalo and P. Aarnio, "Comparison of depletion algorithms for large systems of nuclides," *Ann. Nucl. Energy*, vol. *38*, no. *3*, pp. *261-268*, Mar. 2011, doi: *10.1016/j.anucene.2010.10.019*.

[76] M. Pusa, "Numerical methods for nuclear fuel burnup calculations," Ph.D. dissertation, Dept. Science, Aalto Univ., Espoo, Finland, 2013.

[77] A. Isotalo and P. Aarnio, "Substep methods for burnup calculations with Bateman solutions," *Ann. Nucl. Energy*, vol. 38, no. 9, pp. *1987-1995*, Sept. 2011, doi: *10.1016/j.anucene.2011.04.022*.

[78] F. Michel-Sendis et al., "SFCOMPO-2.0: An OECD NEA database of spent nuclear fuel isotopic assays, reactor design specifications, and operating data," *Ann. Nucl. Energy*, vol. *110*, pp. *779*-788, Dec. 2017, doi: *10.1016/j.anucene.2017.07.022*.

[79] F. Michel-Sendis, "Evaluation Guide for the Evaluated Spent Nuclear Fuel Assay Database (SFCOMPO)," OECD-NEA, Paris, France, Rep. *NEA/NSC/R(2015)8*, Feb. 2016.

[80] C. Alejano, "Spent Nuclear Fuel Assay Data for Isotopic Validation," OECD-NEA, Paris, France, Rep. *NEA/NSC/WPNCS/DOC(2011)5*, June 2011.

[81] Nuclear Energy Agency (NEA). (2024). Database of measured isotopic concentrations of spent nuclear fuel, with operational histories and design data. [Online]. Available: https://www.oecd-nea.org/jcms/pl_21515/sfcompo-2-0-spent-fuel-isotopic-composition.

[82] G. Ilas, I. Gauld, P. Ortego, and S. Tsuda, "SFCOMPO Database of Spent Nuclear Fuel Assay Date – The Next Frontier," in *PHYSOR*, Cambridge, UK, Mar. 29 – Apr. 2, 2020.

[83] M. B. Chadwick et al., "ENDF/B-VII.1 Nuclear Data for Science and Technology: Cross Sections, Covariances, Fission Product Yields and Decay Data," *Nucl. Data. Sheets*, vol. *112*, no. *12*, pp. *2887*-2996, Dec. 2011, doi: *10.1016/j.nds.2011.11.002*.

[84] M. B. Chadwick et al., "ENDF/B-VII.0: Next Generation Evaluated Nuclear Data Library for Nuclear Science and Technology," *Nucl. Data Sheets*, vol. *107*, no. *12*, pp. *2931-3060*, Dec. 2006, doi: *10.1016/j.nds.2006.11.001*.

[85] Y. Nakahara, K. Suyama, and T. Suzaki, "Technical development on burn-up credit for spent LWR fuels," JAERI, Tokyo, Japan, Tech. Rep. *JAERI-TECH--2000-071*, 2000.

[86] IAEA. "Power Reactor Information System: TAKAHAMA-3 Operational." PRIS.IAEA.org. Accessed: Aug. 2, 2024. [Online]. Available: https://pris.iaea.org/PRIS/CountryStatistics/ReactorDetails.aspx?current=354.

[87] S. G. Popov, J. J. Carbajo, V. K. Ivanov, and G. L. Yoder, "Thermophysical Properties of MOX and UO_2 Fuels Including the Effects of Irradiation," ORNL, Oak Ridge, TN, USA, Tech. Rep. *ORNL/TM-2000/351*, 2000.

[88] IAEA - Nuclear Data Section. "Live Chart of Nuclides." nds.iaea.org. Accessed: Apr. 24, 2024. [Online]. Available: https://www-nds.iaea.org/relnsd/vcharthtml/VChartHTML.html.

[89] Y. Nakahara et al., "Nuclide Composition Benchmark Data Set for Verifying Burnup Codes on Spent Light Water Reactor Fuels," *Nucl. Technol.*, vol. *137*, no. *2*, pp. *111-126*, 2002, doi: *10.13182/NT02-2*.

[90] K. Suyama, H. Mochizuki, and T. Kiyosumi, “Revised Burnup Code System SWAT: Description and Validation Using Post-irradiation Examination Data,” *Nucl. Technol.*, vol. *138*, no. *2*, pp. *97-110*, 2002, doi: *10.13182/NT02-A3282*.

[91] Technical Research Centre of Finland, “Surface types.” Serpent.vtt.fi. Accessed: Aug. 2, 2024. [Online]. Available: https://serpent.vtt.fi/mediawiki/index.php/Surface_types

[92] Technical Research Centre of Finland, “Tutorial.” Serpent.vtt.fi. Accessed: Aug. 5, 2024. [Online]. Available: https://serpent.vtt.fi/mediawiki/index.php/Tutorial

[93] Pacific Northwest National Laboratory, “Compendium of Material Composition Data for Radiation Transport Modelling,” PNNL, Richland, WA, USA, Rep. *PNNL-15870*, Rev. 2, Apr. 2021.

[94] Technical Research Centre of Finland, “Input syntax manual.” Serpent.vtt.fi. Accessed: Aug. 5, 2024. [Online]. Available: http://serpent.vtt.fi/mediawiki/index.php/Input_syntax_manual

[95] I. Devold, “A Study of the Temperature Distribution in UO_2 Reactor Fuel Elements,” AE, Stockholm, Sweden, Tech. Rep. *AE-318*, 1968.

[96] K. Suyama, M. Murazaki, K. Ohkubo, Y. Nakahara, and G. Uchiyama, "Re-evaluation of Assay Data of Spent Nuclear Fuel obtained at Japan Atomic Energy Research Institute for validation of burnup calculation code systems," *Ann. Nucl. Energy*, vol. *38*, no. *5*, pp. *930-941*, May 2011, doi: *10.1016/j.anucene.2011.01.025*.

[97] A. H. Harvey, “Thermodynamic Properties of Water: Tabulation from the IAPWS Formulation 1995 for the Thermodynamic Properties of Ordinary Water Substance for General and Scientific Use,” NIST, Boulder, CO, USA, Rep. *NISTIR 5078*, Oct. 1998.

[98] IAEA. “Power Reactor Information System: OHI-2 Permant Shutdown.” PRIS.IAEA.org. Accessed: Aug. 6, 2024. [Online]. Available: https://pris.iaea.org/PRIS/CountryStatistics/ReactorDetails.aspx?current=343.

[99] T. Adachi et al., "Comparison of Calculated Values with Measured Values on the Amount of TRU and FP Nuclides Accumulated in Gadolinium Bearing PWR Spent Fuels," *JNST*, vol. *31*, no. *10*, pp. *1119-1129*, Oct. 1994, doi: *10.1080/18811248.1994.9735266*.

[100] H. Okuno, Y. Naito, and K. Suyama, “OECD/NEA Burn-up Credit Criticality Benchmark Phase III-B Burnup Calculations of BWR Spent Fuel Assemblies in Storage and Transport,” OECD-NEA, Paris, France, Rep. *NEA/NSC/DOC(2002)2*, Feb. 2002.

[101] K. Suyama, T. Iwasaki, and N. Hirakawa, “Integrated burnup calculation code system SWAT,” JAERI, Tokyo, Japan, Tech. Rep. *JAERI-Data/Code-97-047*, 1997.

[102] A. G. Croff, “A User’s Manual for the ORIGEN2 Computer Code,” ORNL, Oak Ridge, TN, USA, Tech. Rep. *ORNL/TM-7174*, 1980.

[103] Y. Kikuchi, “JENDL-3 REVISION-2,” JAERI, Tokai-mura, Japan, Tech. Rep. *IEC-85*, 1994.

[104] K. Suyama, J. Katakura, Y. Ohkawachi, and M. Ishikawa, “Libraries based on JENDL-3.2 for ORIGEN2 code: ORLIBJ32,” JAERI, Tokyo, Japan, Tech. Rep. *JAERI-Data/Code-99-003*, 1999.

[105] K. Suyama, T. Kiyosumi, and H. Mochizuki, “Revised SWAT – The Integrated Burnup Calculation Code System,” JAERI, Tokyo, Japan, Tech. Rep. *JAERI-Data/Code-2000-027*, 2000.

[106] K. Shibata et al., “Japanese Evaluated Nuclear Data Library Version 3 Revision-3,” *J. Nucl. Sci. Technol*, vol. *39*, no. *11*, pp. *1125-1136*, July 2002, doi: *10.1080/18811248.2002.9715303*.

[107] M. Cometto, “Determination of neutron emission from spent fuel for safeguards verification,” B.S. thesis, Dept. Nucl. Eng., SSAS, Roma, Italy, 2011.

List of Appendices

Appendix A: SERPENT-2 Input Code – Takahama Reactor No. 3 Sample “SF96-4” Normalised

```
% --- Takahama Reactor No. 3 Nuclear Power Station (operated by: Kansai Electric Power Co.)
%       Assembly identifier: NT3G23

% --- Information technical reports ALEXANDRIA:
%       (“TAK-001”) [1]  Y. Nakahara, K. Suyama, and T. Suzaki, “Technical development on burn-up credit for spent LWR fuels,” JAERI., Tokyo, Japan, Tech. Rep. JAERI-TECH--2000-071, 2000.
%       (“TAK-002”) [2]  Y. Nakahara et al., “Nuclide Composition Benchmark Data Set for Verifying Burnup Codes on Spent Light Water Reactor Fuels,” Nucl. Technol., vol. 137, no. 2, pp. 111-126, 2002, doi: 10.13182/NT02-2.
%       (“TAK-003”) [3]  K. Suyama, H. Mochizuki, and T. Kiyosumi, “Revised Burnup Code System SWAT: Description and Validation Using Post irradiation Examination Data,” Nucl. Technol., vol. 138, no. 2, pp. 97-110, 2002, doi: 10.13182/NT02-A3282.
%
%       Additional references:
%       [4]  IAEA - Nuclear Data Section. “Live Chart of Nuclides.” nds.iaea.org. Accessed: Apr. 24, 2024. [Online]. Available: https://www-nds.iaea.org/relnsd/vcharthtml/VChartHTML.html.
%       [5]  M. Wang, G. Audi, F. G. Kondev, W. J. Huang, S. Naimi, and Xing Xu, “The AME 2016 atomic mass evaluation,” Chin. Phys. C., vol. 41, no. 3, 2017, doi: 10.1088/1674-1137/41/3/030003.
%       [6]  Pacific Northwest National Laboratory, “Compendium of Material Composition Data for Radiation Transport Modelling,” PNNL., Richland, WA, USA, Rep. PNNL-15870, Rev. 2, Apr. 2021.
%       [7]  A. H. Harvey, “Thermodynamic Properties of Water: Tabulation from the IAPWS Formulation 1995 for the Thermodynamic Properties of Ordinary Water Substance for General and Scientific Use,” NIST., Boulder, CO, USA, Rep. NISTIR 5078, Oct. 1998.
%       [8]  Technical Research Centre of Finland VTT. “Tutorial.” Serpent.vtt.fi. Accessed: Apr. 24, 2024. [Online]. Available: http://serpent.vtt.fi/mediawiki/index.php/Tutorial#Part_1_input.

% --- Reproducing the simulation
set seed 1720487042152

/************************
 * Geometry definitions *
 ************************/

% --- FuelNoGad UO2 pin structure (Rod SF95)
%       Fuel pellet outer diameter 8.05 mm [2, p. 113, Table III]
%       The region between the fuel pellet and cladding can be modelled as void [8, Part 5: Fuel rod geometry]
%       Cladding inner diameter 8.22 mm [2, p. 113, Table III]
%       Cladding outer diameter 9.5 mm [2, p. 113, Table III]
%       All radii are expressed in cm

pin FF
fuelNoGad       0.4025
void            0.4110
zircaloy4       0.4750
coolant

% --- FuelYesGad UO2-Gd2O3 pin structure (Rod SF96)
%       All dimensions are identical to FuelNoGad UO2 pin structure [2, p. 113, Table III]
%       GG: all UO2-Gd2O3 pins
%       GS: Sample UO2-Gd2O3 pin (Rod SF96)
%       All radii are expressed in cm
```

```
pin GG
fuelYesGad      0.4025
void            0.4110
zircaloy4       0.4750
coolant

pin GS
fuelSample      0.4025
void            0.4110
zircaloy4       0.4750
coolant

% --- Empty control channel and instrumentation thimble structure
%       Assumed to have the same dimensions as all other present pins (no information in 'TAK-00X' documents)
%       In practice, they should be wider [Dr. ir. Romojaro]
%       All radii are expressed in cm

pin CC
coolant         0.4110
zircaloy4       0.4750
coolant

% --- Bounding surfaces around the fuel assembly are square surfaces
%       s1 (fuel pin cell pitch) centered at 0.0 0.0 12.6 mm
%       s2 (cell pitch x 17 cells) centered at 0.0 0.0 214.2 mm
%       s3 (fuel assembly pitch) centered at 0.0 0.0 214 +- 0.5% mm (thus 215.07 mm)
%       Half-width expressed in cm

surf s1 sqc 0.0 0.0 0.63
surf s2 sqc 0.0 0.0 10.71
surf s3 sqc 0.0 0.0 10.7535

% --- Universes for the lattice

cell    1 10 fill FF    -s1
cell    2 10 coolant    s1
cell    3 20 fill GG    -s1
cell    4 20 coolant    s1
cell    5 30 fill GS    -s1
cell    6 30 coolant    s1
cell    7 40 fill CC    -s1
cell    8 40 coolant    s1

% --- Pin lattice definition, name of the lattice "lat1"
%       Lattice type 1 (square lattice)
%       Lattice centered at 0.0 0.0
%       17 x 17 lattice elements
%       Lattice pitch 12.6 mm
%       Pitch expressed in cm

lat lat1 1 0.0 0.0 17 17 1.26
        10 10 10 10 10 10 10 10 10 10 10 10 10 10 10 10 10
        10 10 10 10 10 10 10 10 10 10 10 10 10 10 10 10 10
        10 10 10 10 20 40 10 10 40 10 10 40 20 10 10 10 10
        10 10 10 40 10 10 10 10 20 10 10 10 10 40 10 10 10
```

```
        10 10 20 10 10 10 10 10 10 10 10 10 10 20 10 10
        10 10 40 10 10 40 10 10 40 10 10 40 10 10 40 10 10
        10 10 10 10 10 10 20 10 10 10 20 10 10 10 10 10 10
        10 10 10 10 10 10 10 10 10 10 10 10 10 10 10 10 10
        10 10 40 10 10 40 10 10 40 10 10 40 10 10 40 10 10
        10 10 10 10 10 10 10 10 10 10 10 10 10 10 10 10 10
        10 10 10 10 10 10 20 10 10 10 20 10 10 10 10 10 10
        10 10 40 10 10 40 10 10 40 10 10 40 10 10 40 10 10
        10 10 30 10 10 10 10 10 10 10 10 10 10 20 10 10
        10 10 10 40 10 10 10 10 20 10 10 10 10 40 10 10 10
        10 10 10 10 20 40 10 10 40 10 10 40 20 10 10 10 10
        10 10 10 10 10 10 10 10 10 10 10 10 10 10 10 10 10
        10 10 10 10 10 10 10 10 10 10 10 10 10 10 10 10 10

% --- Geometry

cell 11 0 fill lat1 -s2
cell 12 0 coolant s2 -s3
cell 13 0 outside s3

/*************************
 * Material definitions *
 *************************/

% --- FuelNoGad UO2 material (Rod SF95) mass density: 10.412 g/cm3 (95% of theoretical density) [1, p. 363, Table A.2.5]
%       Uranium isotopic composition: 0.04 wt-% 234U; 4.11 wt-% 235U; and 95.85 wt-% 238U [2, p. 114, Table V]
%       Oxygen natural isotopic abundance: 99.757 wt-% 16O; 0.03835 wt-% 17O; and 0.2045 wt-% 18O [4]
%       Fuel temperature is set to 900.0 K [1, p. 148]
%       Fuel rod is burnable
%       4 separate burnable divisions of the material
%       Mass isotopic composition (-) is calculated via Excel and molar mass data [5]

mat fuelNoGad     -10.412 tmp 900.0 rgb 255 255 150 burn 4
8016.09c          -0.11825903
8017.09c          -0.000287892
92234.09c         -0.000352581
92235.09c         -0.036227714
92238.09c         -0.844872605

% --- FuelYesGad UO2-Gd2O3 (Rod SF96) material: 6.00 wt-% natural Gd; mass density: 10.412 g/cm3 (95% of theoretical density) [1, p. 363, Table A.2.5]
%       Uranium isotopic composition: 0.02 wt-% 234U; 2.63 wt-% 235U; and 97.25 wt-% 238U [2, p. 114, Table V]
%       Oxygen natural isotopic abundance: 99.757 wt-% 16O; 0.03835 wt-% 17O; and 0.2045 wt-% 18O [4]
%       Gadolinium natural isotopic abundance: 0.20 wt-% 152Gd; 2.18 wt-% 154Gd; 14.80 wt-% 155Gd; 20.47 wt-% 156Gd; 15.65 wt-% 157Gd; 24.84 wt-% 158Gd; and 21.86 wt-% 160Gd [4]
%       Fuel temperature is set to 900.0 K [1, p. 148]
%       Fuel rod is burnable
%       10 separate burnable divisions of the material
%       Mass isotopic composition (-) is calculated via Excel and molar mass data [5]
%       'fuelSample' mass composition and parameters are identical to FuelYesGad

mat fuelYesGad    -10.412 tmp 900.0 rgb 150 255 150 burn 10
8016.09c          -0.112490082
8017.09c          -0.000273848
64152.09c         -0.000106468
```

```
64154.09c       -0.001160505
64155.09c       -0.007878655
64156.09c       -0.010897031
64157.09c       -0.008331145
64158.09c       -0.013223364
64160.09c       -0.011636986
92234.09c       -0.000166800
92235.09c       -0.021934246
92238.09c       -0.811066699

mat fuelSample  -10.412 tmp 900.0 rgb 150 255 150 burn 10
8016.09c        -0.112490082
8017.09c        -0.000273848
64152.09c       -0.000106468
64154.09c       -0.001160505
64155.09c       -0.007878655
64156.09c       -0.010897031
64157.09c       -0.008331145
64158.09c       -0.013223364
64160.09c       -0.011636986
92234.09c       -0.000166800
92235.09c       -0.021934246
92238.09c       -0.811066699

% --- Zircaloy-4 (i.e. Zry-4) [1, p. 363, Table A.2.5] cladding material: mass density: 6.56 g/cm3 [6, p. 273]
%       Cladding temperature is set to 600.0 K [1, p. 148]
%       Atomic isotopic composition (+) is copied from [6, p. 273]
%       Oxygen natural isotopic abundance: 99.757 wt-% 16O; 0.03835 wt-% 17O; and 0.2045 wt-% 18O [4]
%       Chromium natural isotopic abundance: 4.345 wt-% 50Cr; 83.789 wt-% 52Cr; 9.501 wt-% 53Cr; and 2.365 wt-% 54Cr [4]
%       Iron natural isotopic abundance: 5.845 wt-% 54Fe; 91.754 wt-% 56Fe; 2.119 wt-% 57Fe; and 0.282 wt-% 58Fe [4]
%       Zirconium natural isotopic abundance: 51.45 wt-% 90Zr; 11.22 wt-% 91Zr; 17.15 wt-% 92Zr; 17.38 wt-% 94Zr; and 2.80 wt-% Zr96 [4]
%       Tin natural isotopic abundance: 0.97 wt-% 112Sn; 0.66 wt-% 114Sn; 0.34 wt-% 115Sn; 14.54 wt-% 116Sn; 7.68 wt-% 117Sn; 24.22 wt-% 118Sn; 8.59 wt-% 119Sn; 32.58 wt-% 120Sn; 4.63 wt-% 122Sn; and 5.79 wt-% 124Sn [4]

mat zircaloy4   -6.56 tmp 600 rgb 200 200 200
8016.06c        0.006788
8017.06c        0.000003
24050.06c       0.000076
24052.06c       0.001459
24053.06c       0.000165
24054.06c       0.000041
26054.06c       0.000189
26056.06c       0.002975
26057.06c       0.000069
26058.06c       0.000009
40090.06c       0.502949
40091.06c       0.109681
40092.06c       0.167650
40094.06c       0.169898
40096.06c       0.027371
50112.06c       0.000104
50114.06c       0.000070
50115.06c       0.000036
```

```
50116.06c       0.001552
50117.06c       0.000820
50118.06c       0.002586
50119.06c       0.000917
50120.06c       0.003479
50122.06c       0.000494
50124.06c       0.000618

% --- Coolant is water with an average 550 ppm soluble boric acid added (average of three listed cycle averages)
%       START concentration neglects the first point of provided curvature [Dr. ir. Romojaro]
%       Boron concentration cycle 5 START: 894 ppm; cycle 5 END: 210 ppm; AVERAGE: 552 ppm [2, p. 166, Table X]
%       Boron concentration cycle 6 START: 864 ppm; cycle 6 END: 228 ppm; AVERAGE: 546 ppm [2, p. 166, Table X]
%       Boron concentration cycle 7 START: 1001 ppm; cycle 7 END: 104 ppm; AVERAGE: 553 ppm [2, p. 166, Table X]
%
%       Coolant temperature is set to 570.82 K (specific for sample: "SF96-4") [1, p. 149, Table 3.3.6]
%       Water mass density is interpolated based on a pressure of 16.0 MPa and temperature of 570.82 K [2, p. 113, Table
        II] and [7, pp. 58-59]
%       Hydrogen is flagged as a bound scatterer with the “moder” -card
%       Boron mass density is 2.37 g/cm3 at temperature 293.15 K [6, p. 43]
%       Boron natural isotopic abundance: 19.65 wt-% 10B; and 80.35 wt-% 11B [4]
%       Oxygen natural isotopic abundance: 99.757 wt-% 16O; 0.03835 wt-% 17O; and 0.2045 wt-% 18O [4]

mat water       -0.732017 tmp 570.82 moder lwtr 1001 rgb 200 200 255
1001.05c        2.0
8016.05c        0.999615
8017.05c        0.000384

mat boron       -2.37 tmp 570.82
5010.05c        0.19650
5011.05c        0.80350

mix coolant
water           -0.999450
boron           -550.0E-6

% --- Define thermal scattering libraries associated with hydrogen in light water
%       Interpolate using two bounding libraries for 570.82 K (ENDF/B-VII.1):
%       lwtr.15t (discrete ZAID notation) for temp. 550 K
%       lwtr.16t (discrete ZAID notation) for temp. 600 K

therm lwtr 570.82 lwtr.15t lwtr.16t

% --- Cross section directory file path
%       Isomeric branching library file path

set acelib "/srv/sci/pack/nuclear-data/endfb_71/ace/xsdata.endfb71"
set bralib "/srv/sci/pack/nuclear-data/endfb_71/bralib.endfb71"

/******************
 * Run parameters *
 ******************/

% --- Boundary conditions (1 = black, 2 = reflective, 3 = periodic)

set bc 2
```

```
% --- Use of unresolved resonance probability tables

set ures 1

% --- Neutron population: 10 000 neutrons per cycle; and criticality cycles: 250 active / 50 inactive cycles
%           Test simulations: 10 000 neutrons per cycle
%           Final simulations: 100 000 neutrons per cycle
%           Number of active/inactive cycles discussed with [Dr. ir. Romojaro]

set pop 100000 250 50

% --- XY plot (3)
%           1024 pixels by 1024 pixels

plot 3 1024 1024


/*****************************************
 * Settings for the burn-up calculations *
 *****************************************/

% --- Decay and fission field libraries

set declib "/srv/sci/pack/nuclear-data/endfb_71/decay/rdd.endfb71"
set nfylib "/srv/sci/pack/nuclear-data/endfb_71/nfy/nfy.endfb71"
set sfylib "/srv/sci/pack/nuclear-data/endfb_71/sfy/sfy.endfb71"


% --- Use of double indexing method
%           Copied from sample -file [Dr. ir. Romojaro]

set dix 0

% --- Cut-offs
%           Copied from sample -file [Dr. ir. Romojaro]

set fpcut  0.0E+00

% --- Switch group constant generation off
%           Copied from sample -file [Dr. ir. Romojaro]

set gcu -1

% --- Options for the burn-up calculations
%           Copied from sample -file [Dr. ir. Romojaro]

set bumode          2
set pcc             0
set xscalc          1
set printm          1
```

```
%       Irradiation history from "SF96-4" [1, p. 382, Table A.2.22.]
%       Power density expressed in kW/g
%       Cycle 5: 26 January 1990 to 15 February 1991 (385 days UP)
%       Cooling: 15 February 1991 to 14 May 1991 (88 days DOWN)
%       Cycle 6: 14 May 1991 to 19 June 1992 (402 days UP)
%       Pre-normalisation Neodymium-148 C/E ratio: 0.980888

set powdens 0.0037517 fuelSample
dep daystep 12
set powdens 0.0150170 fuelSample
dep daystep 8
set powdens 0.0159243 fuelSample
dep daystep 27
set powdens 0.0169234 fuelSample
dep daystep 35
set powdens 0.0190644 fuelSample
dep daystep 28
set powdens 0.0213378 fuelSample
dep daystep 21
set powdens 0.0241720 fuelSample
dep daystep 35
set powdens 0.0301462 fuelSample
dep daystep 35
set powdens 0.0336634 fuelSample
dep daystep 28
set powdens 0.0372112 fuelSample
dep daystep 27
set powdens 0.0404939 fuelSample
dep daystep 49
set powdens 0.0431956 fuelSample
dep daystep 15
set powdens 0.0458666 fuelSample
dep daystep 37
set powdens 0.0466822 fuelSample
dep daystep 19
set powdens 0.0476711 fuelSample
dep daystep 9
set powdens 0.00 fuelSample
dep decstep 88
set powdens 0.0212359 fuelSample
dep daystep 10
set powdens 0.0427368 fuelSample
dep daystep 11
set powdens 0.0433077 fuelSample
dep daystep 20
set powdens 0.0437665 fuelSample
dep daystep 23
set powdens 0.0440213 fuelSample
dep daystep 28
set powdens 0.0442762 fuelSample
dep daystep 28
set powdens 0.0445617 fuelSample
dep daystep 28
set powdens 0.0448471 fuelSample
```

```
dep daystep 35
set powdens 0.0451020 fuelSample
dep daystep 28
set powdens 0.0453263 fuelSample
dep daystep 34
set powdens 0.0456117 fuelSample
dep daystep 43
set powdens 0.0456117 fuelSample
dep daystep 28
set powdens 0.0455302 fuelSample
dep daystep 28
set powdens 0.0456321 fuelSample
dep daystep 35
set powdens 0.0456831 fuelSample
dep daystep 15
set powdens 0.0457035 fuelSample
dep daystep 8

% --- Nuclide inventory: these nuclides will be included in the depletion output file.
%         All nuclides which were measured in "SF96-4" via destructive analysis [1, p. 389, Table A.3.28.]

set inventory
441060
511250
551340
551370
581440
601430
601440
601450
601460
601480
601500
631540
922340
922350
922360
922380
932370
942380
942390
942400
942410
942420
952410
952421
952430
962420
962440
```

Appendix B: Results of Destructive Radiochemical Analyses for “SF96” Samples

Table 23: Results of destructive radiochemical analyses for the "SF96" samples [85, p. 389]

Nuclide	Measured Nuclide Concentrations [g/g$_{HM}$]					Method	Uncertainty
	SF96-1	SF96-2	SF96-3	SF96-4	SF96-5		
Ru-106	2.830E-05	6.053E-05	1.402E-04	1.291E-04	1.344E-04	GS	5%
Sb-125	1.433E-06	2.829E-06	3.658E-06	4.645E-06	3.690E-06	GS	10%
Cs-134	8.609E-06	3.759E-05	1.002E-04	1.047E-04	7.146E-05	GS	3%
Cs-137	2.813E-04	5.983E-04	1.018E-03	1.053E-03	8.572E-04	GS	3%
Ce-144	1.179E-04	2.250E-04	3.362E-04	3.453E-04	3.145E-04	GS	10%
Nd-143	2.521E-04	4.778E-04	7.158E-04	7.184E-04	6.433E-04	IDMS	0.1%
Nd-144	1.536E-04	3.588E-04	7.292E-04	7.513E-04	5.927E-04	IDMS	0.1%
Nd-145	1.800E-04	3.575E-04	5.766E-04	5.880E-04	5.095E-04	IDMS	0.1%
Nd-146	1.536E-04	3.266E-04	5.795E-04	5.948E-04	4.910E-04	IDMS	0.1%
Nd-148	8.770E-05	1.851E-04	3.201E-04	3.280E-04	2.733E-04	IDMS	0.1%
Nd-150	4.130E-05	8.972E-05	1.591E-04	1.628E-04	1.331E-04	IDMS	0.1%
Eu-154	2.309E-06	8.538E-06	1.973E-05	1.992E-05	1.423E-05	GS	3%
U-234	1.805E-04	1.522E-04	1.251E-04	1.250E-04	1.354E-04	IDMS	1%
U-235	1.944E-02	1.408E-02	8.638E-03	8.064E-03	9.937E-03	IDMS	0.1%
U-236	1.421E-03	2.411E-03	3.244E-03	3.302E-03	3.013E-03	IDMS	2%
U-238	9.660E-01	9.580E-01	9.476E-01	9.475E-01	9.522E-01	IDMS	0.1%
Np-237	6.125E-05	1.323E-04	2.168E-04	2.252E-04	1.875E-04	AS	10%
Pu-238	8.536E-06	4.172E-05	1.206E-04	1.248E-04	7.978E-05	IDMS	0.5%
Pu-239	3.781E-03	5.459E-03	6.001E-03	5.819E-03	5.519E-03	IDMS	0.3%
Pu-240	6.764E-04	1.494E-03	2.303E-03	2.327E-03	1.964E-03	IDMS	0.3%
Pu-241	2.622E-04	8.684E-04	1.498E-03	1.480E-03	1.203E-03	IDMS	0.3%
Pu-242	2.440E-05	1.615E-04	5.103E-04	5.411E-04	3.551E-04	IDMS	0.3%
Am-241	5.985E-06	1.735E-05	2.845E-05	3.094E-05	2.149E-05	MS, AS	2%
Am-242m	1.218E-07	4.579E-07	6.413E-07	6.793E-07	5.647E-07	MS, AS	10%
Am-243	1.147E-06	1.728E-05	8.872E-05	9.598E-05	5.078E-05	MS, AS	5%
Cm-242	8.502E-07	5.781E-06	1.628E-05	1.679E-05	1.115E-05	MS, AS	10%
Cm-244	9.560E-08	3.092E-06	2.862E-05	3.128E-05	1.280E-05	MS, AS	2%

Appendix C: ‘C/E’ Results by SWAT for “SF96” Samples

Table 24: ‘C/E’ results by SWAT for the “SF96” samples [85, p. 154]

Nuclide	SF96-1	SF96-2	SF96-3	SF96-4	SF96-5	Average	SD
Ru-106	N.A.	N.A.	N.A.	N.A.	N.A.	N.A.	N.A.
Sb-125	N.A.	N.A.	N.A.	N.A.	N.A.	N.A.	N.A.
Cs-134	N.A.	0.905	0.965	0.949	0.966	0.95	0.03
Cs-137	N.A.	1.031	1.042	1.033	1.061	1.04	0.01
Ce-144	N.A.	0.961	0.958	0.962	0.951	0.96	0.01
Nd-143	N.A.	1.036	1.143	1.142	1.067	1.10	0.05
Nd-144	N.A.	0.937	0.886	0.900	0.922	0.91	0.02
Nd-145	N.A.	0.996	0.995	0.999	0.992	1.00	0.00
Nd-146	N.A.	0.975	0.970	0.970	0.972	0.97	0.00
Nd-148	N.A.	0.991	0.990	0.991	0.992	0.99	0.00
Nd-150	N.A.	0.979	0.978	0.977	0.984	0.98	0.00
Eu-154	N.A.	1.483	1.265	1.241	1.387	1.34	0.11
U-234	N.A.	1.056	1.044	1.039	1.050	1.05	0.01
U-235	N.A.	1.011	1.010	1.014	0.998	1.01	0.01
U-236	N.A.	0.947	0.950	0.948	0.957	0.95	0.00
U-238	N.A.	1.000	1.001	1.001	1.001	1.00	0.00
Np-237	N.A.	1.311	1.534	1.478	1.403	1.43	0.10
Pu-238	N.A.	0.825	0.843	0.814	0.853	0.83	0.02
Pu-239	N.A.	0.978	0.988	0.982	0.985	0.98	0.00
Pu-240	N.A.	0.992	0.983	0.971	0.997	0.99	0.01
Pu-241	N.A.	0.992	0.980	0.968	0.993	0.98	0.01
Pu-242	N.A.	0.974	0.958	0.943	0.990	0.97	0.02
Am-241	N.A.	1.382	1.197	1.057	1.368	1.25	0.15
Am-242m	N.A.	0.715	0.800	0.701	0.721	0.73	0.04
Am-243	N.A.	0.939	0.959	0.917	0.982	0.95	0.03
Cm-242	N.A.	0.800	0.789	0.769	0.822	0.79	0.02
Cm-244	N.A.	0.779	0.822	0.778	0.848	0.81	0.03

Appendix D: ‘C/E’ Results by ORIGEN2.1 for “SF96” Samples

Table 25: ‘C/E’ results by ORIGEN2.1 for the “SF96” samples [85, p. 177]

Nuclide	SF96-1	SF96-2	SF96-3	SF96-4	SF96-5	Average	SD
Ru-106	N.A.	N.A.	N.A.	N.A.	N.A.	N.A.	N.A.
Sb-125	N.A.	N.A.	N.A.	N.A.	N.A.	N.A.	N.A.
Cs-134	N.A.	1.013	1.075	1.079	1.127	1.07	0.05
Cs-137	N.A.	1.030	1.043	1.034	1.061	1.04	0.01
Ce-144	N.A.	1.040	1.141	1.136	1.060	1.09	0.05
Nd-143	N.A.	0.952	0.928	0.939	0.935	0.94	0.01
Nd-144	N.A.	0.993	0.935	0.936	0.953	0.95	0.03
Nd-145	N.A.	1.000	0.988	0.990	0.983	0.99	0.01
Nd-146	N.A.	0.989	0.984	0.985	0.986	0.99	0.00
Nd-148	N.A.	0.993	0.995	0.996	0.996	0.99	0.00
Nd-150	N.A.	0.965	0.977	0.981	0.988	0.98	0.01
Eu-154	N.A.	1.539	1.237	1.256	1.455	1.37	0.15
U-234	N.A.	1.072	1.048	1.035	1.044	1.05	0.02
U-235	N.A.	0.957	0.958	0.996	0.987	0.97	0.02
U-236	N.A.	0.939	0.931	0.924	0.934	0.93	0.01
U-238	N.A.	1.001	1.001	1.001	1.000	1.00	0.00
Np-237	N.A.	1.270	1.501	1.484	1.453	1.43	0.11
Pu-238	N.A.	0.744	0.831	0.845	0.912	0.83	0.07
Pu-239	N.A.	0.971	1.026	1.062	1.080	1.03	0.05
Pu-240	N.A.	0.843	0.899	0.908	0.925	0.89	0.04
Pu-241	N.A.	0.951	1.011	1.044	1.090	1.02	0.06
Pu-242	N.A.	0.844	0.920	0.913	0.955	0.91	0.05
Am-241	N.A.	1.141	1.166	1.087	1.391	1.20	0.13
Am-242m	N.A.	0.514	0.668	0.641	0.672	0.62	0.07
Am-243	N.A.	0.799	0.943	0.939	1.020	0.93	0.09
Cm-242	N.A.	0.634	0.736	0.747	0.795	0.73	0.07
Cm-244	N.A.	0.653	0.812	0.825	0.933	0.81	0.12

Appendix E: Results of Destructive Radiochemical Analyses for “C5” and “O13” Samples

Table 26: Results of destructive radiochemical analyses for the "C5" and "O13" samples [96, p. 935]

Nuclide	Measured Nuclide Concentrations [g/g$_{HM}$]			Method	Uncertainty
	C5-89G01	C5-89G03	O13-89G05		
Ru-106	5.26E-06	7.52E-06	6.70E-06	GS	2.6%
Ag110m	2.24E-09	3.69E-09	3.10E-09	GS	5.6%
Sb-125	1.53E-06	2.05E-06	1.72E-06	GS	4%
Cs-134	1.23E-05	2.13E-05	1.69E-05	GS	2.2%
Cs-137	7.00E-04	9.61E-04	8.34E-04	GS	2.4%
Ce-144	3.45E-06	3.91E-06	3.94E-07	GS	2%
Nd-142	9.28E-06	1.70E-05	1.75E-05	IDMS	0.52%
Nd-143	5.16E-04	6.14E-04	5.67E-04	IDMS	0.2%
Nd-144	7.51E-04	1.04E-03	8.86E-04	IDMS	0.11%
Nd-145	4.24E-04	5.40E-04	4.84E-04	IDMS	0.33%
Nd-146	4.16E-04	5.68E-04	4.92E-04	IDMS	0.32%
Nd-148	2.37E-04	3.19E-04	2.79E-04	IDMS	0.29%
Nd-150	1.21E-04	1.65E-04	1.43E-04	IDMS	0.34%
Eu-154	9.74E-06	1.43E-05	1.20E-05	GS	2%
U-232	1.26E-09	1.76E-09	1.53E-09	IDMS	1.6%
U-234	8.75E-05	7.47E-05	8.13E-05	IDMS	1.1%
U-235	5.47E-03	3.65E-03	4.42E-03	IDMS	0.5%
U-236	1.97E-03	2.23E-03	2.14E-03	IDMS	0.5%
U-238	9.60E-01	9.53E-01	9.56E-01	IDMS	0.5%
Np-237	2.21E-04	2.86E-04	2.45E-04	IDMS	5%
Pu-236	3.78E-10	7.21E-10	5.72E-10	IDMS	3.1%
Pu-238	6.82E-05	1.21E-04	9.35E-05	IDMS	0.58%
Pu-239	5.36E-03	5.51E-03	5.52E-03	IDMS	0.5%
Pu-240	2.15E-03	2.61E-03	2.42E-03	IDMS	0.5%
Pu-241	1.24E-03	1.55E-03	1.43E-03	IDMS	0.5%
Pu-242	4.28E-04	7.58E-04	6.05E-04	IDMS	0.5%
Am-241	2.75E-05	3.65E-05	2.72E-05	MS, AS	7.7%
Am-242m	4.77E-07	8.07E-07	5.09E-07	MS, AS	1.3%
Am-243	6.32E-05	1.47E-04	1.23E-04	MS, AS	0.97%
Cm-242	1.21E-05	1.99E-05	1.47E-05	MS, AS	0.84%
Cm-243	1.91E-07	4.99E-07	3.92E-07	MS, AS	19%
Cm-244	1.62E-05	5.70E-05	3.26E-05	MS, AS	1.3%
Cm-245	6.56E-07	2.88E-06	1.5E-06	MS, AS	0.94%
Cm-246	5.74E-08	3.67E-07	1.58E-07	MS, AS	1.1%
Cm-247	5.50E-10	4.88E-09	N.A.	MS, AS	4.7%

Appendix F: ‘C/E’ Results by SWAT2.1 for “C5” and “O13” Samples

Table 27: ‘C/E’ results by SWAT2.1 for the "C5" and "O13" samples [96, p. 938]

Nuclide	C5-89G01	C5-89G03	O13-89G05	Average
Ru-106	0.96	0.98	0.99	0.98
Ag-110m	2.39	2.75	2.63	2.59
Sb-125	1.21	1.24	1.32	1.26
Cs-134	0.95	0.95	0.97	0.96
Cs-137	1.03	1.00	1.01	1.01
Ce-144	0.93	1.07	1.03	1.01
Nd-142	0.86	0.85	0.63	0.78
Nd-143	1.03	1.05	1.05	1.04
Nd-144	1.01	1.01	1.02	1.01
Nd-145	1.02	1.03	1.02	1.02
Nd-146	1.00	1.00	1.00	1.00
Nd-148	1.00	1.00	1.00	1.00
Nd-150	1.02	1.01	1.01	1.01
Eu-154	1.41	1.29	1.32	1.34
U-232	0.14	0.15	0.14	0.14
U-234	1.02	1.02	1.01	1.02
U-235	1.03	1.05	1.05	1.04
U-236	1.00	0.99	0.99	0.99
U-238	1.00	1.00	1.00	1.00
Np-237	0.93	0.98	0.99	0.97
Pu-236	1.37	1.30	1.28	1.32
Pu-238	0.88	0.86	0.85	0.86
Pu-239	0.98	0.99	0.97	0.98
Pu-240	0.98	0.96	0.96	0.97
Pu-241	0.99	0.98	0.98	0.98
Pu-242	0.97	0.93	0.93	0.94
Am-241	1.11	0.91	1.02	1.01
Am-242m	0.98	0.65	0.85	0.83
Am-243	1.01	0.96	0.82	0.93
Cm-242	0.90	0.86	0.89	0.88
Cm-243	1.03	0.80	0.71	0.85
Cm-244	0.94	0.82	0.88	0.88
Cm-245	1.07	0.93	0.99	1.00
Cm-246	0.95	0.80	0.88	0.88
Cm-247	0.81	0.67	N.A.	0.74